Molecular Modeling of Hydrate-Clathrates via ab initio, Cell Potential, and Dynamic Methods

by

Brian Anderson

B.S. in Chemical Engineering
West Virginia University, 2000

M.S. in Chemical Engineering Practice
Massachusetts Institute of Technology, 2004

Submitted to the Department of Chemical Engineering
in partial fulfillment of the requirements for the degree of

Doctor of Philosophy

at the

Massachusetts Institute of Technology

August 2005
[September 2005]

Signature of Author: _____
Department of Chemical Engineering
August 11, 2005

Certified by: _____
Jefferson Tester
Herman P. Meissner Professor of Chemical Engineering
Thesis Supervisor

Certified by: _____
Bernhardt Trout
Associate Professor of Chemical Engineering
Thesis Supervisor

Accepted by: _____
Daniel Blankschtein
Professor of Chemical Engineering
Chairman, Committee for Graduate Students

Molecular Modeling of Hydrate-Clathrates via ab initio, Cell Potential, and Molecular Dynamic Methods

by

Brian Anderson

Submitted to the Department of Chemical Engineering on
August 11, 2005 in partial fulfillment of the requirements for
the degree of Doctor of Philosophy in Chemical Engineering

ABSTRACT

High level *ab initio* quantum mechanical calculations were used to determine the intermolecular potential energy surface between argon and water, corrected for many-body interactions, to predict monovariant and invariant phase equilibria for the argon hydrate and mixed methane-argon hydrate systems. A consistent set of reference parameters for the van der Waals and Platteeuw model, $\Delta\mu_w^0$=1077±5 kcal/mol and ΔH_w^0=1294±11 kcal/mol, were developed for Structure II hydrates and are not dependent on any fitted parameters. Our previous methane-water *ab initio* energy surface has been recast onto a site-site potential model that predicts guest occupancy experiments with improved accuracy compared to previous studies. This methane-water potential is verified via *ab initio* many-body calculations and thus should be generally applicable to dense methane-water systems. New reference parameters, $\Delta\mu_w^0$=1203±3 kcal/mol and ΔH_w^0=1170±19 kcal/mol, for Structure I hydrates using the van der Waals and Platteeuw model were also determined. Equilibrium predictions with an average absolute deviation of 3.4% for the mixed hydrate of argon and methane were made. These accurate predictions of the mixed hydrate system provide an independent test of the accuracy of the intermolecular potentials. Finally, for the mixed argon-methane hydrate, conditions for structural changes from the Structure I hydrate of methane to the Structure II hydrate of argon were predicted and await experimental confirmation.

We present the application of a mathematical method reported earlier[1] by which the van der Waals-Platteeuw statistical mechanical model with the Lennard-Jones and Devonshire approximation can be posed as an integral equation with the unknown function being the intermolecular potential between the guest molecules and the host molecules. This method allows us to solve for the potential directly for hydrates for which the Langmuir constants are computed, either from experimental data or from *ab initio* data. Given the assumptions made in the van der Waals-Platteeuw model with the spherical-cell approximation, there are an infinite number of solutions; however, the only solution without cusps is a unique central-well solution in which the potential is at a finite minimum at the center to the cage. From this central-well solution, we have found the potential well depths and volumes of negative energy for sixteen single-component hydrate systems: ethane (C_2H_6), cyclopropane (C_3H_6), methane (CH_4), argon (Ar), and chlorodifluoromethane (R-22) in structure I; and ethane (C_2H_6), cyclopropane (C_3H_6), propane (C_3H_8), isobutane (C_4H_{10}), methane (CH_4), argon (Ar), trichlorofluoromethane

(R-11), dichlorodifluoromethane (R-12), bromotrifluoromethane (R-13B1), chloroform ($CHCl_3$), and 1,1,1,2-Tetrafluoroethane (R-134a) in structure II.

This method and the calculated cell potentials were validated by predicting existing mixed hydrate phase equilibrium data without any fitting parameters and calculating mixture phase diagrams for methane, ethane, isobutane, and cyclopropane mixtures. Several structural transitions that have been determined experimentally as well as some structural transitions that have not been examined experimentally were also predicted. In the methane-cyclopropane hydrate system, a structural transition from structure I to structure II and back to structure I is predicted to occur outside of the known structure II range for the cyclopropane hydrate. Quintuple (L_w-SI-SII-L_{hc}-V) points have been predicted for the ethane-propane-water (277.3 K, 12.28 bar, and $x_{eth,waterfree} = 0.676$) and ethane-isobutane-water (274.7 K, 7.18 bar, and $x_{eth,waterfree} = 0.81$) systems.

A two-fold mechanism for hydrate inhibition has been proposed and tested using molecular dynamic simulations for PEO, PVP, PVCap, and VIMA. This mechanism hypothesizes that (1) as potential guest molecules become coordinated by water, form nuclei, and begin to grow, nearby inhibitor molecules disrupt the organization of the forming clathrate and (2) inhibitor molecules bind to the surface of the hydrate crystal precursor and retards further growth along the bound growth plane resulting in a modified planar morphology. This mechanism is supported by the results of our molecular dynamic simulations for the four inhibitor molecules studied. PVCap and VIMA, the more effective inhibitors, shows strong interactions with the liquid water phase under hydrate forming conditions, while PVP and PEO appear relatively neutral to the surrounding water.

Thesis Supervisors:

Jefferson W. Tester	Herman P. Meissner Professor of Chemical Engineering
Bernhardt L. Trout	Assistant Professor of Chemical Engineering

Acknowledgements

Throughout the course of one's life, many individuals who make an impact pass through. I would first like to thank all those in my life that have stopped by, if only for a moment, and influenced who I am. There are too many to mention here, but I do sincerely thank you all.

I am blessed to have numerous friends and family that have stayed the course and enriched my life. First and foremost, I must thank my family for always encouraging me and believing in me. My mother, who has been there to see me develop from the shy sixth grader that did not want to go to school, to someone who wants to spend all his time at school. My father, who is always ready with an encouraging and inspiring word. My sister, who has always supported me, looked after me, and toughened me up. Grandpa and Grandma Poling, who always make me feel like the decisions I make are the right decisions. Judy, who is the best step-mother that anyone could ask for. Finally, Mikale, Shannon, and Bobby who are everything but blood to me.

I would like to thank my advisors, Professors Jeff Tester and Bernhardt Trout, for their unending support and direction. I have learned much more than simply how to conduct research from them. I feel that we have created a team, with perfect balance between advisor and student and I only hope that someday I can become half of the advisor that each of them has been to me. I would have never imagined that I would grow to consider both of them my friends, in addition to having the utmost respect for their intuition, understanding, and professionalism.

I sincerely thank all the past and present members of the Trout and Tester groups for all their camraderie through the years. I want to give a special thanks to Zhitao Cao, Patty Sullivan, Mike Timko, Murray Height, Paul Yelvington, Brian Baynes, Jason Ploeger, Heather Stern, Baron Peters, and Gregg Beckham.

Finally, I would like to thank those people in my life that have been there through everything, especially Michelle Hinkle. She been an inspiration to me in so many ways, opening up her home to me and always there when I need her. Thank you Ann Herman and Dan Thunberg for teaching me what I deserve and for showing me true friendship. Thank you Bill Cutter and John Oliver for encouraging me to sing and sing loudly.

Thank you all, thank you very much.

Brian Anderson
August 11, 2005

Table of Contents

List of Figures

List of Tables

Chapter 1. Introduction

1.1 Overview and historical perspective

1.1.1 Discovery of gas hydrates

Natural gas clathrate-hydrates (called gas hydrates) are nonstiochiometric inclusion compounds consisting of a three-dimensional host lattice of water molecules, in which guest molecules, such methane and/or carbon dioxide, are encaged in polyhedral cells formed by the hydrogen-bonded water molecules. The existence of gas hydrates was first reported in 1810 by Sir Humphrey Davy[1] who observed a yellow precipitate while passing chlorine gas through water at temperature near 0°C. In addition, there was some evidence that SO_2 gas hydrates were detected by Joseph Priestley[2] more than 30 years prior to Davy's observation.

1.1.2 Hydrates in various industries

Early studies on gas hydrates focused on identifying the guest molecules that formed hydrates and the pressure-temperature conditions at which the formation occurred. In 1934, it was recognized that solid gas hydrates could deposit in natural gas pipelines, leading to restricted flow and blockage[3]. Shortly thereafter, intense research programs studying gas hydrates were initiated by the oil and gas industry, the government, and academia, with the objective of preventing the formation of gas hydrate.

Deposits of natural gas hydrates were first discovered in the Soviet Union in the early 1960's. The most commonly cited global hydrate reserve estimations are those of Trofimuk[4] with $57 \times 10^{12}\,m^3$ of gas in continental hydrates, and $5 - 25 \times 10^{15}\,m^3$ of gas in

subsea hydrates on the ocean floor. The resource of hydrates has the potential of providing a clean energy source for up to 10,000 years[5]. Hydrates have also been considered as a possible solution to the global CO_2 problem. Hydrates have been considered as a possible means of sequestrating CO_2 to help buffer the buildup of the greenhouse gas in the atmosphere.[6] The hydrate formation-dissociation conditions of CH_4, CO_2, and H_2S are different (see Figure 1.1). Therefore, it is thermodynamically possible to replace CH_4 in the natural gas hydrate with CO_2. Gas hydrates have been proposed as a means in mass and energy storage and separation. They have been used successfully in the desalination of seawater[7] and in the separation of light gases. Since 1970, hydrate research has been motivated by production, transport and processing problems in unusual environments, such as on the North Slope of Alaska.

The deep-sea injection of liquid CO_2 from large concentrated sources could provide a means for CO_2 sequestration as a solid clathrate in the deep regions of the ocean at depths greater than 1000 meters. The kinetic limitations are, however, not known and they may be significant. In general, very little is known about the nucleation of hydrates and the kinetics of their formation and dissociation, since these dynamic processes are extremely difficult to study experimentally. Accurate molecular simulations thus should prove to be a key tool in studying these dynamic processes, since they are not restricted by experimental limitations.

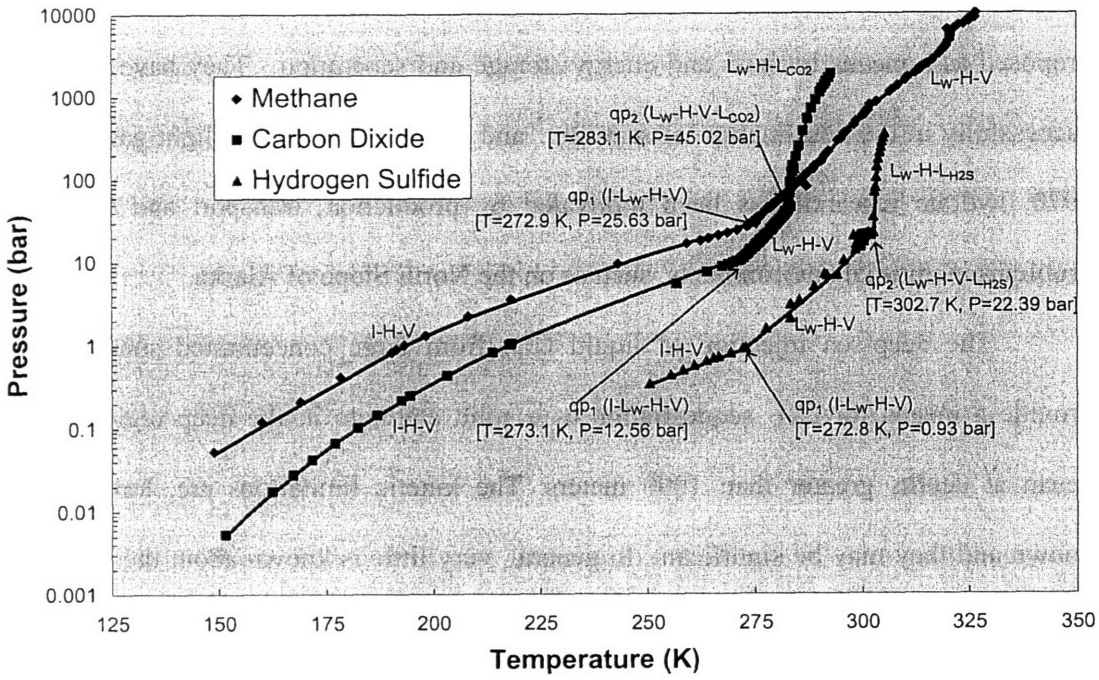

Figure 1.1: Thermodynamic phase diagrams for CH_4, CO_2, and H_2S hydrate clathrates

1.1.3 Experimental measurements of gas hydrates

The methods of obtaining data on the macroscopic properties of natural gas hydrate clathrates have not changed much since the 1930's. The simplest apparatus is often the most elegant and provides reliable simulation of hydrate formation for industrial conditions. Experimentalists typically measure the composition of fluid phases and estimate the composition of the hydrate phase, since measurements of solid hydrates are confounded by experimental difficulties such as fluid occlusion, phase inhomogeneity, non-representative sampling and poor solid sample characterization. Nevertheless, significant improvements in solid phase measurements have been made recently with advances in apparatuses that allow *in situ* diffraction and molecular spectroscopy[8].

In the early stage of experimental work, apparatuses were designed for use above the ice point; requiring a sight glass used to observe the formation and dissociation of gas hydrates[9]. Safety issues increased interest in non-visual means of hydrate detection, especially at high pressures[10]. Apparatuses especially designed for use below the ice point and for two-phase equilibria were also designed for modeling hydrate systems[8].

Compared to PTx_i phase equilibrium measurements, determining other thermal properties of gas hydrates is much more difficult. This is due to the high-pressure decomposition of pre-formed hydrate phases, general hydrate metastability and component entrainment and occlusion. Experimental methods for determining hydrate heat capacity, heat of dissociation and thermal conductivity are detailed by Sloan[8].

The classic method to obtain information on hydrate crystal structures is via X-ray diffraction crystallography. Neutron diffraction studies have the advantage of being able

to determine both the oxygen position and proton placement. However, diffraction methods are problematic because single crystals are required to define hydrate structures, but single hydrate crystals are very difficult to obtain, due to mutual immiscibility and mass transfer effects. Consequently, most diffraction studies were done on powder samples.

With the development of modern analytical tools, three types of spectroscopy have been used to study hydrates. Nuclear Magnetic Resonance (NMR) spectroscopy using ^{129}Xe, ^{13}C or ^{1}H is able to identify the structure and determine relative cage occupation, water reorientation and diffusion[11-13]. Infrared spectroscopy by Bertie and co-workers suggested that the strength of hydrogen bonds in hydrates is very similar to that in ice[14,15]. Recently, Sum et al.[16] used Raman spectroscopy to measure the hydration number and relative cage occupation numbers for pure components and guests. In the future, experimental apparatuses may include a combination of equipment typically used for both macroscopic and microscopic experiments: TPx_i measurements complemented by such techniques as fiber optics Raman spectroscopy[8].

1.2 Clathrate structures

1.2.1 Crystallographic structure

Clathrate hydrates are solids consisting mostly of H_2O molecules, but their structures are different from any of the known forms of ice. To this point three different structures have been identified. Structure I consists of 46 H_2O molecules per unit cell and has 2 12-sided cages (5^{12}, pentagonal dodecahedra) and 6 14-sided cages ($5^{12}6^2$, tetrakaidecahedra)[17]. Structure II has a unit cell of 136 water molecules with 16

pentagonal dodecahedral cages and 8 16-sided cages ($5^{12}6^4$, hexakaidecahedra)[18]. Recently, a new type H structure was found to be composed of 34 water molecules forming 3 cages of 5^{12}, two cages of $4^3 5^6 6^3$ and one cage of $5^{12}6^8$ [19]. The typical guest compounds that form Structure I gas hydrates are methane, ethane, carbon dioxide and cyclopropane (cyclopropane can form both types) while argon, nitrogen, oxygen and cyclopropane form Structure II hydrates. The cavities of structure I and structure II hydrates are shown in Figure 1.2 and Figure 1.3.

The structure I unit cell has a lattice constant of 12.0 Å and is shown in Figure 1.4. The structure II unit cell shown in Figure 1.5 has a lattice constant of 17.3 Å and consists of 136 water molecules that form 16 pentagonal dodecahedral cavities (cell A) and 8 hexakaidecahedral cavities (cell B). Thus for a completely occupied structure II system, the ideal stoichiometry would be (16A, 8B)·136 H_2O. The structure I ideal stoichiometry would be (2A, 6B)·46 H_2O.

For decades, it was believed that small molecules, particularly those smaller than propane formed only structure I clathrates. More recently, crystallographic measurements[1,20,21] have shown that Ar, Kr, N_2, and O_2 can form structure II clathrates. For the argon-water clathrate, both cells A and B can be occupied by argon molecules, so the fully occupied stoichiometry becomes 24 Ar·136 H_2O or Ar·5 $^2/_3$ H_2O.

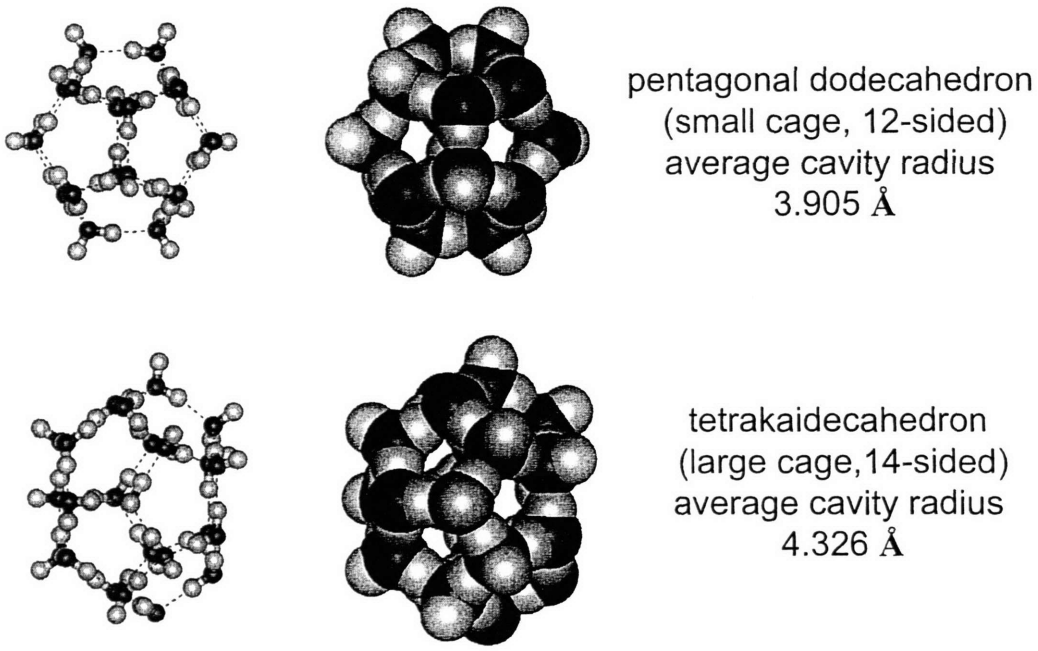

Figure 1.2: Cavities of structure I clathrates

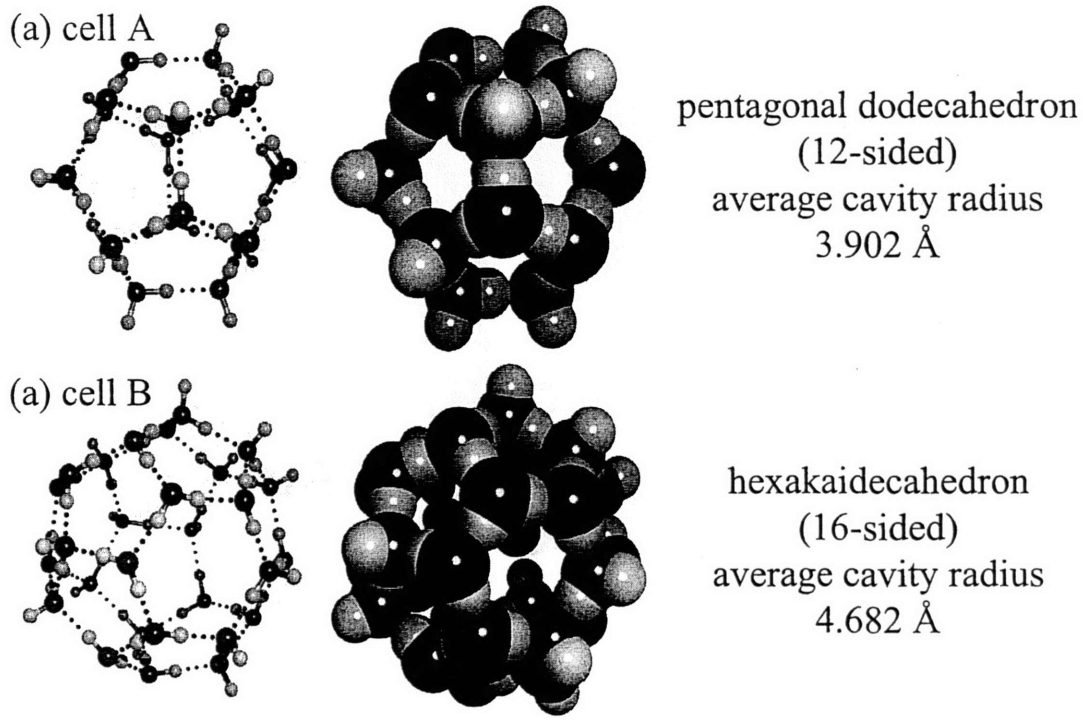

Figure 1.3: Cavities of structure II clathrates

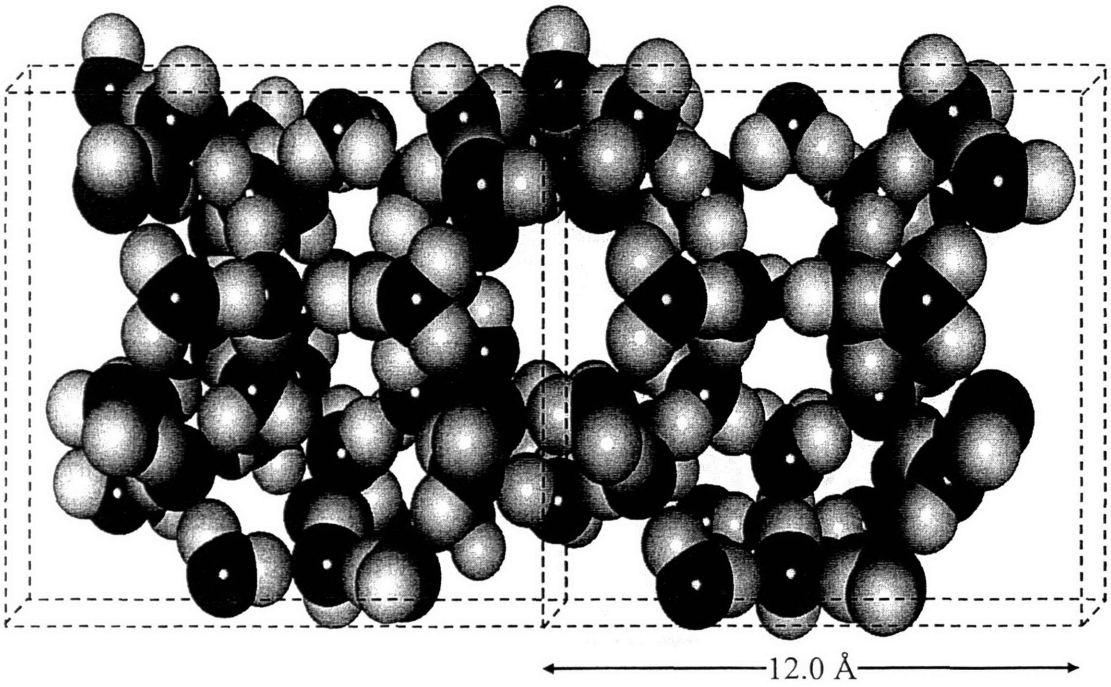

Figure 1.4: Space filling model of the structure I clathrate

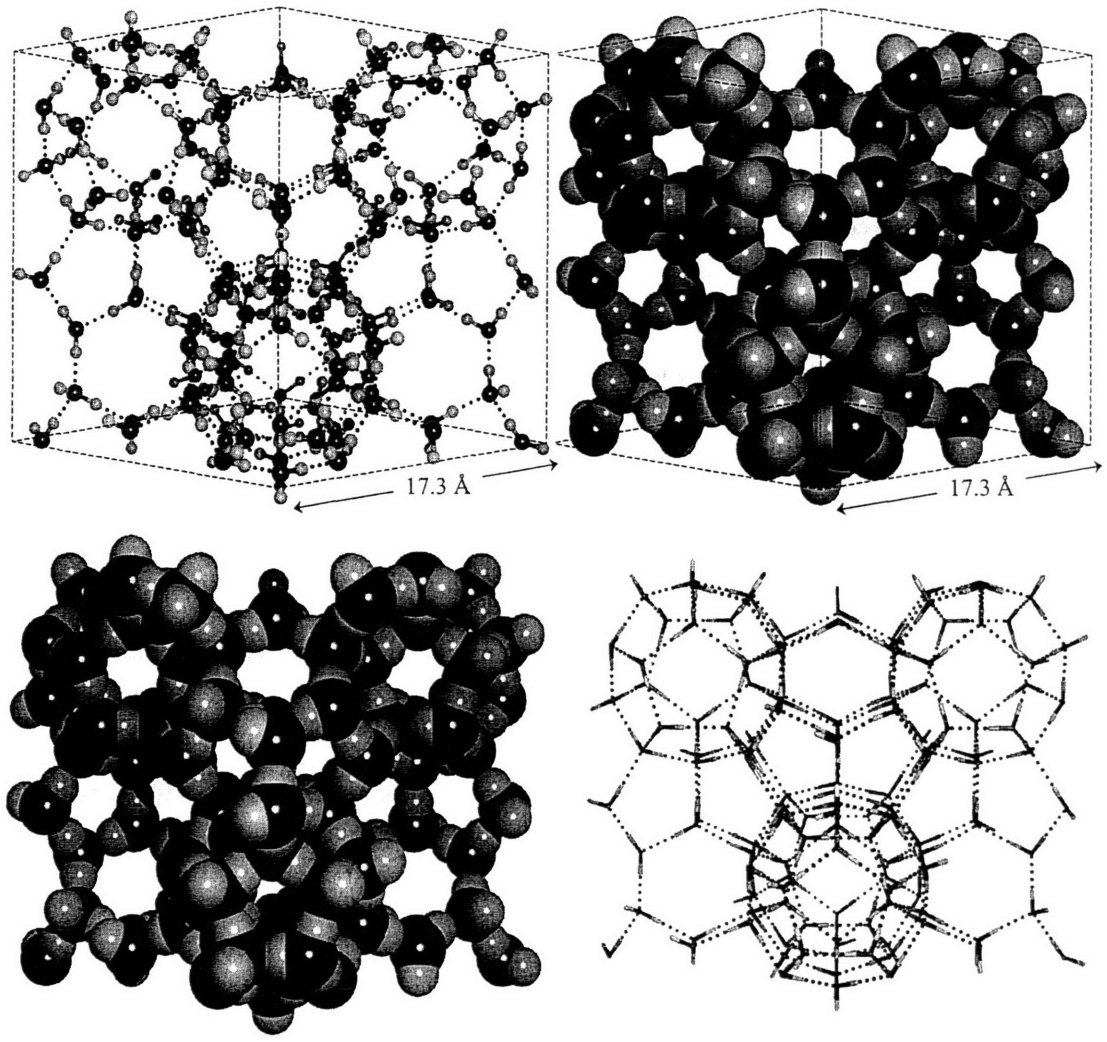

Figure 1.5: Ball and stick and space filling models of the structure II clathrate

1.2.2 Lattice structure used in this study

X-ray diffraction techniques[17,18] were used to determine the structural aspect of water clathrates, and neutron scattering techniques[22] were also used to further refine the crystalline structure determined in the X-ray studies. In this work, the fractional positional parameter reported by McMullan and Jeffery[17] and Mark and McMullan[18] were selected to represent the oxygen positions within structure I and II water clathrates.

1.2.3 Proton placement

In order to understand the configurational characteristics of guest-host intermolecular interactions, the water proton distribution that forms the clathrate cages must be known. Unfortunately, it is extremely difficult to measure the positions of protons directly from conventional diffraction type studies. Conforming to Bernal-Fowler Rules[23] and the constraint that the net dipole of the whole system should be zero, an algorithm was constructed to generate randomly nearly half a million configurations with the desired water geometry[24], and the resulting configuration with the lowest net dipole moment was then selected as a valid proton assignment. Either the experimentally determined structure of water molecules ($r_{OH} = 0.9572\text{Å}, \angle HOH = 104.52°$) or the simple point charge (SPC) model of water ($r_{OH} = 1.0\text{Å}, \angle HOH = 109.47°$) as proposed by Berendson et al.[25] can be used as a desired geometry of water. The Bernal-Fowler Rules[23], further refined by Rahman and Stillinger[26], are outlined below:

(a) The water clathrate host lattice consists of non-dissociated water molecules.

(b) The oxygens form the host lattice with nearly tetrahedral coordination.

(c) Each hydrogen bond between two neighboring oxygens is composed of a single proton covalently bonded to one oxygen and hydrogen bonded to the other.

(d) All proton configurations satisfying the above conditions are equally probable.

1.3 Overview of previous theoretical work to model gas hydrates

1.3.1 Hydrate phase chemical potential

A thermodynamic model corresponding to the three dimensional generalization of ideal localized adsorption was proposed by van der Waals and Platteeuw[27]. This model is based on the following four assumptions:

1. Cage distortions can be neglected.
2. Each cage can be occupied by, at most, one guest molecules.
3. Guest-guest interactions can be neglected.
4. Classical statistics are valid.

The van der Waals and Platteeuw model has been widely used in various applications of gas hydrate systems, since it provides a bridge between the molecular interactions that stabilize crystal structures and the macroscopic thermodynamic properties. A key term in the van der Waals and Platteeuw model is the Langmuir constant. The Langmuir constant is related to the configurational intermolecular interaction between the guest gas molecule and all surrounding host water molecules.

Significant efforts to relate the Langmuir constant to guest-host potential parameters have been made. In their original work, van der Waals and Platteeuw[27] assumed that guest-host interactions can be represented by a guest molecule at a distance r from the cavity center in a spherically symmetrical potential $\Phi(r)$ induced by the water

hosts. This approximation is comparable to that made by Lennard-Jones and Devonshire[28,29], which is referred to as the LJD approximation in this work. A systematic approach to extended to multi-component hydrate guest mixtures was made by Parrish and Prausnitz[30]. With a spherical core Kihara-type potential function to provide an analytical form of the potential used to compute the Langmuir constant, this method gained wide acceptance and has been used in modified forms[31].

However, predictions based on the LJD approximation were still far from satisfactory as shown by several studies[32-34]. Two of the main reasons for the errors are cavity asymmetry and multi-shell water host effects. John and Holder[35] studied the choice of the cell size in the LJD cell theory and provided optimal cell sizes and water coordination numbers for different cavities. However, these parameters are not consistent with the crystallographic structure of clathrate hydrates and are merely additional adjustable parameters to which experimental data is fitted. They then proposed a further modification – to use the addition of terms to account for the contribution of second and subsequent water shells to the potential energy of the guest-host interactions[36]. Subsequently, John and Holder used the crystallographic locations of the host water molecules and binary guest-host Kihara type interactions and carried out more precise calculations of the Langmuir constants[37]. They compared the results to those obtained using the LJD approach. Based on previous studies, John and Holder proposed to use an aspherical correction to account for all nonidealities in the molecular interactions between the encaged gas and the hydrate cavity in their generalized model for predicting equilibrium conditions for gas hydrates[38].

Most recently, Bazant and Trout[39] proposed a novel method to evaluate the Langmuir constant. The spherical-cell statistical formula for the Langmuir constant versus temperature can be viewed as a nonlinear integral equation for the cell potential, and exact potential forms can be found as solutions to this integral equation. A variety of exact analytical solutions were derived in the study, with a significant conclusion being that very simple polynomial forms of the potential, such as quadratic or cubic, can be used to describe the data extremely well. More details regarding the derivation, use, and application of this cell potential method is found in Chapter 4.

A few studies were performed which avoided the use of the LJD approximation for calculating the corresponding configurational integral[40,41]. Work by Sparks and Tester[42] presented a rigorous treatment of multiple water shells and guest-guest potential energy effects in water clathrates, where a modified lattice sum approach was used to characterize the quantitative extent of these effects on the configurational partition function and the three-dimensional Langmuir constant. The results for both sI and sII hydrates confirmed the results of a previous study[36], that subsequent water shell interactions do indeed have a significant effect on the value of Langmuir constants. The spherical LJD approximation was avoided in Sparks' dissertation[24] and the work by Cao, et al.[43-45], where the Langmuir constant was evaluated numerically as a six-dimensional integral based purely on crystallographic data.

1.3.2 Guest–host potential energy functions

The intermolecular potential energy functions used in Owichi and Scheraga[46] and Swaminathan's[47] studies were based on *ab initio* calculations employed in MC studies of methane in aqueous solutions. In their study, up to 256 configurations were generated by

independent random positional and orientational operations of water molecules with respect to methane, with a center of mass separation of no more than 5.5 Å. The calculated potential energy surface was then used to obtain the best least-squares fit by adjusting the parameters of an empirical, distance-based potential function.

In order to accurately evaluate the CH_4-OH_2 contact interaction energy, Novoa et al.[48] performed *ab initio* calculations on methane-water at the self-consistent-field molecular orbital (SCF-MO) and MP2 levels with various quality basis sets including one near Hartree-Fock limit (HFL) case. They employed diffuse functions in the basis set and used the counterpoise (CP) method to reduce the deviation caused by basis set superposition error (BSSE). The predicted interaction energy with the near HFL basis set was 0.59±0.05 kcal/mol corresponding to the minimum-energy structure with C-H···O contact. MP2/6-31++G(2d,2p) was thus chosen as the main method and basis set in Novoa's later work[49]. The potential energy surfaces of the water···hydrocarbon complexes H_2O···CH_4, H_2O···C_2H_4 and H_2O···C_2H_2 were examined to locate several minimum energy structures and estimate the hydrogen bond energies and the corresponding vibrational frequencies.

Szczesniak et. al.[50] explored more configurations between methane and water using the fourth-order Moller-Plesset perturbation theory with the well-tempered basis set 6-31++G(2d,2p). The absolute minimum occurs at the new configuration involving the C···H-O hydrogen-bond with a bond energy of 0.83±0.05 kcal/mol.

Novoa[51] continued to perform a numerical test of evaluating interaction energy using near complete basis sets on H_2O···HF and CH_4···H_2O at the MP2 level. It was suggested that CP method provides reasonable interaction energies when the basis set is

flexible enough. The qualified adequate basis sets consist of NHFL(4d3f,4p3d) and 6-31++G(4d3f,4p3d).

Cao et al.[52] recently computed the methane-water potential energy hypersurface and demonstrated the ability of this *ab initio* potential to accurately predict methane hydrate dissociation pressures across a large range of temperatures[53]. They used the MP2 method with a 6-31++G(2d,2p) basis set, corrected to the cc-pVQZ basis set level. They were able to reach accuracies of < 0.1 kcal/mol with 18,000 calculations at the 6-31++G(2d,2p) level and 100 calculations at the cc-pVQZ level.

In addition, recent work by Klauda and Sandler[54] showed that many-body interactions should be accounted for when applying computed potentials to the hydrate clathrate system. Proper determination of the form of the intermolecular interaction potential is also necessary both to compute equilibrium thermodynamic properties and to perform dynamic molecular simulations of kinetic phenomena such as diffusion and hydrate crystal nucleation, growth, and decomposition.

1.4 Inhibition of Hydrate Formation

The prevention of hydrate formation is a major research focus area for pipeline transport. Typically, large amounts (up to 50 vol %) of methanol are used to help avoid hydrate plugging by lowering the formation temperature, with economic and potential environmental ramifications. In the last 15 years or so, many research efforts have been focused on developing what are termed "low-dosage hydrate inhibitors", or LDHIs, that can kinetically inhibit hydrate formation.[55]

There has been much discussion and disagreement regarding the mechanism by which LDHIs inhibit hydrate formation[56-61]. Furthermore, no proposed mechanism fully

explains all of the phenomena associated with hydrate kinetic inhibition such as increased induction time with sudden growth coupled with the crystal morphology changes observed in inhibited growth conditions.[59,62-64]

1.5 Thesis Objectives and Approach

The overall goal of this thesis is to better understand hydrate processes, namely hydrate phase equilibrium and mechanisms of inhibition, at a molecular level through the use of quantum chemical, statistical mechanical, and molecular dynamic approaches. Specifically, this thesis seeks to:

- Perform *ab initio* quantum mechanical calculations to determine guest-host interaction energies
- Develop accurate intermolecular interaction potentials from *ab initio* calculations
- Determine an accurate and efficient method to calculate the potential energy surface considering the fineness of the intermolecular orientation grid as well as other factors, such as many-body effects, correlation dependencies, and basis set convergence
- Determine with a low degree of uncertainty reference parameters for both structure I and structure II for use in the van der Waals and Platteeuw model for hydrate clathrate systems
- Validate both the determined potential energy surfaces and the van der Waals and Platteeuw model by predicting the cage occupancies for the methane hydrate system and then used to calculate pure argon hydrate

phase behavior and predict the phase behavior of the argon-methane mixed hydrate system.

- Further validate the methane-water potential for molecular dynamic simulations
- Identify the molecular factors favoring/controlling the interaction of inhibition molecules with the surface of hydrates
- Gain insight into molecular parameters and inhibitor properties that can be used to control hydrate nucleation or crystal growth and the tendency of hydrate solids to agglomerate

1.6 References

(1) Davy, H. *Phil. Trans. Roy. Soc. London* **1811**, *101*, 1.
(2) Priestley, J. *Experiments and observations on different kinds of air, and other branches of natural pholosophy, connected with the subject*; Thomas Perrson: Birmingham, 1790; Vol. 2.
(3) Hammerschmidt, E. G. *Ind. Eng. Chem.* **1934**, *26*, 851.
(4) Trofimuk, A. A.; Makogon, Y. F.; Tolkachev, M. V. *Geologiya nefti i Gaza* **1981**, *10*, 15.
(5) Holder, G. D.; John, V. T.; Yen, S. "Geological implications of gas production from In-situ gas hydrates"; SPE/DOE symposium on unconventional gas recovery, 1980.
(6) Warzinski, R. P.; Lynn, R. J.; Holder, G. D. *Annals of the New York Academy of Sciences* **2000**, *912*, 226.
(7) Barduhn, A. J.; Towlson, H. E.; Ho, Y. C. *AIChE J* **1962**, *8*, 176.
(8) Sloan, E. D., Jr. *Clathrate hydrates of natural gases - 2nd ed., rev. and expanded*; Marcel Dekker, Inc.: Monticello, 1998.
(9) Deaton, W. M.; Frost, E. M. *Gas hydrates and their relation to the operation of natural-gas pipe lines*, 1946.
(10) Galloway, T. J.; Ruska, W.; Chappelear, P. S.; Kobayashi, R. *Industrial & Engineering Chemistry Fundamentals* **1970**, *9*, 237.
(11) Davidson, d. W.; Gough, S. R.; Ripmeester, J. A.; Nakayama, H. *Can. J. Chem.* **1981**, *59*, 2587.
(12) Ripmeester, J. A.; Ratcliffe, C. I.; Tse, J. S. *J. Chem. soc Faraday Trans.* **1988**, *84*, 3731.
(13) Ripmeester, J. A.; Ratcliffe, C. A.; Klug, D. D.; Tse, J. S. *Annals of New York Academy of Sciences*, 1994.
(14) Bertie, J. E.; Bates, F. E.; Hendricksen, D. K. *Can. J. Chem.* **1975**, *53*, 71.
(15) Bertie, J. E.; Jacobs, S. M. *J. Chem. Phys.* **1978**, *69*, 4105.
(16) Sum, A. K.; Burruss, R. C.; Sloan, E. D. *Journal of Physical Chemistry B* **1997**, *101*, 7371.
(17) McMullan, R. K.; Jeffrey, G. A. *J. Chem. Phys.* **1965**, *42*, 2725.
(18) Mark, T. C. W.; McMullan, R. K. *J. Chem. Phys.* **1965**, *42*, 2732.
(19) Ripmeester, J. A.; Tse, J. S.; Ratcliffe, C. I.; Powell, B. M. *Nature* **1987**, *352*, 135.
(20) Davidson, D. W.; Garg, S. K.; Gough, S. R.; Handa, Y. P.; Ratcliffe, C. I.; Ripmeester, J. A. *J. Inclusion Phenomena* **1984**, *2*, 231.
(21) Tse, J. S.; Handa, Y. P.; Ratcliffe, C. I.; Powell, B. M. *J. Inclusion Phenomena* **1986**, *4*, 235.
(22) Hollander, F.; Jeffrey, G. A. *J. Chem. Phys.* **1977**, *66*, 4699.
(23) Bernal, J. D.; Fowler, R. H. *J. Chem. Phys.* **1933**, *1*, 515.
(24) Sparks, K. A. Configurational properties of water clathrates through molecular simulation, PhD Thesis, Massachusetts Institute of Technology, 1991.
(25) Berendsen, H. J. C.; Postma, J. P. M.; Van Gunsteren, W. F.; Hermans, J. *Interaction Models for Water in Relation to Protein Hydration.*Reidel, Dordrecht, 1981.

(26) Rahman, A.; Stillinger, F. H. *J. Chem. Phys.* **1972**, *57*, 4009.
(27) van der Waals, J. H.; Platteeuw, J. C. *Adv. Chem. Phys.* **1959**, *2*, 1.
(28) Lennard-Jones, J. E.; Devonshire, A. F. *Proc. Roy Soc.* **1932**, *A163*, 53.
(29) Lennard-Jones, J. E.; Devonshire, A. F. *Proc. Roy. Soc.* **1938**, *165*, 1.
(30) Parrish, W. R.; Prausnitz, J. M. *Industrial & Engineering Chemistry Process Design and Development* **1972**, *11*, 26.
(31) Anderson, F. E.; Prausnitz, J. M. *AIChE J.* **1986**, *32*, 1321.
(32) Ng, H. J.; Robinson, D. B. *Industrial & Engineering Chemistry Fundamentals* **1976**, *15*, 293.
(33) Ng, H.-J.; Robinson, D. B. *AIChE J.* **1977**, *23*, 477.
(34) Schroeter, J. P.; Kobayashi, R.; Hildebrand, M. A. *Ind. Eng. Chem. Fundam.* **1983**, *22*, 361.
(35) John, V. T.; Holder, G. D. *J. Phys. Chem.* **1981**, *85*, 1811.
(36) John, V. T.; Holder, G. D. *J. Phys. Chem.* **1982**, *86*, 455.
(37) John, V. T.; Holder, G. D. *J. Phys. Chem.* **1985**, *89*, 3279.
(38) John, V. T.; Papadopoulos, K. D.; Holder, G. D. *AIChE J* **1985**, *31*, 252.
(39) Bazant, M. Z.; Trout, B. L. *Physica A* **2001**, *300*, 139.
(40) Tester, J. W.; Bivins, R. L.; Herrick, C. C. *AIChE J* **1972**, *18*, 1220.
(41) Tse, J. S.; Davidson, D. W. "Intermolecular potentials in gas hydrates"; Proc. 4th canadian permafrost conf., 1982.
(42) Sparks, K. A.; Tester, J. W. *Journal of Physical Chemistry* **1992**, *96*, 11022.
(43) Cao, Z. T.; Tester, J. W.; Sparks, K. A.; Trout, B. L. *J. Phys. Chem. B.* **2001**, *105*, 10950.
(44) Cao, Z. T.; Tester, J. W.; Trout, B. L. *Journal of Physical Chemistry B* **2002**, *106*, 7681.
(45) Cao, Z. Modeling of Gas Hydrates from First Principles, PhD Thesis, Massachusetts Institute of Technology, 2002.
(46) Owicki, J. C.; Scheraga, H. A. *J. Am. Chem. Soc.* **1977**, *99*, 7413.
(47) Swaminathan, S.; Harrison, S. W.; Beveridge, D. L. *J. Am. Chem. Soc.* **1978**, *100*, 5705.
(48) Novoa, J. J.; Tarron, B.; Whangbo, M.-H.; Williams, J. M. *J. Chem. Phys.* **1991**, *95*, 5179.
(49) Rovira, M. C.; Novoa, J. J.; Whangbo, M.-H.; Williams, J. M. *Chemical Physics* **1995**, *200*, 319.
(50) Szczesniak, M. M.; Chalasinski, G.; Cybulski, S. M.; Cieplak, P. *J. Chem. Phys.* **1993**, *98*, 3078.
(51) Novoa, J. J.; Planas, M.; Rovira, M. C. *Chem. Phys. Lett.* **1996**, *251*, 33.
(52) Cao, Z.; Tester, J. W.; Trout, B. L. *J. Chem. Phys.* **2001**, *115*, 2550.
(53) Cao, Z.; Tester, J. W.; Sparks, K. A.; Trout, B. L. *J. Phys. Chem. B* **2001**, *105*, 10950.
(54) Klauda, J. B.; Sandler, S. I. *Journal of Physical Chemistry B* **2002**, *106*, 5722.
(55) Lederhos, J. P.; Long, J. P.; Sum, A.; Christiansen, R. L.; Sloan, E. D. *Chemical Engineering Science* **1996**, *51*, 1221.
(56) Koh, C. A.; Westacott, R. E.; Zhang, W.; Hirachand, K.; Creek, J. L.; Soper, A. K. *Fluid Phase Equilibria* **2002**, *194*, 143.

(57) Storr, M. T.; Rodger, P. M. A molecular dynamics study of the mechanism of kinetic inhibition. In *Gas Hydrates: Challenges for the Future*; NEW YORK ACAD SCIENCES: New York, 2000; Vol. 912; pp 669.
(58) Makogon, T. Y.; E. Dendy Sloan, J. "Mechanism of Kinetic Hydrate Inhibitors"; Fourth International Conference on Gas Hydrates, 2002, Yokohama, Japan.
(59) Storr, M. T.; Taylor, P. C.; Monfort, J. P.; Rodger, P. M. *Journal of the American Chemical Society* **2004**, *126*, 1569.
(60) Zeng, H.; Wilson, L. D.; Walker, V. K.; Ripmeester, J. A. *Canadian Journal of Physics* **2003**, *81*, 17.
(61) Hutter, J. L.; King, H. E.; Lin, M. Y. *Macromolecules* **2000**, *33*, 2670.
(62) Makogon, T. Y.; Larsen, R.; Knight, C. A.; Sloan, E. D. *Journal of Crystal Growth* **1997**, *179*, 258.
(63) Larsen, R.; Knight, C. A.; Sloan, E. D. *Fluid Phase Equilibria* **1998**, *151*, 353.
(64) Sakaguchi, H.; Ohmura, R.; Mori, Y. H. *Journal of Crystal Growth* **2003**, *247*, 631.

Chapter 2. Theoretical Background

2.1 Overview of the statistical mechanical model

A thermodynamic model corresponding to the three dimensional generalization of ideal localized adsorption was proposed by van der Waals and Platteeuw[1]. This model is based on the following four assumptions:

1. Cage distortions can be neglected.
2. Each cage can be occupied by, at most, one guest molecules.
3. Guest-guest interactions can be neglected.
4. Classical statistics are valid.

The difference in chemical potential between clathrate and empty host lattice can then be expressed as

$$\Delta\mu^{\beta-H} = kT\sum_i \nu_i \ln(1+\sum_J C_{Ji}\hat{f}_J) \tag{2.1}$$

where ν_i is the number of type i cavities per water molecule, $\hat{f}_J$ is the fugacity of guest molecule J which is usually calculated from Peng-Robinson equation of state[2], and C_{Ji} is the Langmuir constant defined as

$$C_{Ji} \equiv \frac{Z_{Ji}}{kT} \tag{2.2}$$

where Z_{Ji} is the configurational integral, which depends on the interaction potential between guest and host molecules. Since the structure I unit cell has 2 small cavities, 6 large cavities, and 46 water molecules, the complete expression for a pure component Structure I (sI) water clathrate system is

$$\frac{\Delta\mu_w^{\beta-H}}{kT} = \frac{1}{23}\ln(1+C_{J1}\hat{f}_J) + \frac{3}{23}\ln(1+C_{J2}\hat{f}_J) \tag{2.3}$$

while since the structure II (sII) unit cell has 16 small cavities, 8 large cavities, and 136 water molecules,, the equivalent expression for sII is

$$\frac{\Delta\mu_w^{\beta-H}}{kT} = \frac{2}{17}\ln(1+C_{J1}\hat{f}_J) + \frac{1}{17}\ln(1+C_{J2}\hat{f}_J) \tag{2.4}$$

Clathrate hydrates can be thought of as non-stoichiometric compounds. Therefore the probability of finding a guest molecule of type J in a type i cavity, usually referred to as cage occupancy y_{Ji}, is ≤ 1.0 and a function of equilibrium conditions. Mathematically, the cage occupancy y_{Ji} is related to the Langmuir constants as follows:

$$y_{Ji} = \frac{C_{Ji}\hat{f}_J}{1+\sum_J C_{Ji}\hat{f}_J} \tag{2.5}$$

As a result, the vdWP statistical model can also be expressed in terms of the cage occupancies as

$$\Delta\mu_w^{\beta-H} = -kT\sum_i \nu_i \ln(1-\sum_J y_{Ji}) \tag{2.6}$$

2.2 Thermodynamic analysis of phase equilibria

2.2.1 Phase equilibria

With this thermodynamic model, we can consider clathrate as a two-component system. Thus the phase equilibrium of clathrate hydrates can be described by

$$\begin{aligned} \mu_w^H &= \mu_w^{L,\alpha} \\ \mu_w^\beta - \mu_w^H &= \mu_w^\beta - \mu_w^{L,\alpha} \\ \mu_w^{\beta-H} &= \Delta\mu_w^{\beta-L,\alpha} \end{aligned} \tag{2.7}$$

where μ_w^{β} is the chemical potential hypothetical empty hydrate lattice with no cages occupied by guest molecules, μ_w^{H} is the chemical potential of water in the hydrate phase, and μ_w^{α} or μ_w^{L} is the chemical potential of water in the solid ice phase or liquid aqueous phase depending on whether the temperature is below 273.15 K or not. Following the convention proposed by Holder[3], the chemical potential difference between water in the hypothetical empty lattice and the water in the hydrate phase can be expressed as

$$\frac{\Delta\mu_w^{\beta-L,\alpha}(T,P)}{kT} = \frac{\Delta\mu_w^{\beta-L,\alpha}(T_0,0)}{kT_0} - \int_{T_0}^{T}[\frac{\Delta H_w^{\beta-L,\alpha}}{kT^2}]_P dT + \int_0^P[\frac{\Delta V_w^{\beta-L,\alpha}}{kT}]_T dP - \ln a_w^L \quad (2.8)$$

where $\Delta\mu_w^{\beta-L,\alpha}(T_0,0)$ is the reference chemical potential difference at the reference temperature, T_0, and zero pressure. The temperature dependence of the enthalpy difference is given by

$$\Delta H_w^{\beta-L,\alpha} = \Delta H_w^{\beta-L,\alpha}(T_0) + \int_{T_0}^{T} \Delta C_p^{\beta-L,\alpha} dT \quad (2.9)$$

where the heat capacity difference is approximated by

$$\Delta C_{p_w}^{\beta-L,\alpha} = \Delta C_{p_w}^{\beta-L,\alpha}(T_0) + b^{\beta-L,\alpha}(T-T_0) \quad (2.10)$$

where $b^{\beta-L,\alpha}$ is the constant representing the dependence of heat capacity on the temperature. The volume difference is assumed to be constant. The additional term involving the activity of water, a_w^L, is defined by

$$a_w^L = \frac{\hat{f}_w^L}{\hat{f}_w^+} \quad (2.11)$$

where $\hat{f}_w^L$ is the fugacity of water in the water-rich aqueous phase and $\hat{f}_w^+$ is the water fugacity in the reference state, which is chosen to be f_w, the pure water phase. T_0, the

reference temperature, is usually taken to be 273.15 K. Reference parameters found in the literature are given in Table 2.1 and values used in this work are found in Table 2.2.

Table 2.1: Thermodynamic reference properties for Structure I and II water clathrates[4]

Structure I (J/mol)		Structure II (J/mol)		Source[a]
$\Delta\mu^{\beta-L,\alpha}(T_0,0)$	$\Delta H^{\beta-L,\alpha}(T_0,0)$	$\Delta\mu^{\beta-L,\alpha}(T_0,0)$	$\Delta H^{\beta-L,\alpha}(T_0,0)$	
699	0	820	0	van der Waals and Platteeuw (1959)
-	-	366-537	-	Barrer and Ruzicka (1962)
-	-	833	-	Sortland and Robinson (1964)
1255.2	753	795	837	Child (1964)
1264	1150	-	808	Parrish and Prausnitz (1972)
1155	381	-	0	Holder (1976)
1297	1389	937	1025	Dharmawardhana, Parrish and Sloan (1980)
1299	1861	-	-	Holder, Malekar, and Sloan (1984)
1120	931	1714	1400	John, Papadopoulos, and Holder (1985)
1297	-	-	-	Davidson, Handa, and Ripmeester (1986)
1287	931	1068	764	Handa and Tse (1986)
1236	1703	-	-	Cao, Tester, and Trout (2002)

[a]Ref 1,5-15

Table 2.2: Thermodynamic reference properties for structure I and II hydrates: T_0 = 273.15 K

	structure I	structure II	source
$\Delta\mu_w^0$ (J/mol)[a]	1203	1077	16
ΔH_w^0 (J/mol)	1170	1294	16
$\Delta V_w^{\beta-\alpha}$ ($m^3 \cdot mol^{-1}$)	3.0×10^{-6}	3.4×10^{-6}	17
$\Delta H_w^{L-\alpha}$ (J/mol)	6009.5		
$\Delta V_w^{L-\alpha}$ ($m^3 \cdot mol^{-1}$)	-1.598×10^{-6}		
$\Delta C_p^{\beta-L}$ (J/mol·K)	$-37.32 + 0.179(T - T_0)$		3
$\Delta C_p^{\beta-\alpha}$ (J/mol·K)	$0.565 + 0.002(T - T_0)$		3

[a]superscripts/subscripts
w = water
^{0} = reference state
β = empty hydrate lattice
α = ice phase
L = liquid phase

2.3 Configurational partition function

In the thermodynamic model, Equations (2.1) and (2.7), $\mu^{\beta-L,\alpha}$ can be determined from experimental data and $\hat{f}_J$ from an equation of state. Next, the Langmuir constant must be obtained. For a guest molecule J in a cavity of type i, C_{Ji} is directly related to the six-dimensional configurational integral defined by

$$Z_{Ji} \equiv \frac{1}{8\pi^2} \int_V \exp(-\Phi(r,\theta,\phi,\alpha,\beta,\gamma)/kT) r^2 \sin\theta dr d\theta d\phi d\alpha d\beta d\gamma \qquad (2.12)$$

where Z_{Ji} is the full configurational integral, which depends on the total interaction potential $\Phi = \sum_{ij} \Phi_{ij}$ between guest and host molecules[18,19] and is, in general, a function of r, θ, and ϕ, the spherical coordinates of the guest molecule, and α, β, and γ, the Euler angles that describe the orientation of the guest. In order to calculate the configurational integral accurately, the total interaction potential between the guest molecule and all of the host water molecules must be represented properly. In early work the potential was approximated by a two-parameter spherically symmetric Lennard-Jones potential[1]. Later, a Kihara potential, with three parameters, was used to improve accuracy. However, these empirically fitted potentials are not fundamentally based on the guest-host interactions, have been shown to be aphysical, and do not match those determined using gas-phase experimental data[4,12,20].

2.3.1 LJD approximation

Since analytical integration of Equation (2.12) is intractable given the asymmetries of the host-guest potential, several approximations have been applied. Most

commonly, the LJD cell model is used to simplify the 6-dimensional integration to one-dimensional. The potential is averaged and uniformly distributed on a single spherical surface for each cage that is located at the average radius of that cavity. The guest molecule is also usually assumed to be spherically symmetric (Φ independent of α, β, γ). The averaging in this case is over both spherical angles (θ and ϕ) and effectively smoothes the potential function $\Phi_{Ji}(r, \theta, \phi)$ to a dependence on radial distance only[21]. The LJD approximation thus expresses the Langmuir constant as a one-dimensional integral,

$$C_{Ji}(\text{LJD}) \equiv C^* = \frac{4\pi}{kT}\int e^{-\langle W(r)\rangle / kT} r^2\, dr \tag{2.13}$$

where the integration is carried out over the cavity radius and $\langle W(r\rangle = \langle \Phi_{Ji}(r,\theta,\phi)\rangle_{\text{LJD}}$ is the angle-averaged, spherically symmetric cell potential defined at each r by

$$\langle W(r)\rangle = \frac{1}{4\pi}\int_0^{2\pi}\int_0^{\pi} \Phi_{Ji}(r,\theta,\phi)\sin\theta\, d\theta\, d\phi \tag{2.14}$$

The actual choice of the guest-host intermolecular interaction potential is a point of great concern and therefore discussed in Section 2.3.3. To illustrate the use of the LJD model, we give the spherically averaged LJD form of $\langle W(r)\rangle$ in Equation (2.15) when the Kihara potential (see Equation (2.22)) is chosen to represent guest-host interactions[22].

$$\langle W(r)\rangle = 2z_{c,i}\varepsilon\left[\frac{\sigma^{12}}{R_i^{11}r}\left(\delta^{10} + \frac{a}{R_i}\delta^{11}\right) - \frac{\sigma^{6}}{R_i^{5}r}\left(\delta^{4} + \frac{a}{R_i}\delta^{5}\right)\right] \tag{2.15}$$

where

$$\delta^N = \frac{1}{N}\left[\left(1 - \frac{r}{R_i} - \frac{a}{R_i}\right)^{-N} - \left(1 + \frac{r}{R_i} - \frac{a}{R_i}\right)^{-N}\right] \tag{2.16}$$

where $z_{c,i}$ = coordination number of cavity i, R_i = effective cavity i radius, a = core radius of interaction, σ = the distance between molecular cores at which there is no interaction, and ε = the depth of the intermolecular potential well.

2.3.2 Integration methods

In order to calculate the configurational integral correctly, the total interaction potential between the guest molecule and all of the host water molecules must be represented properly. Early work was done by approximating the potential with a two-parameter spherical symmetric Lennard-Jones potential. Later, a Kihara potential, with three parameters, was used to improve accuracy. More recent studies showed that the spherical approximation can lead to large deviation because it did not consider the asymmetry of the cages[22,23]. The asymmetry of the cages can be taken into account by computing this integral via quadrature or by using MC method. Previous work was done by Sparks et al.[24] using 10-point multi-interval Gauss-Legendre quardrature formula (n=10)[25]

$$\int_a^b f(x)dx = \int_a^{b/n} f(x)dx + \int_{b/n}^{2b/n} f(x)dx + \cdots + \int_{(n-1)b/n}^{b} f(x)dx \tag{2.17}$$

2.3.3 Choice of intermolecular potential

Generally, the total interaction potential between each guest molecule i and all host molecules is modeled as the sum of two-body potentials

$$\Phi(r,\theta,\phi,\alpha,\beta,\gamma) = \sum_{j=1}^{N} \Phi_{ij}(r_{ij},\theta,\phi,\alpha,\beta,\gamma) \tag{2.18}$$

where the sum is over all the N interacting host water molecules.

Van der Waals and Platteeuw chose to model the guest-host interaction using the Lennard-Jones (6-12) interaction potential with the Lennard-Jones Devonshire (LJD) spherical cell approximation. The LJD spherical cell approach simplifies the integration considerably to a one-dimensional integral in *r*:

$$C_{Ji} = \frac{4\pi}{kT}\int e^{-W(r)/kT} r^2 dr \tag{2.19}$$

where the spherically symmetric cell potential, *W(r)*, is determined from

$$W(r) = \frac{1}{4\pi}\int_0^{2\pi}\int_0^{\pi}\Phi_{ij}(r_{ij},\theta,\phi)\sin\theta d\theta d\phi \tag{2.20}$$

For the Lennard-Jones (6-12) potential is

$$\Phi_{ij}^{LJ}(r) = 4\varepsilon\left[\left(\frac{\sigma}{r_{ij}}\right)^{12} - \left(\frac{\sigma}{r_{ij}}\right)^{6}\right] \tag{2.21}$$

This works reasonably well for small guest molecules such as argon[1], but large discrepancies exists for the more complex and larger molecules such as ethane and cyclopropane. To reduce errors, the Kihara potential was used with Lennard-Jones Devonshire (LJD) spherical cell approximation. The form of the Kihara potential[26] is

$$\begin{aligned}\Phi_{ij}^{K}(r) &= \infty \qquad\qquad r \le 2a \\ \Phi_{ij}^{K}(r) &= 4\varepsilon\left[\left(\frac{\sigma-2a}{r_{ij}-2a}\right)^{12} - \left(\frac{\sigma-2a}{r_{ij}-2a}\right)^{6}\right] \quad r > 2a\end{aligned} \tag{2.22}$$

However, the Kihara potential is only empirically superior since it has three adjustable parameters.

In order to evaluate the total interaction potential, the summations must be cut off at a certain radius, because it is practically impossible to sum over all the host molecules. Only the first shell of water molecules surrounding the guest molecule was considered in

the early calculation of total guest-host interaction[27]. However, Sparks et al.[24] showed that the shells other than the first shell also contribute non-negligibly to the total potential. At least four shells of host water molecules are required to obtain asymptotic value from lattice summation over the infinite host water molecules.

The parameters that go into these potential are generally found by fitting experimentally determined curve of dissociation pressure as a function of T. Thus, they lack a molecular basis, and must be determined ad hoc for each hydrates studies. Furthermore, they cannot be used where more than one cage are occupied. The potential surface generated from first principle (*ab initio*) quantum mechanical calculations becomes a promising alternative to describe more accurately the interactions between guest and host molecules[28].

2.4 Prediction of hydrate phase diagram

The prediction of the three-phase hydrate equilibrium curves is inherently an iterative process. Parrish and Prausnitz[8] laid out the groundwork for predicting dissociation pressures of gas hydrates formed by gas mixtures. This algorithm is used in our prediction of pure component hydrate phase diagrams with a simplification to eliminate the reference hydrate suggested by Holder et al.[3], as shown in Equation (2.8). A first order estimation for the equilibrium pressure-temperature curves that are used as an initial guess can be expressed by a 3-parameter equation:

$$\ln P = A + B/T + C\ln T \tag{2.23}$$

where A, B and C are empirical parameters determined from experimental data[4]. Details regarding the computational iterative algorithm for equilibrating the chemical potentials of the phases in question can be found in the Ph.D. thesis of Zhitao Cao[29] at MIT.

2.4.1 Three different approaches to calculate the Langmuir constants

Common fit potentials.

The ability to predict behavior in mixed systems, in which there is more than one type of guest molecule, is essential in predictions of naturally occurring hydrate systems. Commonly, the Lennard-Jones 6-12 or Kihara models are chosen to represent average interactions between the host water lattice and the guest molecules (methane, ethane, etc.) and are adjusted to fit experimental 3-phase, monovariant dissociation pressure data as a function of *T*. Reference parameters are chosen *a priori* (Table 2.1) and the resulting fitted potential depends on the values of the reference parameters used. Thus, the potentials lack a physical basis, and must be determined *ad hoc* from data from each hydrate system studied. Furthermore, they cannot be consistently used where multiple clathrate cage types are occupied. Generating the potential surface from *ab initio* calculations becomes a promising alternative to these earlier empirical methods as interactions between guest and host molecules can be described in a molecularly consistent, quantitative manner.[28] For example, *ab initio* methods can be used to compute accurately the interaction energy of any particular orientation of the molecule pair. Suitable averages can then be obtained to functionally represent the spatial dependence of Φ_{ij} for all guest-host interactions needed to evaluate Equation (2.12).

Independently determined potentials.

Lennard-Jones parameters for liquid hydrocarbons have been optimized to reproduce experimental densities and heats of vaporization with an accuracy of approximately 5% in what is termed the OPLS model[30]. A popular model for water is the TIP3P model, which has three point charges on the oxygen and hydrogens to represent

the dipole, and Lennard-Jones parameters for the oxygen only. The TIP3P model has been parameterized to reproduce liquid water properties at ambient conditions[31]. However, using a simple mixing rule, the TIP3P model and the OPLS model for hydrocarbons failed to give a reasonable Langmuir constant, a key term in the van der Waals and Platteeuw statistical model, for several hydrates[19,24,32]. In our previous work,[32,33] we use an intermolecular potential developed for methane clathrate-hydrates in order to capture, from first principles, accurate Structure I methane clathrate reference parameters. This potential has been studied further in this work and modified according to the new methods employed for our new argon-water potential.

Inversion of Langmuir Curves.

Earlier, Bazant and Trout[34] described such a method by which the functional form of the inter-molecular potential can be found by solving Equation (2.19) analytically for $w(r)$. First, Equation (2.19) is restructured as

$$C_{Ji}(\beta) = 4\pi\beta \int_0^\infty e^{-\beta w(r)} r^2 dr \tag{2.24}$$

where $\beta = 1/kT$. The upper limit of integration is extended to $R = \infty$, which introduces negligible errors due to the low temperatures accessible in clathrate experiments.

In order to invert Equation (2.24), a functional form of $C_{Ji}(\beta)$ must be found. We do this by computing $C_{Ji}(\beta)$ from experimental data and *ab initio* data and fitting the computed values of $C_{Ji}(\beta)$ to a functional form. More details on this methodology can be found in Chapter 4.

2.5 References

(1) van der Waals, J. H.; Platteeuw, J. C. *Adv. Chem. Phys.* **1959**, *2*, 1.
(2) Peng, D.-Y.; Robinson, D. B. *Ind. Eng. Chem. Fund.* **1976**, *15*, 59.
(3) Holder, G. D.; Corbin, G.; Papadopoulos, K. D. *Industrial & Engineering Chemistry Fundamentals* **1980**, *19*, 282.
(4) Sloan, E. D., Jr. *Clathrate hydrates of natural gases - 2nd ed., rev. and expanded*; Marcel Dekker, Inc.: Monticello, 1998.
(5) Barrer, R. M.; Ruzicka, D. J. *Trans. Faraday Soc.* **1962**, *58*, 2253.
(6) Sortland, L. D.; Robinson, D. B. *Canadian Journal of Chemical Engineering* **1964**, *42*, 38.
(7) Child, W. C., Jr. *J. Phys. Chem.* **1964**, *68*, 1834.
(8) Parrish, W. R.; Prausnitz, J. M. *Industrial & Engineering Chemistry Process Design and Development* **1972**, *11*, 26.
(9) Holder, G. D.; Katz, D. L.; Hand, J. H. *AAPG Bulletin-American Association of Petroleum Geologists* **1976**, *60*, 981.
(10) Dharmawardhana, P. B.; Parrish, W. R.; Sloan, E. D. *Industrial & Engineering Chemistry Fundamentals* **1980**, *19*, 410.
(11) Holder, G. D.; Malekar, S. T.; Sloan, E. D. *Ind. Eng. Chem. Fundam.* **1984**, *23*, 123.
(12) John, V. T.; Papadopoulos, K. D.; Holder, G. D. *AIChE J* **1985**, *31*, 252.
(13) Davidson, D. W.; Handa, Y. P.; Ripmeester, J. A. *Journal of Physical Chemistry* **1986**, *90*, 6549.
(14) Handa, Y. P.; Tse, J. S. *Journal of Physical Chemistry* **1986**, *90*, 5917.
(15) Cao, Z. T.; Tester, J. W.; Trout, B. L. *Journal of Physical Chemistry B* **2002**, *106*, 7681.
(16) Anderson, B. J.; Tester, J. W.; Trout, B. L. *Journal of Physical Chemistry B* **2004**, *108*, 18705.
(17) Stackelberg, M. v.; Müller, H. R. *Zeitschrift für Elektrochemie* **1954**, *58*, 25.
(18) Sparks, K. A.; Tester, J. W. *Journal of Physical Chemistry* **1992**, *96*, 11022.
(19) Sparks, K. A.; Tester, J. W.; Cao, Z. T.; Trout, B. L. *Journal of Physical Chemistry B* **1999**, *103*, 6300.
(20) John, V. T.; Holder, G. D. *J. Phys. Chem.* **1985**, *89*, 3279.
(21) Hirschfelder, J. O.; Curtiss, C. F.; Bird, R. B. *Molecular theory of gases and liquids*; John Wiley &Sons, Inc.: New York, 1964.
(22) McKoy, V.; Sinanoglu, O. *J. Chem. Phys.* **1963**, *38*, 2946.
(23) John, V. T.; Holder, G. D. *J. Phys. Chem.* **1981**, *85*, 1811.
(24) Sparks, K. A. Configurational properties of water clathrates through molecular simulation, PhD Thesis, Massachusetts Institute of Technology, 1991.
(25) Carnahan, B.; Luther, H. A.; Wilkes, J. O. *Applied Numerical Methods*; Wiley: New York, 1969.
(26) Kihara, T. *Reviews of Mod. Phys.* **1953**, *25*, 831.
(27) Tester, J. W.; Bivins, R. L.; Herrick, C. C. *AIChE J* **1972**, *18*, 1220.
(28) Cao, Z.; Tester, J. W.; Trout, B. L. *J. Chem. Phys.* **2001**, *115*, 2550.
(29) Cao, Z. Modeling of Gas Hydrates from First Principles, PhD Thesis, Massachusetts Institute of Technology, 2002.

(30) Jorgensen, W. L.; Madura, J. D.; Swenson, C. J. *J. Am. Chem. Soc.* **1984**, *106*, 6638.
(31) Sun, Y.; Kollman, P. A. *J. Comp. Chem.* **1995**, *16*, 1164.
(32) Cao, Z. T.; Tester, J. W.; Sparks, K. A.; Trout, B. L. *J. Phys. Chem. B.* **2001**, *105*, 10950.
(33) Cao, Z. T.; Tester, J. W.; Trout, B. L. *J. Chem. Phys.* **2001**, *115*, 2550.
(34) Bazant, M. Z.; Trout, B. L. *Physica A* **2001**, *300*, 139.

Chapter 3. Development of Argon-Water Potential via Ab Initio Methods and its Application to Clathrate Hydrates

3.1 Introduction

High level *ab initio* quantum mechanical calculations were used to determine the intermolecular potential energy surface between argon and water, corrected for many-body interactions, to predict monovariant and invariant phase equilibria for the argon hydrate and mixed methane-argon hydrate systems. A consistent set of reference parameters for the van der Waals and Platteeuw model, $\Delta\mu_w^0$=1077±5 kcal/mol and ΔH_w^0=1294±11 kcal/mol, were developed for structure II hydrates and are not dependent on any fitted parameters. Our previous methane-water *ab initio* energy surface has been recast onto a site-site potential model that predicts guest occupancy experiments with improved accuracy compared to previous studies. This methane-water potential is verified via *ab initio* many-body calculations and thus should be generally applicable to dense methane-water systems. New reference parameters, $\Delta\mu_w^0$=1203±3 kcal/mol and ΔH_w^0=1170±19 kcal/mol, for structure I hydrates using the van der Waals and Platteeuw model were also determined. Equilibrium predictions with an average absolute deviation of 3.4% for the mixed hydrate of argon and methane were made. These accurate predictions of the mixed hydrate system provide an independent test of the accuracy of the intermolecular potentials. Finally, for the mixed argon-methane hydrate, conditions for structural changes from the structure I hydrate of methane to the structure II hydrate of argon were predicted and await experimental confirmation.

3.2 Gas hydrate modeling

A thermodynamic model corresponding to the three-dimensional generalization of ideal localized adsorption was proposed in 1959 by van der Waals and Platteeuw[1]. By assuming single guest occupancy of the available water cages and negligible distortions of the empty lattice, the difference in chemical potential between the clathrate and empty host lattice can then be expressed as

$$\Delta\mu^{\beta-H} = kT\sum_i \nu_i \ln(1+\sum_J C_{Ji}\hat{f}_J) \tag{3.25}$$

where ν_i is the number of type i cavities per water molecule, $\hat{f}_J$ is the fugacity of guest molecule J, which is usually calculated from a mixture form of a PVTN Peng-Robinson equation of state[2], and C_{Ji} is the Langmuir constant for a guest molecule J in a cavity of type i defined as

$$C_{Ji} \equiv \frac{Z_{Ji}}{kT} = \frac{1}{8\pi^2 kT}\int_V \exp(-\Phi(r,\theta,\phi,\alpha,\beta,\gamma)/kT) r^2 \sin\theta\, dr\, d\theta\, d\phi\, d\alpha\, d\beta\, d\gamma \tag{3.26}$$

where Z_{Ji} is the full configurational integral, which depends on the total interaction potential between guest and host molecules[3,4] and which is, in general, a function of r, θ, and ϕ the polar coordinates of the guest molecule and α, β, and γ the Euler angles that describe the orientation of the guest.

With this thermodynamic model, we can consider the clathrate as a two-component system, with monovariant, three-phase equilibrium described by:

$$\begin{aligned} \mu_w^H &= \mu_w^{L,\alpha} \\ \mu_w^\beta - \mu_w^H &= \mu_w^\beta - \mu_w^{L,\alpha} \\ \Delta\mu_w^{\beta-H} &= \Delta\mu_w^{\beta-L,\alpha} \end{aligned} \tag{3.27}$$

where μ_w^{β} is the chemical potential of a hypothetical empty hydrate lattice, μ_w^{H} is the chemical potential of water in the hydrate phase, and $\mu_w^{L,\alpha}$ refers to the chemical potential of water in either a solid ice phase, α, for $T \leq 273.15$ K or liquid aqueous phase, L, for $T \geq 273.15$ K. In the thermodynamic model, $\mu^{\beta-L,\alpha}$ can be determined from experimental data and $\hat{f}_J$ from a *PVTN* equation of state.

Following the convention proposed by Holder[5], the chemical potential difference between water in the hypothetical empty lattice and the water in the hydrate phase can be expressed as

$$\frac{\Delta\mu_w^{\beta-L,\alpha}(T,P)}{kT} = \frac{\Delta\mu_w^{\beta-L,\alpha}(T_0,0)}{kT_0} - \int_{T_0}^{T}[\frac{\Delta H_w^{\beta-L,\alpha}}{kT^2}]_P dT + \int_0^P[\frac{\Delta V_w^{\beta-L,\alpha}}{kT}]_T dP - \ln a_w^L \quad (3.28)$$

where $\Delta\mu_w^{\beta-L,\alpha}(T_0,0)$ is the reference chemical potential difference at the reference temperature, T_0, and zero pressure. The temperature dependence of the enthalpy difference is given by

$$\Delta H_w^{\beta-L,\alpha} = \Delta H_w^{\beta-L,\alpha}(T_0) + \int_{T_0}^{T} \Delta C_p^{\beta-L,\alpha} dT \quad (3.29)$$

where the heat capacity difference is approximated by

$$\Delta C_{p_w}^{\beta-L,\alpha} = \Delta C_{p_w}^{\beta-L,\alpha}(T_0) + b^{\beta-L,\alpha}(T - T_0) \quad (3.30)$$

where $b^{\beta-L,\alpha}$ is the constant representing the dependence of heat capacity on the temperature. The volume difference, $\Delta V_w^{\beta-L,\alpha}$, is assumed to be independent of pressure. The additional term involving the activity of water, a_w^L, is defined by

$$a_w^L = \frac{\hat{f}_w^L}{\hat{f}_w^+} \quad (3.31)$$

where $\hat{f}_w^L$ is the fugacity of water in the water-rich aqueous phase and $\hat{f}_w^+$ is the water fugacity in the reference state, which is chosen to be the pure water phase at T and P of the mixture, thus using the conventional notation $\hat{f}_w^+ = f_w$. The reference temperature, T_0, is usually taken to be 273.15 K. Reference parameters reported in the literature are given in Table 3.1.

Table 3.1: Thermodynamic reference properties for structure I and II water clathrates[6]

structure I (J/mol)		structure II (J/mol)		Source[a]
$\Delta\mu^{\beta-L,\alpha}(T_0,0)$	$\Delta H^{\beta-L,\alpha}(T_0,0)$	$\Delta\mu^{\beta-L,\alpha}(T_0,0)$	$\Delta H^{\beta-L,\alpha}(T_0,0)$	
699	0	820	0	van der Waals and Platteeuw (1959)
-	-	366-537	-	Barrer and Ruzicka (1962)
-	-	833	-	Sortland and Robinson (1964)
1255.2	753	795	837	Child (1964)
1264	1150	-	808	Parrish and Prausnitz (1972)
1155	381	-	0	Holder (1976)
1297	1389	937	1025	Dharmawardhana, Parrish and Sloan (1980)
1299	1861	-	-	Holder, Malekar, and Sloan (1984)
1120	931	1714	1400	John, Papadopoulos, and Holder (1985)
1297	-	-	-	Davidson, Handa, and Ripmeester (1986)
1287	931	1068	764	Handa and Tse (1986)
1236	1703	-	-	Cao, Tester, and Trout (2002)
1203	1170	1077	1294	This Study

[a]Ref 1,9,19-28

Having the ability to model accurately clathrate behavior, specifically phase equilibrium behavior, has been important in practical engineering operations. In 1939 Hammerschmidt[7] discovered that gas hydrates were forming plugs in natural gas transmission lines. This fact led to many investigations aimed at understanding and avoiding hydrate formation. Since the late 1950's, most modeling efforts have been based on the van der Waals and Platteeuw statistical mechanical model using the Lennard-Jones and Devonshire (LJD) spherical cell potential approximation[1,8]. Typically phase data are fit by adjusting potential parameters for a specified pair potential model,

commonly the Kihara potential. Evaluations at the University of Pittsburgh by Holder and coworkers[9] and at MIT[10] have demonstrated the inadequacy of the LJD approximation. These empirically fitted potential parameters are aphysical and cannot be applied to other systems such as mixed hydrate systems[11]. As one might expect, potential parameters computed from gas-hydrate phase data using the spherical LJD approximation do not match those computed from other experimental data[6,9,12]. Consequently, complete three-dimensional integration over the host lattice is necessary to determine correctly the full interaction energy.

In addition, recent work by Klauda and Sandler[13] showed that many-body interactions should be accounted for when applying computed potentials to the hydrate clathrate system. Proper determination of the form of the intermolecular interaction potential is also necessary both to compute equilibrium thermodynamic properties and to perform dynamic molecular simulations of kinetic phenomena such as diffusion and hydrate crystal nucleation, growth, and decomposition.

3.2.1 Common fit potentials.

The ability to predict behavior in mixed systems, in which there is more than one type of guest molecule, is essential in predictions of naturally occurring hydrate systems. Commonly, the Lennard-Jones 6-12 or Kihara models are chosen to represent average interactions between the host water lattice and the guest molecules (methane, ethane, etc.) and are adjusted to fit experimental 3-phase, monovariant dissociation pressure data as a function of T. Reference parameters are chosen *a priori* (Table 3.1) and the resulting fitted potential depends on the values of the reference parameters used. Thus, the potentials lack a physical basis, and must be determined *ad hoc* from data from each

hydrate system studied. Furthermore, they cannot be consistently used where multiple clathrate cage types are occupied. Generating the potential surface from *ab initio* calculations becomes a promising alternative to these earlier empirical methods as interactions between guest and host molecules can be described in a molecularly consistent, quantitative manner.[14] For example, *ab initio* methods can be used to compute accurately the interaction energy of any particular orientation of the molecule pair. Suitable averages can then be obtained to functionally represent the spatial dependence of Φ_{ij} for all guest-host interactions needed to evaluate Equation (3.26).

3.2.2 Independently determined potentials.

Lennard-Jones parameters for liquid hydrocarbons have been optimized to reproduce experimental densities and heats of vaporization with an accuracy of approximately 5% in what is termed the OPLS model[15]. A popular model for water is the TIP3P model, which has three point charges on the oxygen and hydrogens to represent the dipole, and Lennard-Jones parameters for the oxygen only. The TIP3P model has been parameterized to reproduce liquid water properties at ambient conditions[16]. However, using a simple mixing rule, the TIP3P model and the OPLS model for hydrocarbons failed to give a reasonable Langmuir constant, a key term in the van der Waals and Platteeuw statistical model, for several hydrates[4,10,17]. In our previous work,[17,18] we use an intermolecular potential developed for methane clathrate-hydrates in order to capture, from first principles, accurate structure I methane clathrate reference parameters. This potential has been studied further in this work and modified according to the new methods employed for our new argon-water potential.

3.2.3 Reference parameters.

Accurate values for the thermodynamic reference parameters used in the van der Waals and Platteeuw statistical mechanical model are essential. The two critical reference parameters, $\Delta\mu_w^0$ and ΔH_w^0, have been determined by many investigators[1,9,19-28]. Unfortunately, these parameters take on a wide range of values (see Table 3.1) and have so far been used in models to fit experimental data rather than to make predictions[28].

3.3 Objectives of this work

In order to determine accurate, physically based, and model independent interaction parameters, we performed *ab initio* quantum mechanical calculations to determine guest-host interaction energies. First, we developed accurate intermolecular interaction potentials from *ab initio* calculations. Then an accurate and efficient method to calculate the potential energy surface was determined considering the fineness of the intermolecular orientation grid as well as other factors, such as many-body effects, correlation dependencies, and basis set convergence. This accurate intermolecular potential is then used to determine with a low degree of uncertainty reference parameters for the van der Waals and Platteeuw model for hydrate clathrate systems. This model is then validated by predicting the cage occupancies for the methane hydrate system and then used to calculate pure argon hydrate phase behavior and predict the phase behavior of the argon-methane mixed hydrate system.

3.4 Methodology and Approach

In our study, the aug-cc-pVQZ basis set was used for the calculation and the electron correlation energy was corrected by the second-order Møller-Plesset (MP2) perturbation method. Basis set superposition error (BSSE) was corrected by using half of the correction energy in the counterpoise method[29]. The geometry of the water molecules was optimized at the MP2/6-31++G(2d,2p) level. Gaussian 98 was used to perform the *ab initio* calculations.

3.4.1 Determination of potential energy surface.

In our calculation of interaction energies, the distance and orientation between argon and water are varied but the geometry of the water is frozen based on the actual clathrate structure. By inspecting the ball and stick model of a structure II clathrate hydrate (see Figure 3.3), the relative orientations between guest and water molecule can be seen to fall into two types, characterized by the plane containing the water molecule, shown in Figure 3.2. The different orientations are then created by a two-step process: first fixing the planar orientation of the water molecule and then moving the guest molecule in the three-dimension grid to different positions inside the water cage. The center of mass of the guest molecule is moved in a polar coordinate system where the water oxygen is the origin. For guest molecules that are not spherically-symmetric, such as methane, the rigid-body of the guest molecule is further rotated in its own internal coordinate in a fashion consistent with the geometry input file in the Z-matrix form, used in Gaussian 98 software (see Ref. [17]). The combination of these two steps for the spherically-symmetric guest argon maps out a simplified three-dimensional grid as shown in Figure 3.3.

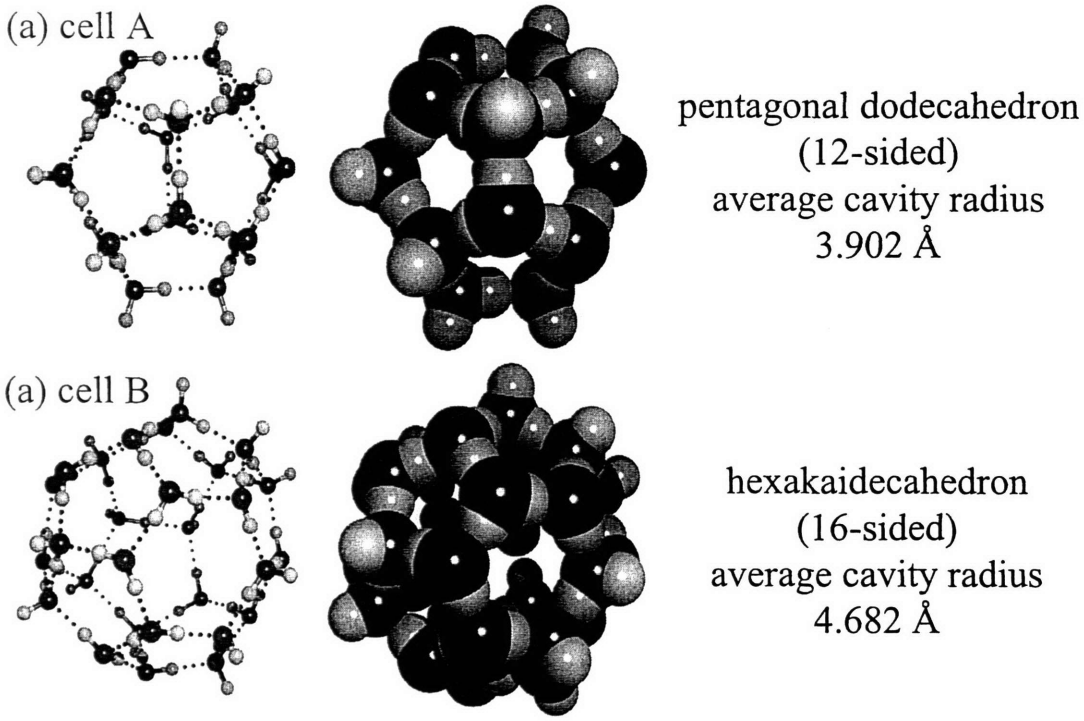

Figure 3.1: Cavities of structure II clathrates.

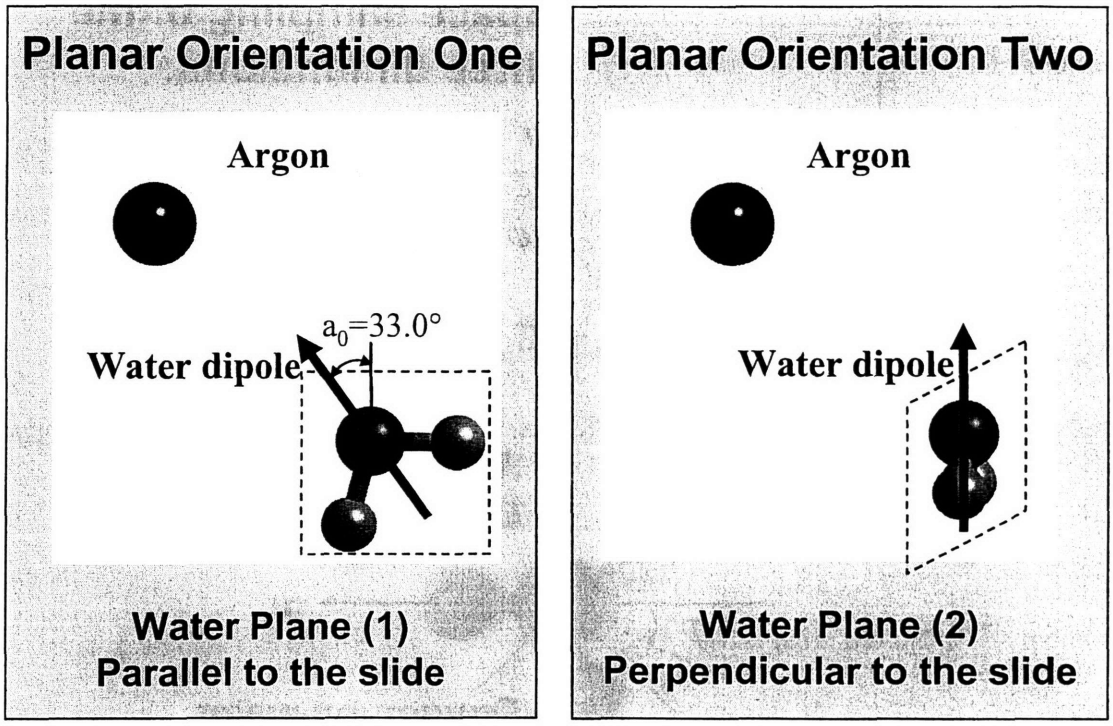

Figure 3.2: Two characteristic water plane orientations in the argon–water clathrate viewed from the center of the cavity.

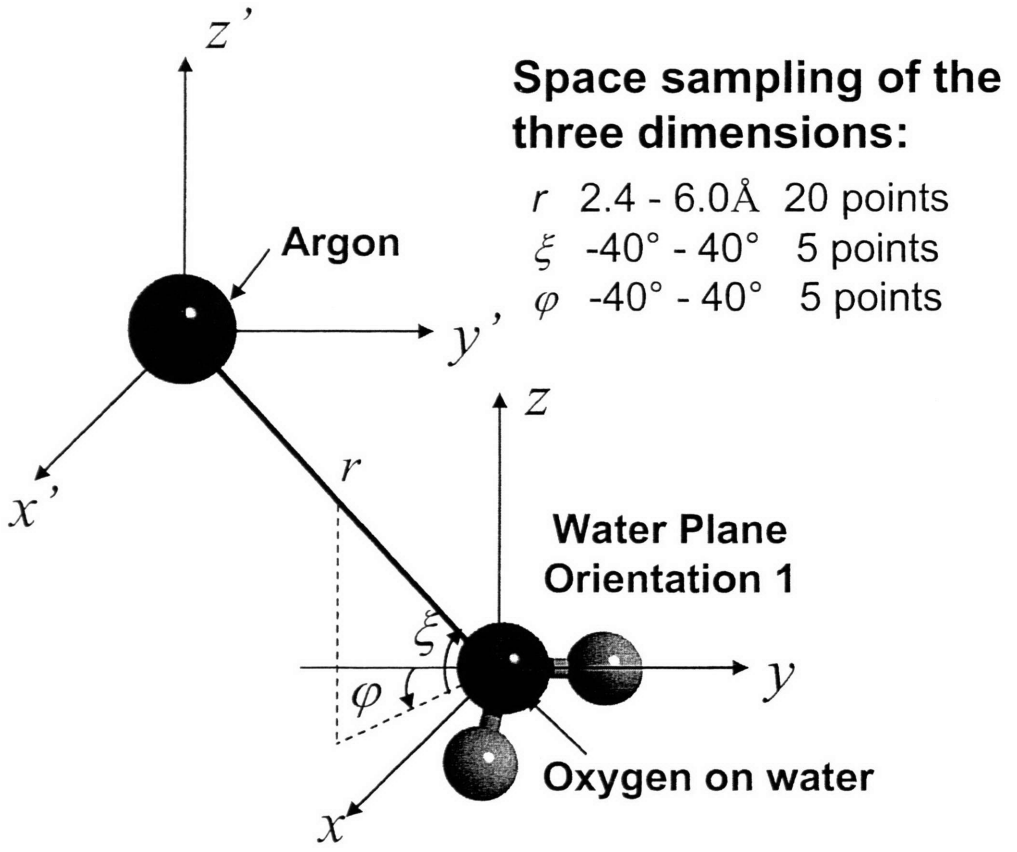

Figure 3.3: The three spherical coordinate dimensions (r, ξ, ϕ) used to define the position and orientation between an argon guest and fixed planar orientation 1 water host

The range of the r, ξ, ϕ dimensions given in Figure 3.3 were determined in the following manner. Because the guest molecule is entrapped in a single cage, the r distance between the center of the argon guest and the oxygen atom of the host water molecule cannot be larger than the maximum diameter of the cage nor any smaller than the hard sphere radius of the Ar-O pair. Also, noting that the interaction energy will become extremely repulsive when the distance is very small, the interval for r was set at 2.4-6.0 Å with 10 equally separated points selected. Ranges for the polar angle ξ and azimuthal angle ϕ were determined by moving a guest molecule over a minimum distance inside the cage not too close to the cage wall. The ξ and ϕ ranges were set from -40° to 40°. Five angular points were considered to be sufficient for sampling the argon-water configuration space.

For each separation distance r, there are two different water planes, and $5 \times 5 = 25$ angular orientations of the argon molecule. Therefore, an algorithm must be applied to combine the set of $25 \times 2 = 50$ interaction energies to obtain a potential that can be incorporated into the configurational integral. Two approaches were examined, an angle-averaging method that results in a potential dependent upon r only, and a site-site method that attempts to account for guest orientation. In general, to determine the angle-averaged interaction, a Boltzmann-weighted average is taken at each radial point r as a representative average of the 5 remaining degrees of freedom (α, β, γ, ξ, and ϕ) following the method outlined in Cao et al., 2001[18]. This angle-averaged potential, we found, results in large errors in the prediction of the occupancies of the clathrate cages. This error is due to the smearing effect of averaging out all of the five orientational and rotational degrees of freedom. The higher energy configurations are weighted out in the

development of the two-dimensional potential, but are calculated in the configurational integral.

To account for all six degrees of freedom in the argon- and methane-water interactions, a site-site model was developed. The 500 different argon-water and 18,000 different methane water orientations were fit to site-site potentials based on the interactions between the center of the guest molecule and the oxygen on the water (**Ar**–**O**H_2 and H_4**C**–**O**H_2), the center of the guest molecule and the hydrogens on the water molecule (**Ar**–**H**OH and H_4**C**–**H**OH), and the methane hydrogens with the oxygen on the water (H_3C**H**–**O**H_2). The **Ar**–**O**H_2 and H_4**C**–**O**H_2 potentials capture the guest position effects while the **Ar**–**H**OH and H_4**C**–**H**OH potential captures the ξ and ϕ orientations. In addition, for methane, the H_3C**H**–**O**H_2 potential captures the Euler orientation of the methane molecule with respect to the water.

To obtain a highly accurate *ab initio* potential, we evaluated three energetic corrections: a correlation correction based on the effects of higher orders of quantum calculations, a basis-set extrapolation to ensure that the basis set employed can estimate interaction energies accurately, and a many-body correction to account for the many-body effects expected to play an important role in clathrate calculations. The effect of the level of correlation was examined by calculating a few selected points at increasing levels of electron correlation. It has been reported[30] that for hydrogen-bonded complexes, the improvements resulting from electron correlation beyond the MP2 level are not large. In this work, that improvement was investigated for the Ar-H_2O pair. An *ab initio* potential was calculated for the Ar-H_2O pair at the MP2 level using the 6-31++G(2*d*,2*p*), aug-cc-pVTZ, aug-cc-pVQZ, and aug-cc-pV5Z basis sets to examine the convergence of the

potential with increasing basis-set size. As shown in Figure 3.4, the binding energy or the Ar-H_2O complex converges (when using diffuse functions in the augmented basis sets) as we approach the size of the aug-cc-pVQZ basis set with 250 basis functions. The deviations of the binding energies, with respect to the aug-cc-pV5Z energy, are 0.015 and 0.006 kcal/mol for the aug-cc-pVTZ and aug-cc-pVQZ energies respectively.

3.4.2 Estimating many-body effects.

The recent study by Klauda and Sandler[13] showed that many-body effects can result in a 35% change in the total energy of interaction between a clathrate cage and the guest molecule. To evaluate these effects in our study, a structure II pentagonal dodecahedron consisting of 20 water molecules surrounding entrapped argon and methane molecules (Figure 3.1a) was divided first into symmetrical halves then into quarters of a cell each containing 5 water molecules, as shown in Figure 3.5. Next the four cell quarters were each dissected into all of the combinations of two and three molecule combinations that could comprise each quarter cell. Finally, each set of two waters and three waters was split into its individual water molecules. The clathrate cage was then reconstructed piece by piece, calculating the energy to do so along the way. Interaction energies between the guest argon and each piece of the cage were calculated using MP2/aug-cc-ATZ *ab initio* methods and the developed **Ar–H**OH and H_4**C–H**OH potentials were corrected to reproduce the many-body cluster calculation.

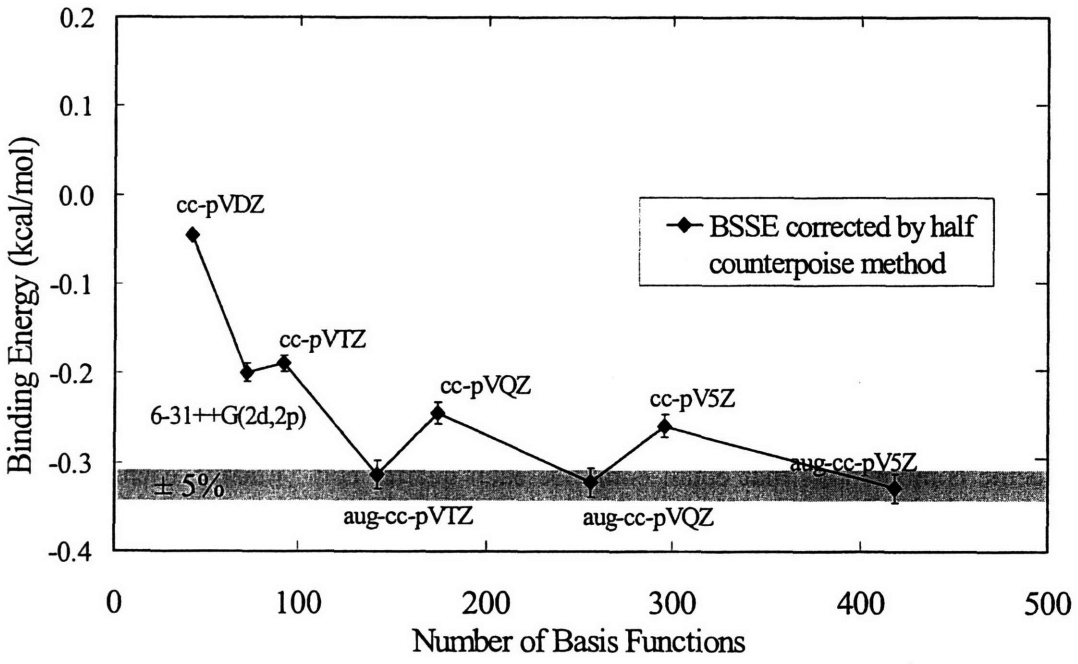

Figure 3.4: The effect of size of the basis set on estimated binding energy of the optimized Ar H_2O pair. ±5% deviation shown from aug-cc-pV5Z basis set calculation.

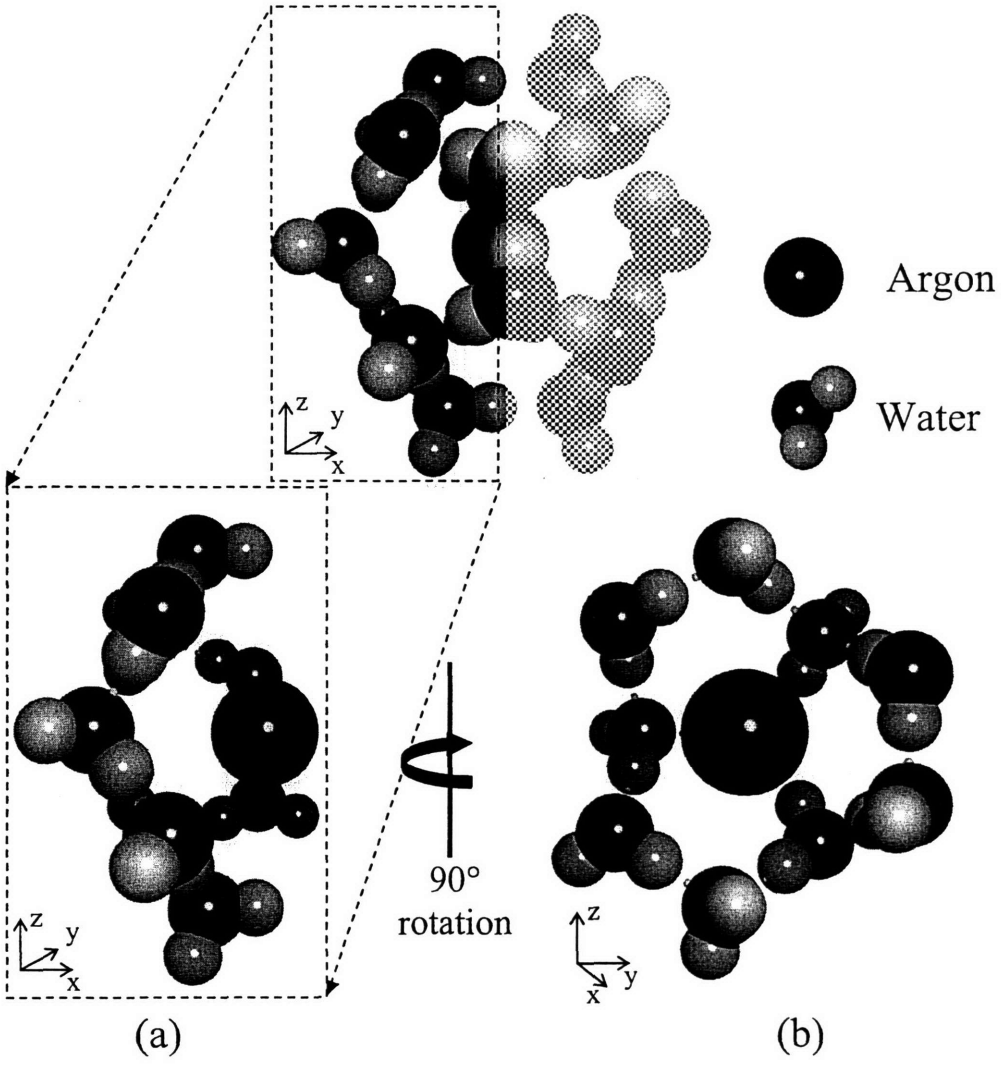

Figure 3.5: Two-dimensional projection of the half-cell configuration for argon in the small cage (pentagonal dodecahedron) of a structure II clathrate. (a) A *z-x* planar orientation and (b) a *z-y* planar orientation rotated 90° from (a) as shown. Relative atom sizes represent different *y* in (a) and *x* in (b) coordinate positions.

3.4.3 Reference parameter evaluation.

In order to determine reference parameters accurately for a structure II clathrate hydrate lattice the approach by Holder et al.[25] was used. One can reformulate the temperature and pressure dependence of the multiphase equilibria criteria equating the chemical potential of water in hydrate (H) and liquid (L) or solid (α) phases, to give,

$$Y = \frac{\Delta\mu_w^0}{RT_0} + \frac{\Delta H_w^0 + \Delta H_w^{\alpha-L}(T_0)}{R}\left[\frac{1}{T} - \frac{1}{T_0}\right] \tag{3.32}$$

where Y is a function of the experimental conditions (T, P, composition) and other properties, namely $\Delta b^{\beta-L \text{ or } \alpha}$, $\Delta C_p^{\beta-L \text{ or } \alpha}(T_0)$ and $\Delta V_w^{\beta-L \text{ or } \alpha}(T_0)$. In an earlier study[28], we found accurate reference parameters for structure I clathrates using methane phase data and our calculated *ab initio* potential describing methane-water interaction (see Table 3.1). A similar approach will be followed here to obtain reference parameters for structure II and structure I clathrates using the *ab initio* site-site potentials for argon and methane respectively in a water clathrate and accompanying phase data.

3.5 Results and Discussion

3.5.1 Basis Set Convergence.

Tsuzuki et al.[30] showed that a large basis set is needed to estimate accurately the interaction energy of hydrogen-bonded complexes. The basis set dependence of the binding energy of the Ar-H_2O complex was evaluated. As a result, the MP2/aug-cc-pVQZ level and basis set were selected for the calculation of the *ab initio* potential energy surface between argon and water. Potential energy surfaces were determined

using the MP2 level of electron correlation and the 6-31++G(2*d*,2*p*), cc-pVTZ, aug-cc-pVTZ, and aug-cc-pVQZ basis sets. These three-dimensional surfaces were then averaged and projected onto a spherically symmetric potential using the method described by Cao et al., 2001[18] As shown in Figure 3.6, the potential converges as the size of the basis set approaches aug-cc-pVQZ.

The use of even larger basis sets was examined for the argon-water pair interaction. Table 3.2 shows the energy of the argon-water pair for the aug-cc-pVQZ and aug-cc-pV5Z basis sets. The difference in energies between the aug-cc-pVQZ and aug-cc-pV5Z basis sets shows that for this system convergence is reached to well within 0.14 kcal/mol, even for the short-range repulsive interaction at 2.4 Å. For distances of 2.8 Å or greater, the difference in energy is lower, ranging from 0.04 to 0.002 kcal/mol, and lower than errors achieved by various basis set extrapolation methods.[31,32] This energy difference would not be visible if plotted in Figure 3.6.

The convergence of the *ab initio* potential was verified by examining the change in the thermodynamic properties resulting from the change in potential. For the argon-water system, convergence to within 0.01 kcal/mol in the attractive region of the potential was necessary to predict phase equilibria to within a 5% range.

Table 3.2: Comparison of aug-cc-pVQZ (AQZ) and aug-cc-pV5Z (A5Z) calculations of the angle-averaged binding energy of an Ar-H_2O pair using the MP2 electron correlation level. Energies reported in kcal/mol.

r (Å)	$\langle E_{cp,\,AQZ}(r)\rangle$ (kcal/mol)	$\langle E_{cp,\,A5Z}(r)\rangle$ (kcal/mol)
2.4	9.365	9.233
2.8	1.097	1.059
3.2	-0.294	-0.305
3.6	-0.347	-0.352
4.0	-0.230	-0.232

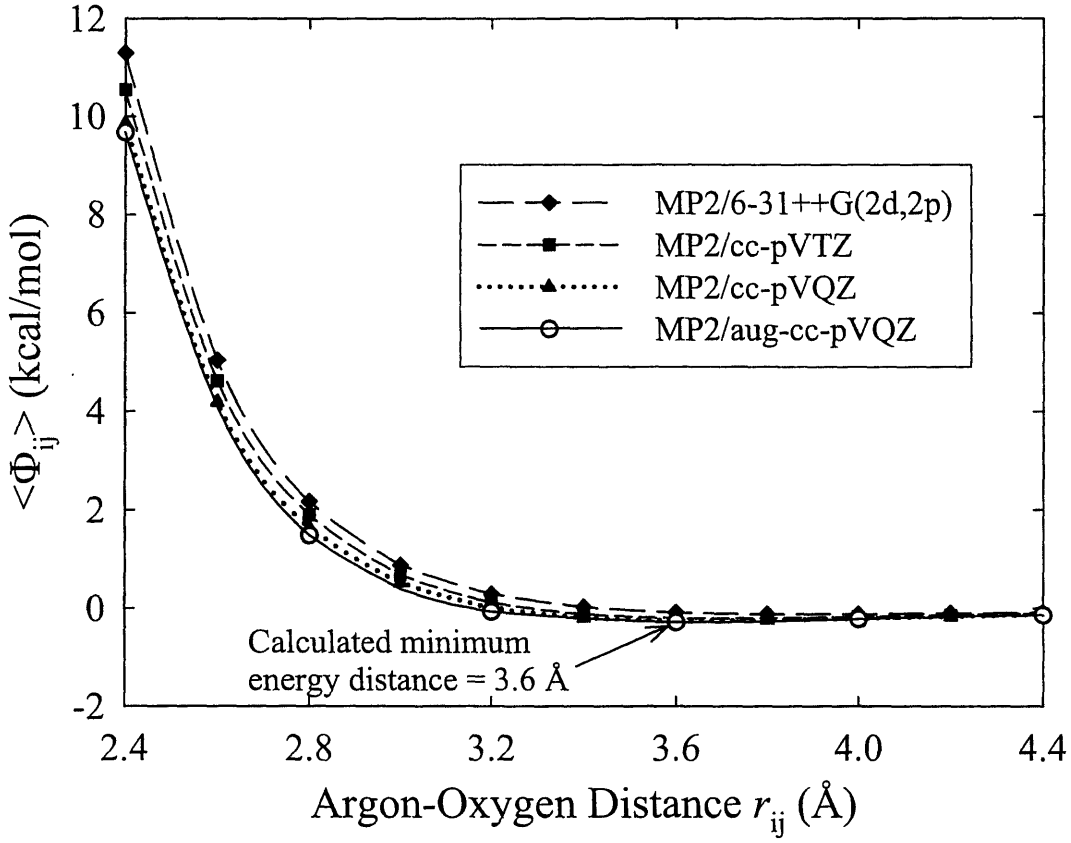

Figure 3.6: The effect of size of the basis set on the calculated *ab initio* pair potential for a binary Ar-H_2O system.

3.5.2 Grid Fineness.

Because accurate *ab initio* calculations are computationally intensive, it is desirable to optimize the grid spacing on the hyperspace (r, ξ, ϕ, α, β, γ) surface to achieve acceptable accuracy with the coarsest grid possible. Minimizing the total number of calculations necessary to achieve convergence of the potential increases efficiency substantially. By examining the sensitivity of the intermolecular potential we can evaluate the convergence of the potential for any grid size.

In order to insure that a fine enough grid was used in the calculation of the final potential energy hypersurface at the MP2/aug-cc-pVQZ level, the effect of angular grid resolution was examined. Selected angular points were systematically removed from the Boltzmann averaging scheme to simulate a coarser mesh. As expected, there was a greater dependence of the potential on the ξ grid points due to the interaction of the argon with the hydrogen atoms on the water molecule. Table 3.3 shows the results of systematically eliminating angular points on the average guest-host interaction energy.

Upon close inspection, one can see that the lower half of Table 3.3 illustrates the stronger dependence of the potential on the ξ grid points. Elimination of grid points in the ϕ direction allows the potential to maintain its value to within 2%, while it diverges in a statistically significant manner from the converged curve when the grid in the ξ direction is made coarser. Data for all 500 grid points per water plane, as discussed in Figure 3, is noted as all points. Elimination of angular grid points, ±20° and ±40°, in the ξ and ϕ directions result in coarser meshes. The 20° spacing detailed earlier is sufficient to capture the effects of different orientations within the clathrate cage.

Table 3.3 : Angle-averaged energy of interaction of the Ar-H_2O pair at different radial separation distances for varying resolution of angular grid size

angles included in calculation (degrees)			% deviation from full mesh				
			r (Å)				
ϕ	ξ	total points per planar orientation	2.4	2.8	3.2	3.6	4.0
-40, -20, 0, 20, 40	-40, -20, 0, 20, 40	500 (all points)	0.0	0.0	0.0	0.0	0.0
-40, 0, 40	-40, -20, 0, 20, 40	300	0.2	-0.1	2.7	0.6	0.6
-20, 0, 20	-40, -20, 0, 20, 40	300	-0.3	-0.1	-5.2	-1.1	-1.0
0	-40, -20, 0, 20, 40	180	-0.5	-0.3	-7.3	-1.4	-1.3
-40, -20, 0, 20, 40	-40, 0, 40	300	0.4	-0.9	-14.3	0.7	1.5
-40, 0, 40	-40, 0, 40	180	0.5	-0.8	-11.3	1.1	1.9
-40, -20, 0, 20, 40	-20, 0, 20	300	-1.1	-5.9	28.1	-1.5	-3.1
-20, 0, 20	-20, 0, 20	180	-1.4	-5.7	23.4	-3.7	-4.8
-40, -20, 0, 20, 40	0	180	-1.7	-15.8	43.3	-2.5	-4.9
0	0	10	-1.7	-16.1	35.8	-6.7	-7.8

3.5.3 Electron Correlation Effects.

Once convergence of the potential due to the grid size was achieved to ±3%, the level of electron correlation was examined. A size-consistent approach[33] was used to verify the convergence of the electron correlation energy using the aug-cc-pVQZ basis set, which was large enough to see convergence of the level of electron correlation.[34] As shown in Table 3.4, the calculated binding energies differ by less than 0.01 kcal/mol for the argon-water dimer at values of $r > 3$ Å between the MP2 and the MP4 level. This is in the attractive ($\Phi < 0$) region near the cell center. In the repulsive region, at smaller values of r, with argon closer to the cell boundaries, the errors are somewhat larger, but are proportionally weighted less due to the exponential Boltzmann factor in the configurational integral (see Equation (3.26)).

Table 3.4: Comparison of MP2 and MP4 calculations of the angle-averaged binding energy of an Ar-H_2O pair using the aug-cc-pVQZ basis set.

r (Å)	$\langle E_{cp,\,MP2}(r)\rangle$ (kcal/mol)	$\langle E_{cp,\,MP4}(r)\rangle$ (kcal/mol)
2.4	9.365	9.489
2.8	1.097	1.109
3.2	-0.294	-0.301
3.6	-0.347	-0.352
4.0	-0.230	-0.232

3.5.4 Potential Forms.

Given a numerical argon-water pairwise *ab initio* potential, it is useful to have a mathematical form that can represent the calculated potential accurately. This would allow the potential to be easily implemented in the configurational integral for thermodynamic calculations or for molecular dynamics or Monte Carlo simulations. Figure 3.7 shows the least-squares fit of the angle-averaged *ab initio* potential to a few common two- and three-parameter potential forms, the Lennard-Jones 6-12, Kihara, and Exponential-6 potentials.

Lennard-Jones 6-12:
$$\Phi_{L-J}(r) = 4\varepsilon\left[\left(\frac{\sigma}{r}\right)^{12} - \left(\frac{\sigma}{r}\right)^{6}\right] \tag{3.33}$$

Kihara:
$$\Phi_{Kihara}(r) = 4\varepsilon\left[\left(\frac{\sigma - 2a}{r - 2a}\right)^{12} - \left(\frac{\sigma - 2a}{r - 2a}\right)^{6}\right] \tag{3.34}$$

Exponential-6:
$$\Phi_{Exp-6}(r) = \frac{\varepsilon}{\alpha - 6}\left[6\exp\left(\alpha\left(1 - \frac{r}{r_m}\right)\right) - \left(\frac{r_m}{r}\right)^{6}\right] \tag{3.35}$$

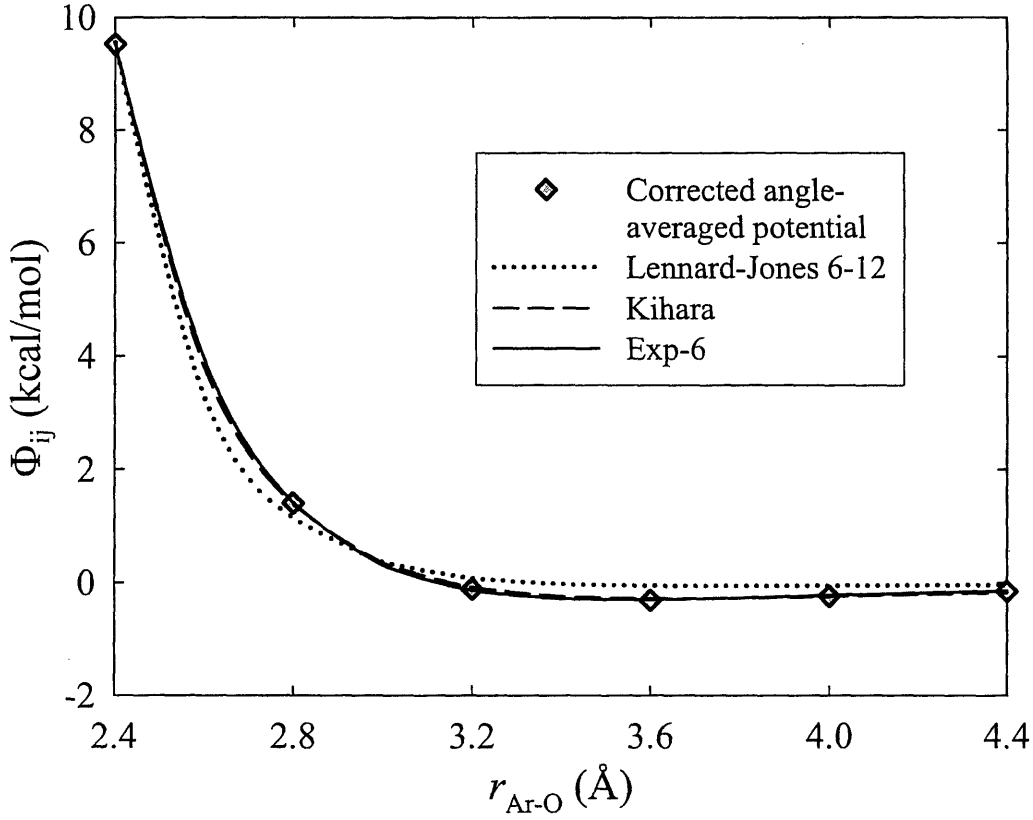

Figure 3.7: Selected potentials forms, Lennard-Jones 6-12, Kihara, and Exp-6, fitted to the *ab initio* calculated Ar-H_2O intermolecular potential.

Figure 3.7 clearly illustrates that the Exponential-6 and the Kihara potential forms provide the best description of the argon-water potential. The best fit for the Kihara potential, however, results in a non-physical negative value for a (-0.418 Å), the repulsive core diameter, so similar to our previous work[18] we conclude that the Exponential-6 potential[35] is the best for this interaction. Therefore, we used the exp-6 form to represent both the **Ar**–**O**H_2 and H_4**C**–**O**H_2 potentials. The Kihara potential form introduces a hard core repulsive effect that is inherently too strong to reproduce accurately the methane-water and argon-water interaction energies. The Kihara potential that best fits the *ab inito* data compensates for this softer core effect by introducing an aphysical attractive core radius (a = -0.418 Å). In a forthcoming paper[36] we report that the Kihara potential can reproduce accurately the methane Langmuir constants for structure I hydrates, but not for structure II, a direct result of this phenomenon. The "hardness" of the Kihara potential for the methane-water interaction in a structure II lattice causes the fitted reference chemical potential[6] to be significantly lower than the value measured by experiment. Further potential parameter adjustment is necessary when modeling systems involving structure I to structure II phase transitions[37], emphasizing the current "*ad hoc*" nature of modeling using such aphysical potential models.

The **Ar**–**H**OH and H_4**C**–**H**OH interactions were characterized by a purely repulsive interaction and modeled using

$$\Phi_{repul}(r) = \frac{B}{r^{12}} \tag{3.36}$$

and the $H_3C\mathbf{H}$–$\mathbf{O}H_2$ interaction modeled using the L-J 6-12 potential. The 500 argon-water *ab initio* energies and the 18,000 methane-water *ab initio* energies were fit to the site-site potentials minimizing χ in the following objective function[13]:

$$\chi = \sum_{i}^{\#\text{ of QM points}} \left[\exp\left(\frac{-\Delta E_{cp,i}}{kT} \right)_{pred} - \exp\left(\frac{-\Delta E_{cp,i}}{kT} \right)_{QM} \right]^2 \tag{3.37}$$

The temperature, T, used in Equation (3.37) was 273 K; however, our sensitivity analysis shows that within the range of temperatures 150-300 K, the choice of T results in deviations of optimum potential parameters of less than 4%. The adjustable parameters in the site-site potentials are the characteristic energy, ε, for both the L-J 6-12 and the exp-6 potentials, the soft core radius, σ, of the L-J 6-12 potential, the radius of minimum energy, r_m, of the exp-6 potential, and B for the repulsive interactions. The α values of the exp-6 potentials were held constant at 12.5 Å for argon and 12.15 Å for methane.

3.5.5 Many-Body Effects.

Many-body interaction effects were also evaluated. In principle, we are interested in estimating the total potential energy for all water molecules in the full cage interacting with a single argon molecule. Due to computational limitations we were only able to calculate many body effects using 10 water molecules in half of the pentagonal dodecahedron – cell A (Figure 3.1a) with a single guest argon at the MP2/aug-cc-pVQZ level. Klauda and Sandler[13] showed at a lower level of accuracy for the CH_4-H_2O system that two half-cell calculations closely resemble the calculation of the full cell. Therefore, we assumed a similar trend would hold for the argon-water system and evaluated a number of partial-cell structures to analyze the many-body effect. Table 3.5 shows the

calculation of the total interaction energy between an argon guest and a structure II pentagonal dodecahedron using various sums of pair and many-body interactions. The quarter cell calculated energies have converged to within 0.04 kcal/mol of the half cell energy and thus will be used in subsequent many-body calculations. The guest molecule was then placed in a number of different configurations within the quarter cell and the interaction energy was calculated for this 6-molecule system.

Table 3.5: Calculation of interaction energy between the entrapped argon guest located at the cell center and full pentagonal dodecahedron cell with 20 host water molecules using half and quarter cell, and sums of pieces of quarter-cells (groups of 2 and 3 waters). Note that only the first shell Ar-H_2O interactions are included.

method of *ab initio* calculation	interaction energy (kcal/mol)
half cell (10 waters)×2	-4.338
quarter cell (5 waters) ×4	-4.371
assembled groups of 2 and 3 waters (20 waters total)	-4.083

The site-site model was then used to calculate the total interaction energy of the many-body system. The water-water interactions within the hydrate lattice are primarily along the cage vertices and the resulting delocalization of electrons along the hydrogen bond will serve to affect the strength of the guest–hydrogen interaction. Consequently, to account for this hydrogen bond effect in the argon-water system, the pairwise *ab initio* site-site potential was corrected by adjusting the characteristic energy, $\varepsilon_{Ar\text{-}H}$, of the **Ar–H**OH L-J potential such that the errors of the predictions of the site-site model w.r.t the *ab initio* quarter cage calculations were minimized. The optimized site-site potential parameters for argon and methane with water are listed in Table 3.6. The results of the predictions of the quarter cell-argon interaction energies using the uncorrected and

corrected site-site potentials are shown in Figure 3.8. Similarly, the methane *ab initio* site-site potential was used to predict the quarter cell–methane interaction energy; however, no correction was needed to represent properly the many-body system. The results of the methane 6-molecule system predicted energies are shown in Figure 3.9.

Table 3.6: Fit potential parameters for the *ab initio* site-site models for Ar – H_2O.

	Exponential-6			repulsive
interaction	ε/k (K)	r_m (Å)	α	B (Å^{12} kcal/mol)
Ar – OH_2	156.8	3.556	12.5	
Ar – HOH				1.259×10^5

Table 3.7: Fit potential parameters for the *ab initio* site-site models for CH_4 – H_2O.

	Exponential-6			repulsive	L-J 6-12	
interaction	ε/k (K)	r_m (Å)	α	B (Å^{12} kcal/mol)	ε/k (K)	σ (Å)
H_4C – OH_2	165.1	3.634	10.15			
H_4C – HOH				2.792×10^5		
H_3CH – OH_2					16.7	2.03

One can see from Figure 3.9 that the methane site-site potential reproduces the interaction energies of the many body system with high accuracy without any correction to the H_4C–HOH potential. Any correction attempt results in a negligible change to $\varepsilon_{C\text{-}H}$. The argon-water interaction is principally dispersive in nature and is much more sensitive to changes in the water electron structure than the methane-water interaction.

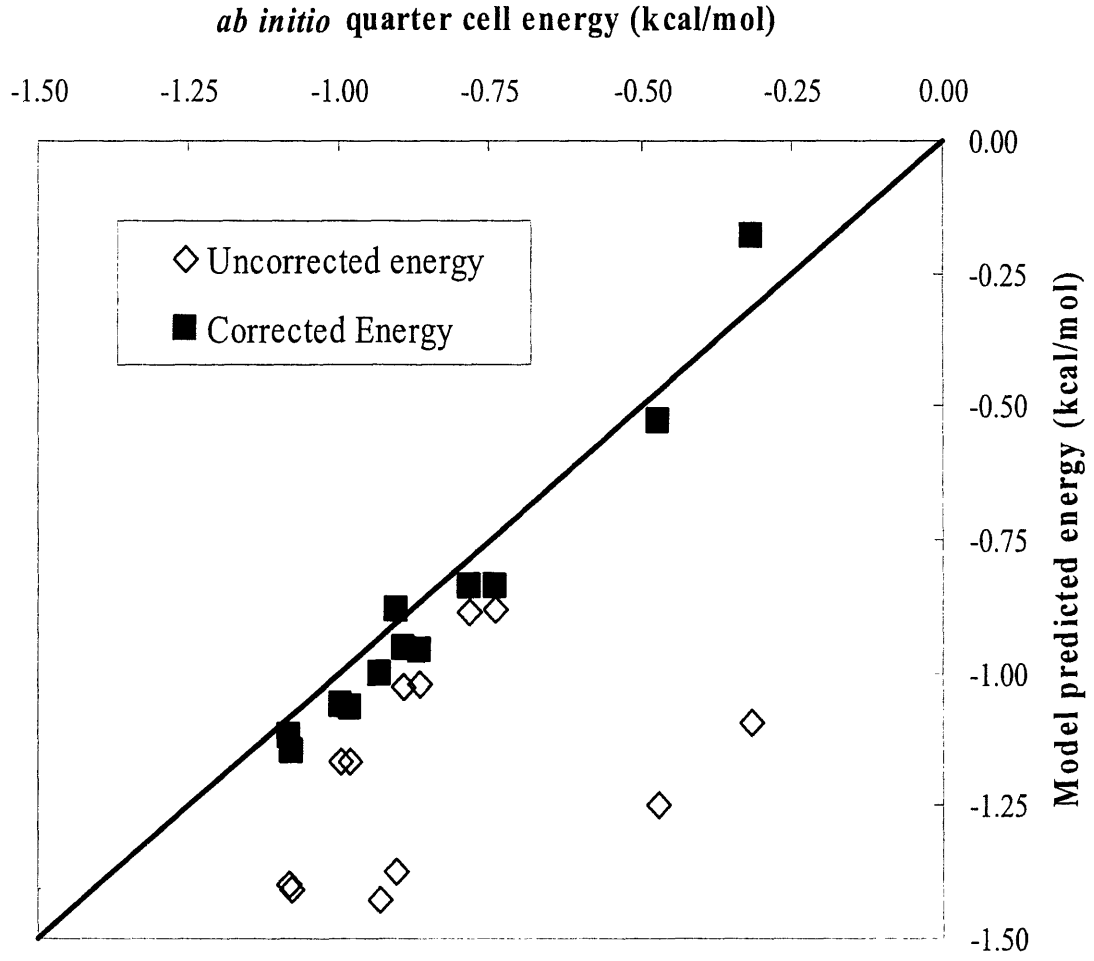

Figure 3.8: Parity plot of the uncorrected and corrected site-site predicted quarter cell–argon interaction energy.

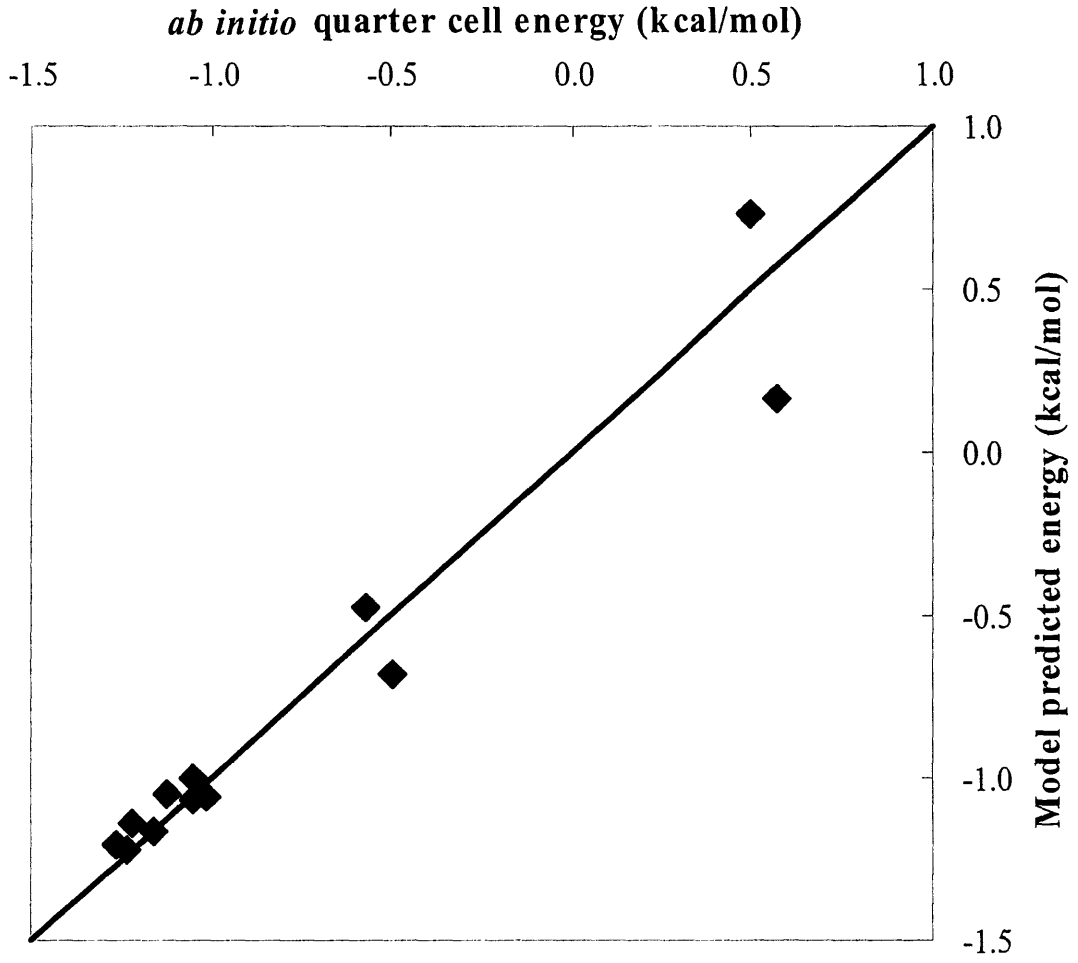

Figure 3.9: Parity plot of the uncorrected site-site predicted quarter cell–methane interaction energies.

3.5.6 Determination of Reference Parameters.

Using the method first developed by Holder et al.[25] and the *ab initio* pair potential for Ar-H_2O interactions we determined the references parameters for a structure II hydrate lattice to be $\Delta\mu_w^0$= 1077±5 J/mol and ΔH_w^0= 1297±11 J/mol (see Figure 3.10). The estimation of the error in the calculation of the reference parameters was found by calculating the 95% confidence intervals on the regression; it slightly underestimates the overall error because experimental errors were not included. The choice of χ in Equation (3.37) will affect the calculated reference parameters; however, over the range of experimental temperatures, the deviations in $\Delta\mu_w^0$ and ΔH_w^0 that result (±4 and ±9 J/mol respectively) are within the 95% confidence intervals. The reference parameter results compare favorably with the structure II reference parameters found by Handa and Tse[38] using thermophysical data from the krypton structure II hydrate. We have also used our method for calculating reference parameters in conjunction with the argon potential found by Tee et al.[39] using second virial coefficients and viscosity data and the potential found by Bickes et al.[40] via molecular-beam differential scattering measurements on argon with water. These results are tabulated in Table 3.8.

Table 3.8: Theoretical empty hydrate reference parameters for structure II hydrates

method of Ar-H_2O interaction	$\Delta\mu_w^0$ (J/mol)	ΔH_w^0 (J/mol)	Sources
2nd Virial/viscosity Kihara	1073	1900	Tee et al.[39]
Molecular-beam scattering L-J 6-12	1180	920	Bickes et al.[40]
Thermophysical properties of krypton SII	1068	764	Handa & Tse[38]
ab initio interaction with many-body correction	1077	1294	This study

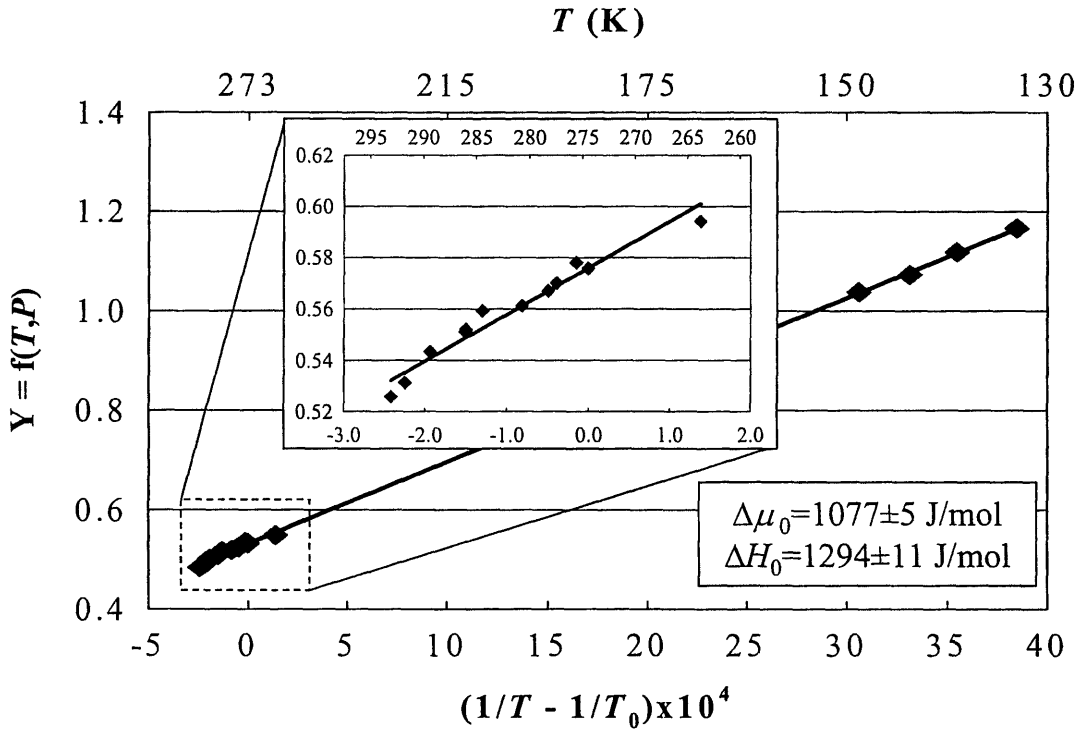

Figure 3.10: Determination of structure II reference parameters using the Holder et al.[25] method, Y=f(T,P) from Eq. , and experimental data from Barrer and Edge[41] and Saito and Kobayashi[42].

This process was repeated for structure I using the calculated *ab initio* site-site potential for methane and water and the reference parameters were determined to be be $\Delta\mu_w^0$= 1203±3 J/mol and ΔH_w^0= 1170±19 J/mol. These results, along with the above structure II results are listed in Table 3.1.

3.5.7 Phase Equilibrium Calculations.

Using the regressed reference parameters given in Figure 3.10 and Table 3.8 for a structure II hydrate, we are now able to reproduce experimental equilibrium data for the argon-water clathrate. Figures 3.11 and 3.12 demonstrate the robustness of the method employed in this paper. The model agrees with experimental results to ±3% over a wide temperature (133-293 K) and pressure range (0.3-850 bar). The reference parameters listed in Table 3.8 were used in for phase equilibria calculations plotted in Figure 3.12 for the three different Ar - H_2O potentials.

The methane-water site-site potential in conjunction with the calculated structure I reference parameters leads to a 3.5% absolute average deviation (AAD) from experimental data. This match is achieved with only two adjustable parameters, $\Delta\mu_w^0$ and ΔH_w^0, that we will show in a forthcoming paper on hydrate cell potentials to be applicable to not only the methane hydrate system but for other structure I hydrate formers[36]. Using the LJD approximation and Sloan's[6] Kihara parameters the AAD is 11% and Klauda and Sandler[13] report an AAD of 3.35% for structure I methane hydrate. The Klauda and Sandler[13] method uses three parameters to fit the pure data, while we achieve 3.5% AAD using two parameters that are applicable to other hydrate systems. The Klauda and Sandler methane potentials are dependent on the cage and the values for

ε in the L-J 6-12 potential vary by as much as 15% with the chosen cage. Our methane and argon potentials are independent of structure and location and should be applicable to any condensed aqueous system.

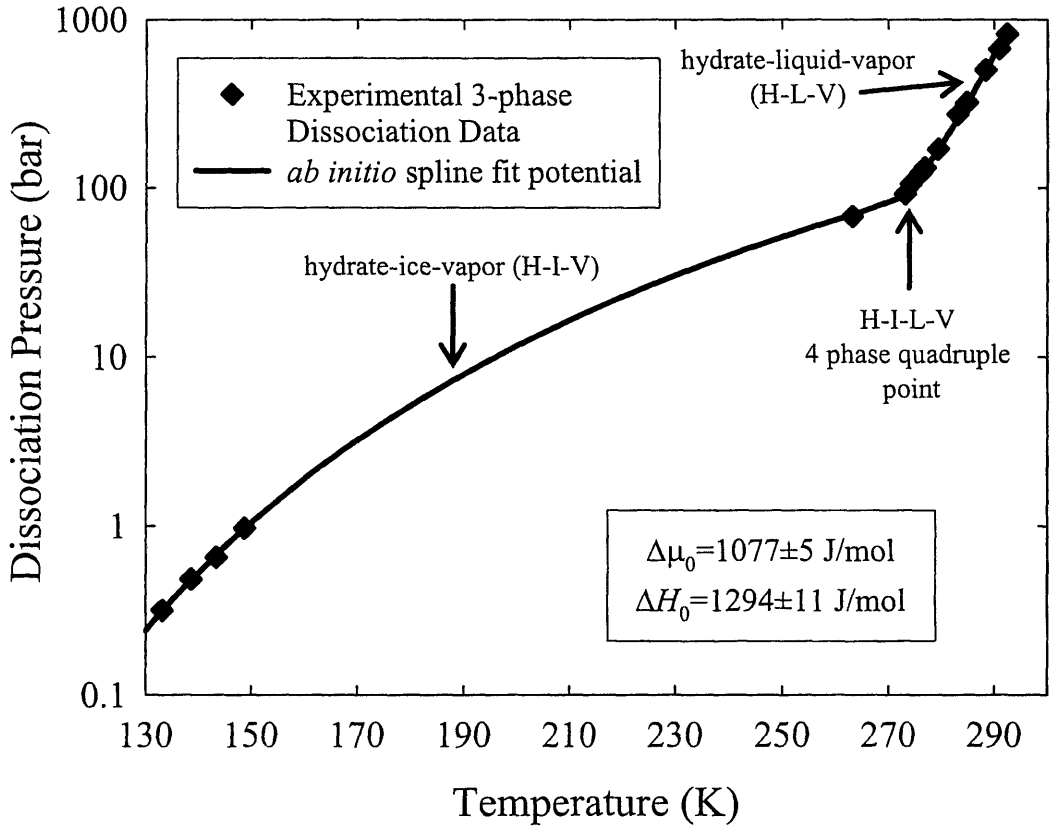

Figure 3.11: Calculation of argon three-phase equilibrium dissociation pressures using the corrected *ab initio* site-site potential with the regressed structure II reference parameters. Experimental data are from Barrer and Edge[41] and Saito and Kobayashi[42].

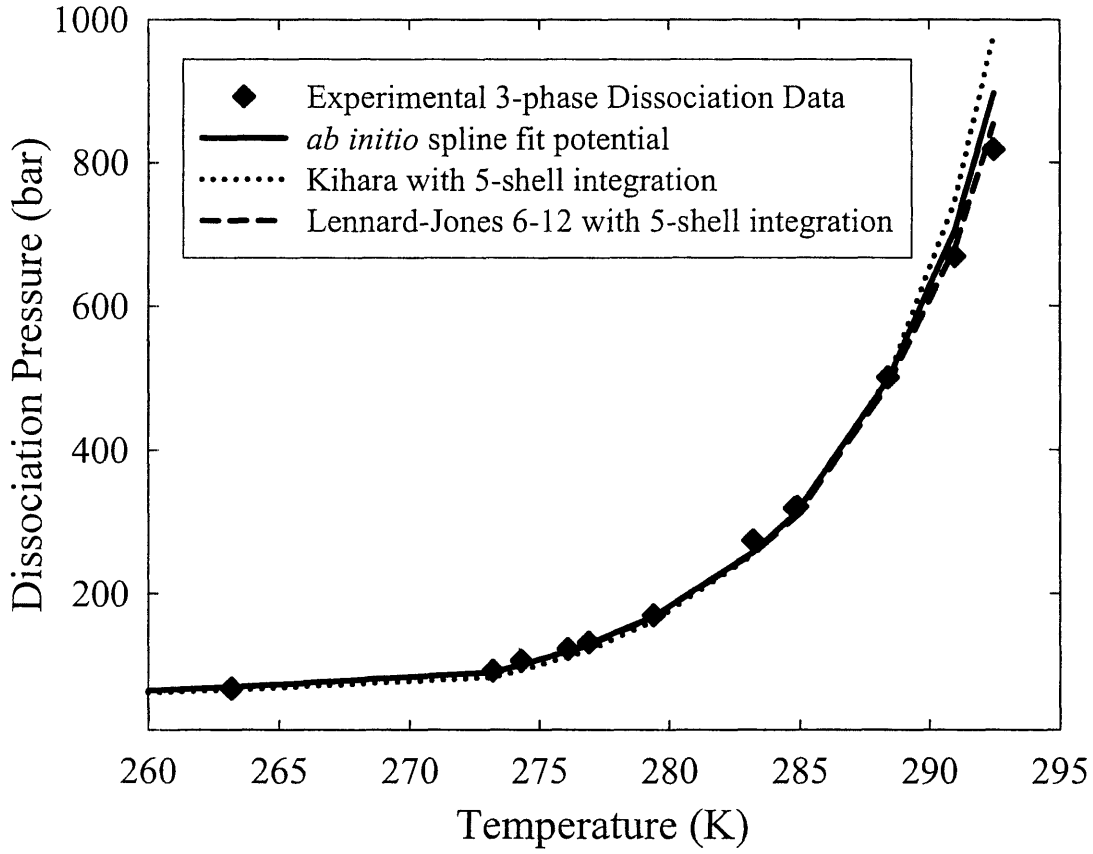

Figure 3.12: Comparison of experimental 3-phase equilibrium dissociation pressures[41,42] for the argon hydrate system with predictions using the *ab initio* potential developed in this study, the Kihara potential found by Tee, et al[39] and the L-J 6-12 parameters found by Bickes, et al[40].

3.5.8 Methane Cage Occupancies.

Cage occupancies have been measured using Raman spectroscopy and nuclear magnetic resonance (NMR) techniques.[43-45] These techniques rely on the integration of signal intensities characteristic of guests occupying different cages. The ratios of the integrated intensities reproduce the ratios of the occupancies of the guest in the lattice cages, scaled by the ratio of the total number of cages in a unit cell. Ripmeester and Ratcliffe[43] used NMR to study the occupancy ratios of methane and methane-propane hydrates. The pure methane hydrate occupancy ratio, θ_S/θ_L was measured to be 0.916, where θ_L and θ_S are large- and small-cage occupancies respectively. The hydrate samples were conditioned for ~3 months at 233 K and then for ~1 week at 260 K. They were then cooled to 77 K and placed into the NMR probe that had been cooled to ~193 K. Using this procedure, the hydrate should exhibit properties of a hydrate conditioned at 260 K, and this is the temperature that was used by Ripmeester and Ratcliffe to calculate the absolute occupancies. We used the Klauda and Sandler[13] method to calculate θ_S/θ_L(193K)=0.84 as they did and then using their potential results in θ_S/θ_L(260 K)=0.84.

Uchida et al.[45] measured methane hydrate occupancy using Raman spectroscopy at pressures above the equilibrium pressure. However, the specific pressure at which the samples were conditioned cannot be determined from their paper. The reaction vessel was pressurized to the specific pressure then as the hydrate formed the pressure dropped. The final pressure is the pressure of importance, though the "specific" pressure is reported. Moreover, with increasing pressure they report a decreasing θ_S/θ_L, which is contrary to expectations. Sum et al. also used Raman spectroscopy to measure methane cage occupancies at the equilibrium pressure.[44] Using our methane *ab initio* site-site

model, we calculate the occupancy ratios reported by the Ripmeester[43] and Sum[44] groups as detailed in Table 3.9.

Table 3.9: Occupancy ratio, θ_S/θ_L of methane structure I hydrates. CSMHYD indicates the phase equilibria program included in Sloan, 1998.[6]

temperature (K)	experimental value[43,44]	CSMHYD[6]	this study
260	0.916 ± 0.01	0.910	0.920
273.65	0.947 ± 0.02	0.900	0.906
274.65	0.925 ± 0.02	0.904	0.910
275.65	0.892 ± 0.03	0.908	0.914
276.65	0.890 ± 0.01	0.912	0.917

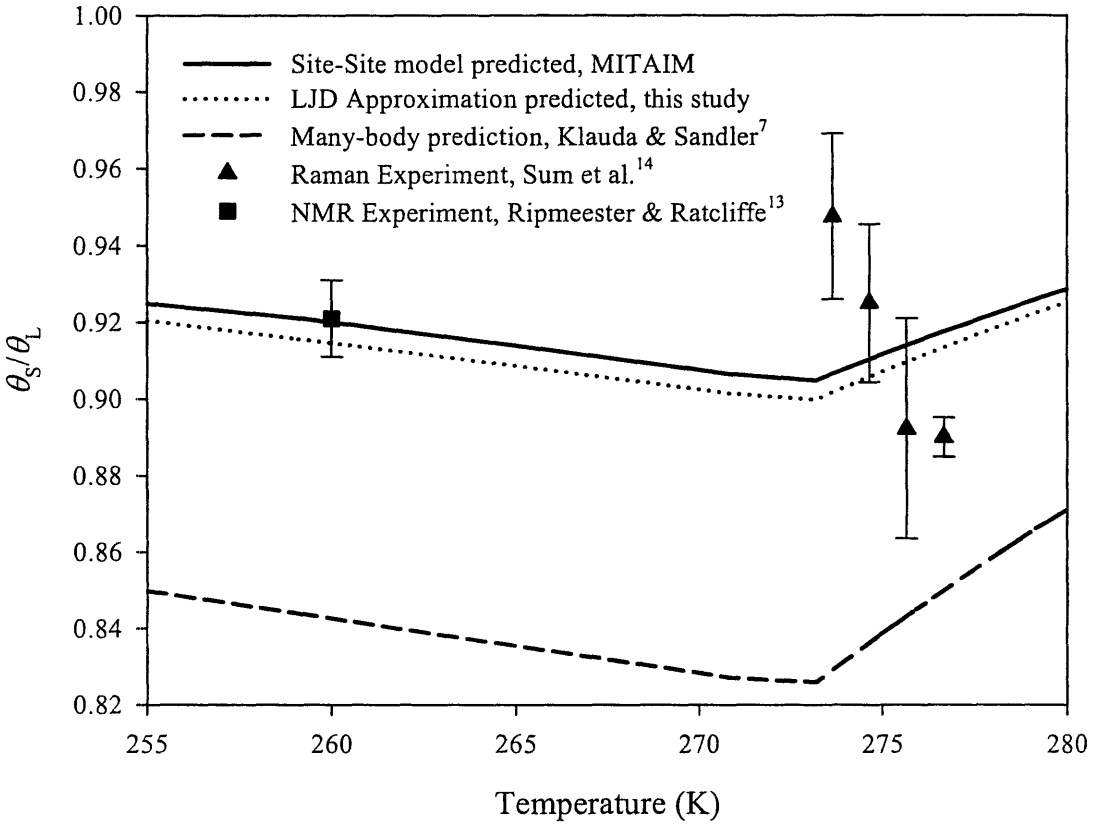

Figure 3.13 : Temperature dependence of the ocupancy ratio θ_S/θ_L of methane structure I hydrates.

3.5.9 Mixed Hydrate Phase Equilibrium.

Because argon preferentially forms a structure II hydrate while methane preferentially forms a structure I hydrate, there should be a surface in the argon-methane-water phase diagram where a structural change would occur. We can calculate and predict where this structural change would occur. The ability of our model to predict phase equilibria in the mixed argon-methane hydrate provides an independent test of our intermolecular potentials and calculated reference parameters of the two hydrate structures as shown in Figure 3.14. Figure 3.14 also illustrates where the structural transition is predicted based on thermodynamic equilibrium.

Within the experimental temperature range, the structure I to structure II transition occurs near 0.4 mol fraction methane. Because the difference in free energy of the two structures near 40% methane is very small, a particular solid hydrate phase once formed could remain in a metastable state even after entering the stable region for the other structure. In other words, if one were to add argon gas to a system in which a structure I hydrate had already been formed with methane as a guest gas, it could continue to crystallize as a structure I hydrate. In general, the structure that would result from nucleating a mixture of argon and methane could be governed by kinetics. Figure 3.15 demonstrates the ability of this model to predict the structural transition that is likely to exist when the composition of an argon-methane gas mixture is changed.

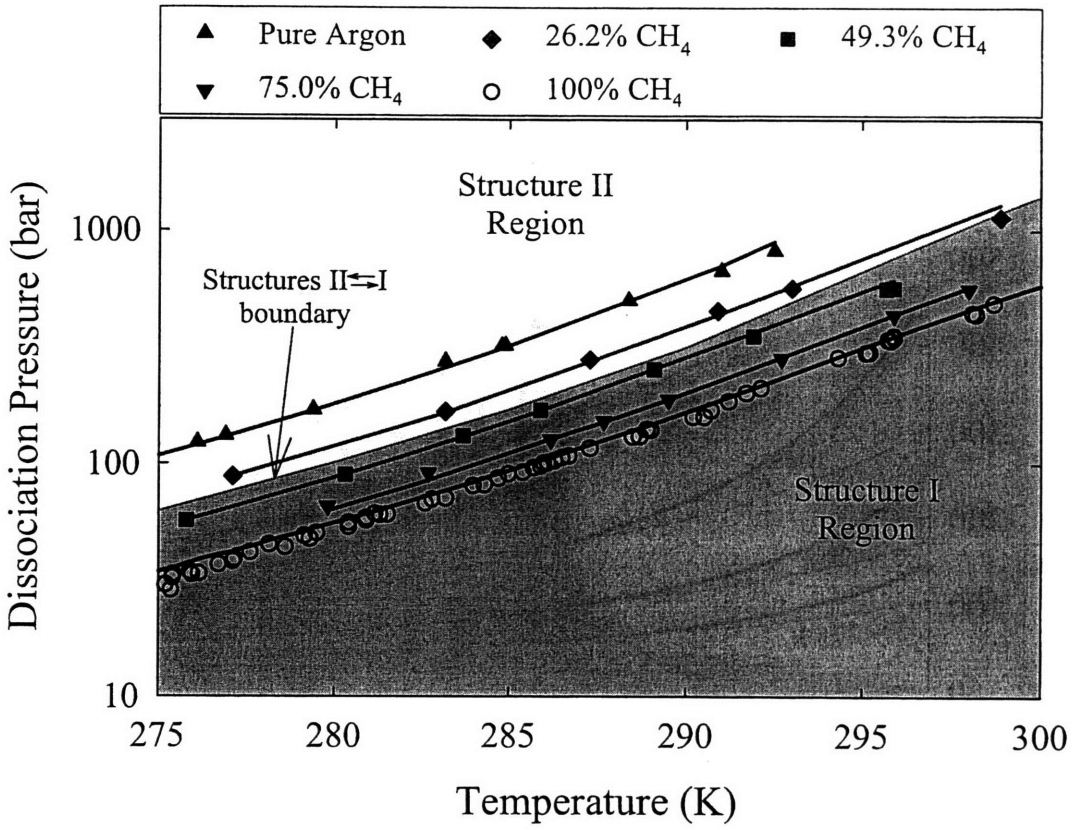

Figure 3.14: Prediction dissociation pressure of mixed CH_4-Ar hydrate in a using the calculated *ab initio* potential for both guest species. Experimental data are given for pure Ar (+), 26.2% CH_4 (■), 49.3% CH_4 (▲), 75% CH_4 (♦), 100% CH_4 (○). Predictions (—) are calculated using the lowest energy structure.

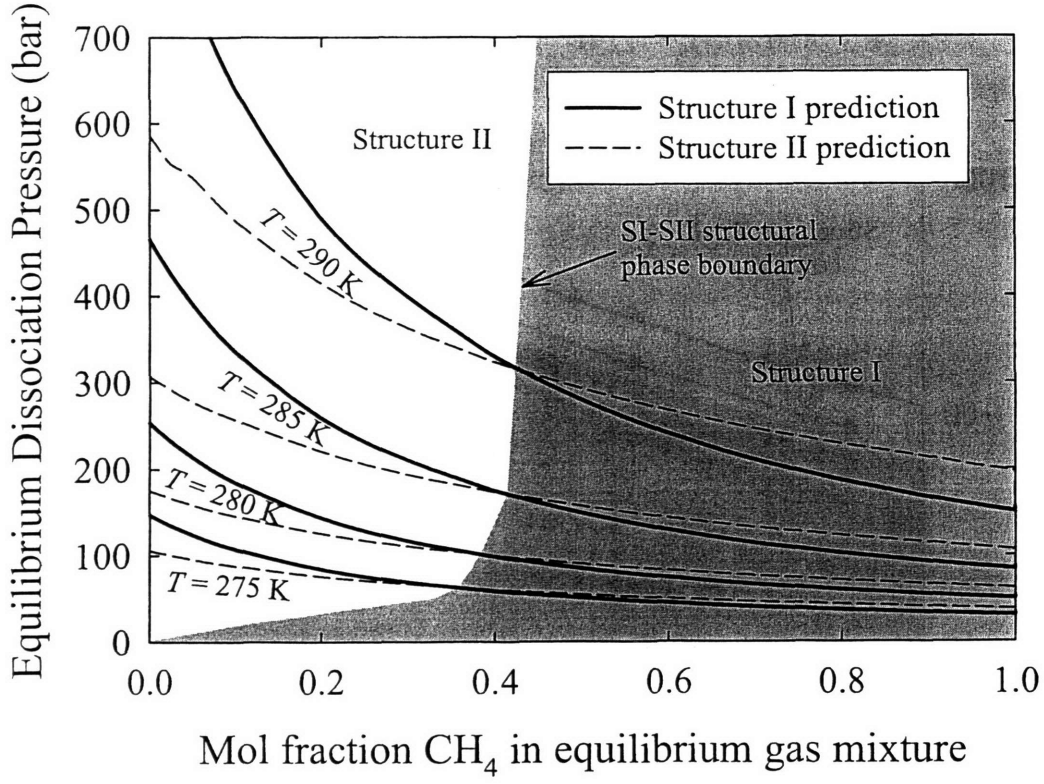

Figure 3.15: Prediction of structural changes in a mixed Ar-CH_4 hydrate at 275, 280, 285, and 290 K. Solid lines are structure I and dotted lines are structure II predicted dissociation pressures for the 3-phase (hydrate-water rich liquid-gas mixture) monovariant systems.

3.6 Conclusions

Accurate quantum mechanical calculations were performed to quantify argon-water interactions for use in modeling the condensed gas hydrate system. Convergence to within 0.01 kcal/mol in the attractive region was reached for the argon-water binary system at the MP2/aug-cc-pVQZ level of correlation and basis-set. A site-site potential was developed that characterizes the three-dimensional hyperspace energy surface of the argon-water interaction and the six-dimensional surface for methane-water interactions. Many-body effects can be significant in the argon-water system due to the delocalization of electrons along the hydrogen bonds. These effects were accounted for by fitting the **Ar–H**OH potential characteristic energy to quantum mechanical calculations on systems with up to five water molecules interacting with the argon. The many-body effects are negligible in the methane-water system when our methane-water site-site potential is used. Precise values for structure II reference parameters, $\Delta\mu_w^0$=1077±5 kcal/mol and ΔH_w^0=1294±11 kcal/mol and structure I reference parameters, $\Delta\mu_w^0$=1203±3 kcal/mol and ΔH_w^0=1170±19 kcal/mol (errors evaluated using 95% confidence intervals), were found using the *ab initio* site-site potentials. Using these reference values together with the *ab initio* site-site potentials, the equilibrium dissociation pressure was computed within ±3% of the experimental value for pure argon hydrates and within ±3.5% of the experimental value for methane hydrates. Over the temperature range studied, we verified that argon forms structure II hydrates as opposed to structure I hydrates. Methane cage occupancies were predicted to within ±5% of experimental values. Phase equilibria for the mixed hydrate of argon and methane were predicted within ±3.4% without any

fitting parameters. Also the existence of structure I to structure II phase transitions was determined using our *ab initio* approach.

3.7 References

(1) van der Waals, J. H.; Platteeuw, J. C. *Adv. Chem. Phys.* **1959**, *2*, 1.
(2) Peng, D.-Y.; Robinson, D. B. *Ind. Eng. Chem. Fund.* **1976**, *15*, 59.
(3) Sparks, K. A.; Tester, J. W. *Journal of Physical Chemistry* **1992**, *96*, 11022.
(4) Sparks, K. A.; Tester, J. W.; Cao, Z. T.; Trout, B. L. *Journal of Physical Chemistry B* **1999**, *103*, 6300.
(5) Holder, G. D.; John, V. T.; Yen, S. "Geological implications of gas production from In-situ gas hydrates"; SPE/DOE symposium on unconventional gas recovery, 1980.
(6) Sloan, E. D., Jr. *Clathrate hydrates of natural gases - 2nd ed., rev. and expanded*; Marcel Dekker, Inc.: Monticello, 1998.
(7) Hammerschmidt, E. G. *Ind. Eng. Chem.* **1934**, *26*, 851.
(8) Fowler, R. H.; Guggenheim, E. A. *Statistical Thermodynamics*; Cambridge University Press, 1952.
(9) John, V. T.; Papadopoulos, K. D.; Holder, G. D. *AIChE J* **1985**, *31*, 252.
(10) Sparks, K. A. Configurational properties of water clathrates through molecular simulation, PhD Thesis, Massachusetts Institute of Technology, 1991.
(11) Bazant, M. Z.; Trout, B. L. *Physica A* **2001**, *300*, 139.
(12) John, V. T.; Holder, G. D. *J. Phys. Chem.* **1985**, *89*, 3279.
(13) Klauda, J. B.; Sandler, S. I. *Journal of Physical Chemistry B* **2002**, *106*, 5722.
(14) Cao, Z.; Tester, J. W.; Trout, B. L. *J. Chem. Phys.* **2001**, *115*, 2550.
(15) Jorgensen, W. L.; Madura, J. D.; Swenson, C. J. *J. Am. Chem. Soc.* **1984**, *106*, 6638.
(16) Sun, Y.; Kollman, P. A. *J. Comp. Chem.* **1995**, *16*, 1164.
(17) Cao, Z. T.; Tester, J. W.; Sparks, K. A.; Trout, B. L. *J. Phys. Chem. B.* **2001**, *105*, 10950.
(18) Cao, Z. T.; Tester, J. W.; Trout, B. L. *J. Chem. Phys.* **2001**, *115*, 2550.
(19) Barrer, R. M.; Ruzicka, D. J. *Trans. Faraday Soc.* **1962**, *58*, 2253.
(20) Sortland, L. D.; Robinson, D. B. *Canadian Journal of Chemical Engineering* **1964**, *42*, 38.
(21) Child, W. C., Jr. *J. Phys. Chem.* **1964**, *68*, 1834.
(22) Parrish, W. R.; Prausnitz, J. M. *Industrial & Engineering Chemistry Process Design and Development* **1972**, *11*, 26.
(23) Holder, G. D.; Katz, D. L.; Hand, J. H. *AAPG Bulletin-American Association of Petroleum Geologists* **1976**, *60*, 981.
(24) Dharmawardhana, P. B.; Parrish, W. R.; Sloan, E. D. *Industrial & Engineering Chemistry Fundamentals* **1980**, *19*, 410.
(25) Holder, G. D.; Malekar, S. T.; Sloan, E. D. *Ind. Eng. Chem. Fundam.* **1984**, *23*, 123.
(26) Davidson, D. W.; Handa, Y. P.; Ripmeester, J. A. *Journal of Physical Chemistry* **1986**, *90*, 6549.
(27) Handa, P. Y.; Tse, J. S. *J. Phys. Chem.* **1986**, *90*, 5917.
(28) Cao, Z. T.; Tester, J. W.; Trout, B. L. *Journal of Physical Chemistry B* **2002**, *106*, 7681.

(29) Dunning, T. H. *Journal of Physical Chemistry A* **2000**, *104*, 9062.
(30) Tsuzuki, S.; Uchimaru, T.; Matsumura, K.; Mikami, M.; Tanabe, K. *Journal of Chemical Physics* **1999**, *110*, 11906.
(31) Truhlar, D. G. *Chemical Physics Letters* **1998**, *294*, 45.
(32) Varandas, A. J. C. *Journal of Chemical Physics* **2000**, *113*, 8880.
(33) Chakravorty, S. J.; Davidson, E. R. *Journal of Physical Chemistry* **1993**, *97*, 6373.
(34) Feller, D. *Journal of Chemical Physics* **1999**, *111*, 4373.
(35) Ree, F. H. *Simple molecular systems at very high density*; Plenum: New York, 1989.
(36) Anderson, B. J.; Bazant, M. Z.; Tester, J. W.; Trout, B. L. *Journal of Physical Chemistry B in press* **2004**.
(37) Ballard, A. L.; Sloan, E. D. *Gas Hydrates: Challenges for the Future* **2000**, *912*, 702.
(38) Handa, Y. P.; Tse, J. S. *Journal of Physical Chemistry* **1986**, *90*, 5917.
(39) Tee, L. S.; Gotoh, S.; Stewart, W. E. *Industrial & Engineering Chemistry Fundamentals* **1966**, *5*, 363.
(40) Bickes, R. W.; Scoles, G.; Smith, K. M. *Canadian Journal of Physics* **1975**, *53*, 435.
(41) Barrer, R. M.; Edge, A. V. J. *Proc. Roy. Soc.* **1967**, *London A300*, 1.
(42) Saito, S.; Kobayashi, R. *AIChE Journal* **1965**, *11*, 96.
(43) Ripmeester, J. A.; Ratcliffe, C. I. *Journal of Physical Chemistry* **1988**, *92*, 337.
(44) Sum, A. K.; Burruss, R. C.; Sloan, E. D. *Journal of Physical Chemistry B* **1997**, *101*, 7371.
(45) Uchida, T.; Hirano, T.; Ebinuma, T.; Narita, H.; Gohara, K.; Mae, S.; Matsumoto, R. *Aiche Journal* **1999**, *45*, 2641.

Chapter 4. Application of the Cell Potential Method to Predict Phase Equilibria of Multi-Component Gas Hydrate Systems

4.1 Introduction

Despite the large database of experimental clathrate phase behavior[1], the theory of clathrates is not well developed and still relies heavily on the *ad hoc* fitting of experimental data. The commonly used fitting procedures can usually reproduce the input data, but have poor predictive ability outside of the range of fitting. The thermodynamic reference parameters that are commonly used while fitting intermolecular potential parameters to the experimental data[1,2] differ greatly from reference parameters that are determined experimentally[3] or computationally[4]. When these procedures are used in attempts to predict hydrate formation from gas mixtures, the intermolecular potential and reference parameters typically need adjusting[2] to reproduce accurately phase equilibria and structural transitions.

Recently, Bazant and Trout showed that the inverse temperature dependence of the Langmuir constant for natural gas hydrates contains all the necessary information to determine intermolecular potentials[5]. Starting from the van der Waals and Platteeuw statistical model[6], cell potentials can be directly and unambiguously extracted from experimental equilibrium data by solving an integral equation analytically. The resulting potentials are physically meaningful and much simpler than the numerically fit Kihara potentials[7]. Finally, given the simplicity of the spherically averaged cell potential, hydrate phase equilibria information can be calculated without the use of numerical integration techniques. When used in conjunction with reference parameters and

intermolecular potentials calculated using *ab initio* methods[4] no fitting parameters are necessary.

This chapter illustrates the validation of the use of the cell potential method by testing its predictive ability against experimental results, and then uses the method to make predictions that await experimental testing. In sections 4.2 and 4.3, we review the classical statistical-mechanical description of hydrates, which relates Langmuir constants to the cell potential of guest molecules. Our method is reviewed in section 4.4, where we obtain the cell potential from an exact solution to an integral equation. For comparison with other methods, in section 4.6 we compute cell potentials for ethane hydrates using standard fitting procedures. In section 4.7, we apply our method to determine cell potentials for a variety of clathrates systems. We also fit commonly used empirical intermolecular potentials to our analytical cell potentials to evaluate the validity of the former in reproducing the temperature dependence of Langmuir constants. In section 4.8, we test our cell potentials by predicting phase equilibria for mixed gas hydrates, including structures that have not yet been observed experimentally. We summarize our results and comment on their implications in section 4.9.

4.2 Hydrate Phase Chemical Potential Model

A thermodynamic model corresponding to the three-dimensional generalization of ideal localized adsorption was proposed in 1959 by van der Waals and Platteeuw[6]. By assuming single guest occupancy of the available water cages, neglecting variations in guest-guest interactions, and assuming negligible distortions of the empty lattice, the difference in chemical potential between clathrate and empty host lattice can then be expressed as

$$\Delta\mu^{\beta-H} = kT\sum_i \nu_i \ln(1+\sum_J C_{Ji}\hat{f}_J) \tag{4.38}$$

where ν_i is the number of type i cavities per water molecule, $\hat{f}_J$ is the fugacity of guest molecule J in the gas or liquid phase, which can, for example, be calculated from a mixture form of a *PVTN* Peng-Robinson equation of state[8], and C_{Ji} is the Langmuir constant for a guest molecule J in a cavity of type i defined as

$$C_{Ji} \equiv \frac{Z_{Ji}}{kT} = \frac{1}{8\pi^2 kT}\int_V \exp(-\Phi(r,\theta,\phi,\alpha,\beta,\gamma)/kT) r^2 \sin\theta\, dr\, d\theta\, d\phi\, d\alpha\, d\beta\, d\gamma \tag{4.39}$$

where Z_{Ji} is the full configurational integral, which depends on the total interaction potential $\Phi = \sum_{ij}\Phi_{ij}$ between guest and host molecules[9,10] and is, in general, a function of r, θ, and ϕ, the spherical coordinates of the guest molecule, and α, β, and γ, the Euler angles that describe the orientation of the guest. In order to calculate the configurational integral accurately, the total interaction potential between the guest molecule and all of the host water molecules must be represented properly. In early work the potential was approximated by a two-parameter spherically symmetric Lennard-Jones potential[6]. Later, a Kihara potential, with three parameters, was used to improve accuracy. However, these empirically fitted potentials are not fundamentally based on the guest-host interactions, have been shown to be aphysical, and do not match those determined using gas-phase experimental data[1,11,12]. Our work is based on computing physically relevant intermolecular potentials directly from *ab initio* calculations and from single component phase data. Given intermolecular interaction potentials, the chemical phase equilibrium is calculated by methods described in our earlier work[4,13] and reference state values for

$\Delta\mu_w^0 \equiv \Delta\mu_w^{\beta-\alpha}(T_0,0)$, $\Delta H_w^0 \equiv \Delta H_w^{\beta-\alpha}(T_0)$, $\Delta C_{p,w}^{\beta-L,\alpha}(T_0)$, and $\Delta V_w^{\beta-L,\alpha}(T_0)$ used are found in Table 4.1.

Table 4.1: Thermodynamic Reference Properties for Structure I and II hydrates: T_0 = 273.15 K

	structure I	structure II	source
$\Delta\mu_w^0$ (J/mol) [a]	1203	1077	4
ΔH_w^0 (J/mol)	1170	1294	4
$\Delta V_w^{\beta-\alpha}$ ($m^3 \cdot mol^{-1}$)	3.0×10^{-6}	3.4×10^{-6}	14
$\Delta H_w^{L-\alpha}$ (J/mol)	6009.5		
$\Delta V_w^{L-\alpha}$ ($m^3 \cdot mol^{-1}$)	-1.598×10^{-6}		
$\Delta C_p^{\beta-L}$ (J/mol·K)	$-37.32 + 0.179(T - T_0)$		15
$\Delta C_p^{\beta-\alpha}$ (J/mol·K)	$0.565 + 0.002(T - T_0)$		15

[a] superscripts/subscripts
w = water
^{0} = reference state
β = empty hydrate lattice
α = ice phase
L = liquid phase

4.3 Calculating the Configurational Integral

Typically, the van der Waals and Platteeuw (vdWP) model[6] is used in conjunction with the spherical-cell approximation to estimate the configurational integral. This approach is analogous to the approximation made by Lennard-Jones and Devonshire is the case of liquids[16]. In the spherical-cell (SC) approximation, the intermolecular potential Φ is replaced by a spherically-averaged cell potential[6,16], reducing the multi-dimensional configurational integral in Equation (4.39) to one-dimension, thus resulting in the following relationship between the potential, $w(r)$, and the Langmuir constant,

$$C_{Ji} = \frac{4\pi}{kT}\int_0^R e^{-w(r)/kT} r^2 dr \tag{4.40}$$

where the cutoff distance R is taken at the average radius of the cage. The exact value of R is rarely significant, because at the temperatures at which clathrates form, the high-energy, repulsive portion of the integral for $r \approx R$ provides a negligible contribution. The spherically symmetric cell potential, $w(r)$, can be determined by angle averaging:

$$w(r) = \frac{1}{4\pi} \int_0^{2\pi} \int_0^{\pi} \Phi_{ij}(r_{ij}, \theta, \phi) \sin\theta \, d\theta \, d\phi \tag{4.41}$$

Applying Equation (4.41) over the first coordination shell to the Kihara potential[17],

$$\begin{aligned} \Phi_{ij}^{K}(r) &= \infty && r \le 2a \\ \Phi_{ij}^{K}(r) &= 4\varepsilon \left[\left(\frac{\sigma - 2a}{r_{ij} - 2a} \right)^{12} - \left(\frac{\sigma - 2a}{r_{ij} - 2a} \right)^{6} \right] && r > 2a \end{aligned} \tag{4.42}$$

yields the following form for $w(r)$:

$$w(r) = 2z\varepsilon \left[\frac{\sigma^{12}}{R^{11} r} \left(\delta_{10} + \frac{a}{R} \delta_{11} \right) - \frac{\sigma^{6}}{R^{5} r} \left(\delta_{4} + \frac{a}{R} \delta_{5} \right) \right] \tag{4.43}$$

where

$$\delta_N = \frac{1}{N} \left[\left(1 - \frac{r}{R} - \frac{a}{R} \right)^{-N} - \left(1 + \frac{r}{R} - \frac{a}{R} \right)^{-N} \right] \tag{4.44}$$

and z is the coordination number, R again is the average cage radius, and σ, ε, and a are the Kihara parameters. The Kihara parameters are generally determined by numerically fitting monovariant phase equilibrium data[1,18]. The resulting Kihara parameters are not unique: many different sets of (ε, σ, and a) values can fit the experimental data well. Furthermore, these fitted Kihara parameters do not match those obtained by fitting other experimental data, such as second virial coefficient, gas viscosity, and molecular beam scattering data[1].

4.4 Inversion of Langmuir Curves

To numerically regress experimental data to preset functional forms, such as the Kihara potential, makes use of awkward and unnecessarily complex equations (Equations (4.43) and (4.44)) and, at any rate, leads to aphysical results. Therefore, it would be preferable to find a functional form of the interatomic potential without requiring any *ad hoc* assumptions, *a priori*. Ideally, this approach should also provide accurate predictions of the properties of mixed guest systems without refitting any potential or reference parameters.

Earlier, Bazant and Trout[5] described such a method by which the functional form of the inter-molecular potential can be found by solving Equation (2.19) analytically for $w(r)$. First, Equation (2.19) is restructured as

$$C_{Ji}(\beta) = 4\pi\beta \int_0^\infty e^{-\beta\, w(r)} r^2 dr \tag{4.45}$$

where $\beta = 1/kT$. The upper limit of integration is extended to $R = \infty$, which introduces negligible errors due to the low temperatures accessible in clathrate experiments.

In order to invert Equation (2.24), a functional form of $C_{Ji}(\beta)$ must be found. We do this by computing $C_{Ji}(\beta)$ from experimental data and *ab initio* data (Sections 4.4.1 and 4.4.2) and fitting the computed values of $C_{Ji}(\beta)$ to a functional form (Section 4.4.3).

4.4.1 Hydrates That Occupy Only the Large Cage

In order to calculate Langmuir constants directly from the experimental dissociation data without ambiguity it is necessary to focus on clathrate-hydrates for which only the larger of the two sets of cavities are occupied by the guest molecules.

These include ethane, cyclopropane, propane, isobutane, and certain CFC water clathrates. With single occupancy Equation (4.38) reduces to

for structure I $$\frac{\Delta\mu_w^{\beta-H}}{kT} = \frac{3}{23}\ln(1+C_{J,2}\hat{f}_J) \tag{4.46}$$

for structure II $$\frac{\Delta\mu_w^{\beta-H}}{kT} = \frac{1}{17}\ln(1+C_{J,2}\hat{f}_J) \tag{4.47}$$

The "experimental" Langmuir constants can then be obtained by solving for the C_{Ji}'s in Equations (4.46) and (4.47), and using the fact that at three-phase vapor, hydrate (*H*), and ice (α) or liquid water (*L*) equilibrium at a specified temperature, $\Delta\mu_w^{\beta-H} = \Delta\mu_w^{\beta-L,\alpha}$.

for structure I $$C_{J2} = \frac{\exp\left(\frac{23}{3}\Delta\mu_w^{\beta-L,\alpha}/kT\right)-1}{\hat{f}_J} \tag{4.48}$$

for structure II $$C_{J2} = \frac{\exp\left(\frac{17}{1}\Delta\mu_w^{\beta-L,\alpha}/kT\right)-1}{\hat{f}_J} \tag{4.49}$$

where $\hat{f}_J$ is calculated for the fluid phase from the $P\underline{V}TN_i$ mixture form of the Peng-Robinson equation of state[8], used to represent the $P\underline{V}TN_i$ properties of the fluid phase. This equation provides a simple way to relate the "experimental" Langmuir constant of a type *J* guest in the larger cavity to $\hat{f}_J$, the fugacity of guest component *J*, and $\Delta\mu_w^{\beta-H}$, the chemical potential difference between water in the hypothetical empty hydrate, and water in either an aqueous liquid phase or ice phase.

4.4.2 Hydrates That Occupy Both Large and Small Cages – Using Ab Initio Data

The procedure discussed above cannot be applied directly to the methane-water clathrate system or the argon-water clathrate system because methane and argon occupy

both the small and the large cages in the structure I and structure II clathrates formed by the simple hydrates of methane and argon respectively. Thus, there are two terms on the right side of Equation (4.38), and a single set of monovariant phase data cannot be used to determine uniquely the two C_{Ji}'s in Equation (4.38). Consequently, we need another method for obtaining the Langmuir constants of these systems. Using the *ab initio* potentials developed by Cao et al.[19-22] and Anderson et al.[4] is just such a method. Here, we use these to calculate the Langmuir constant at various temperatures by integrating the full 6-dimensional configurational integral over 5 hydrate shells. This method allows us to compute the Langmuir constant not only for the cages of the structure I hydrate, but also for the cages of the theoretical (unstable) structure II methane hydrate. Methane does not form a structure II hydrate as a simple (pure) hydrate[1], but will form a structure II hydrate with other hydrate guests[1,23-26]. Using these *ab initio* Langmuir constants, cell potentials were determine for methane and argon.

4.4.3 Functional Form of "Experimental" Langmuir Constants

Typical sets of experimental Langmuir constant data are described well by a van't Hoff temperature dependence, given by,

$$C(\beta) = C_0 e^{m\beta} \tag{4.50}$$

where C_0 and m are specific to guest molecule J and cavity i. This empirical van't Hoff behavior is illustrated in Figure 2 of Bazant and Trout[5] and could be anticipated using general thermodynamic considerations[27]. Combining Equations (2.24) and (4.50) yields

$$C_0 e^{m\beta} = 4\pi\beta \int_0^\infty e^{-\beta w(r)} r^2 dr \tag{4.51}$$

a well-posed integral equation. Although there are an infinite number of solutions to the integral equation, all but one, a unique central-well solution, are aphysical, having discontinuities and/or cusps (discontinuous derivatives) in the potential. Therefore, we selected the central-well solution to Equation (4.51) to represent the van't Hoff temperature dependence shown in Equation (4.50). Thus,

$$C_{Ji}(\beta) = \beta F(\beta) \mathrm{e}^{-w(r_0)\beta} \tag{4.52}$$

where

$$F(\beta) = \beta \int_0^\infty \mathrm{e}^{-\beta y} \mathrm{g}(\mathrm{y}) \mathrm{d}y \tag{4.53}$$

and $\mathrm{g}(\mathrm{y})$ is the inverse Laplace transform of the function

$$G(\beta) = \frac{F(\beta)}{\beta} = \frac{C(\beta)\mathrm{e}^{\beta w_0}}{\beta^2} \tag{4.54}$$

These lead to the general expression for the central-well potential $w(r)$:

$$w(r) = w_0 + g^{-1}\left(\frac{4}{3}\pi r^3\right) \tag{4.55}$$

4.5 Computation of Unique, Central-Well Potentials

In the case of perfect van't Hoff behavior, one can see that $F(\beta) = C_0/\beta$ and $G(\beta) = C_0/\beta^2$. The inverse Laplace transforms of these functions are $f(y) = C_0 H(y)$ and $g(y) = C_0 y H(y)$, respectively, where $H(y)$ is the Heaviside step function. Thus, the unique, central well potential (Solution to Equation (4.51)) is:

$$w(r) = \frac{4\pi r^3}{3C_0} - m \qquad r \geq 0 \tag{4.56}$$

where the slope of the van't Hoff plot of the Langmuir constant is equal to the well depth $m = -w_0$ and the y-intercept $\log C_0$ is related to the well size measured by the volume of negative energy mC_0 with a spherical radius of

$$r_s = \left(\frac{3mC_0}{4\pi} \right)^{1/3} \tag{4.57}$$

The cell potential may then be simplified into the following form

$$w(r) = m\left[\left(\frac{r}{r_s} \right)^3 - 1 \right] \qquad r \geq 0 \tag{4.58}$$

Equations (4.56)-(4.58) allow facile implementation of the cell potential method. The two unknown parameters in Equation (4.56), C_0 and m, can be found by first calculating the Langmuir constants for a given guest molecule in the hydrate cage over a range of temperatures. Then, one can regress C_0 and m directly from the van't Hoff plot where $m = -w_0$.

4.6 Determining Cell Potentials for One Structure Based on Known Potential Parameters for Another Structure

Pure ethane, like methane, forms a structure I hydrate only occupying the large cages. However, when mixed with larger guest molecules, such as propane and isobutane, ethane forms a structure II hydrate. Unexpectedly, a mixture of ethane and methane, both simple structure I formers, will form a structure II hydrate[23-25]. Models have been developed that characterize this structural transition[2,26,28], but the parameters used in these models were found by incorporating the mixture data and transition points in the parameter optimization process. To have models capable of predicting equilibria in

systems outside the range of available experimental data, for example for other gas mixtures or at other temperatures, unique, physically relevant ethane potential parameters are needed.

The approach that we employed to find the cell potential for ethane in a structure II is as follows. (1) Various spherically averaged intermolecular potential forms (i.e. the Kihara and various Lennard-Jones L-J 6-N potentials) were applied and fit to the calculated cell potentials for methane in both cages of structure I. It has been stated that the repulsive interaction between the guest and host lattice that is paramount[29,30]; however, when calculating the Langmuir constant of a guest in a hydrate cage, the potential is effectively Boltzmann-weighted, see Equation (2.19). Therefore, it is the volume of the attractive region, or the integration of the attractive region, that determines the Langmuir constant. Thus, we minimized a Boltzmann-weighted objective function, χ, in order to fit the spherically averaged potentials to the calculated cell potentials.

$$\chi = \sum_{i}^{\#\text{ of radial points}} \left[\exp\left(\frac{-w_{\text{cell potential}}}{kT} \right) - \exp\left(\frac{-w_{\text{fit potential}}}{kT} \right) \right]^2 \tag{4.59}$$

(2) The spherically averaged potential form chosen above was fit to the ethane structure I cell potential using Equation (4.59). (3) This fit potential was applied to ethane in a structure II lattice and the Langmuir constants were calculated. (4) From these predicted Langmuir constants, the cell potential for structure II ethane was determined. This procedure could be extended to other guests to provide a theoretical link between the cell potentials of guests in different cages, thus allowing these analytical cell potentials to be used in hydrate systems in which the guest occupies both types of cavities.

4.7 Resulting Cell Potentials

4.7.1 Single Occupancy Hydrates – Extracting Cell Potentials from Experimental Data

The methods for extracting cell potentials for guest molecules that occupy only the large cage is discussed in Section 4.4.1 and the resulting potentials are shown in Figure 4.1. Cell potentials for all structure I and structure II guests studied are listed in Table 4.2 and Table 4.3 respectively. The reported confidence intervals are calculated using the 95% confidence on the regression parameters, m and C_0, of the van't Hoff plots (see Equation (4.50)). Although the experimental errors of the equilibrium dissociation pressures were not reported, their effect can be estimated. If the experimental error for the dissociation pressure of ethane is assumed to be a few percent, the resulting error bars on the cell potential for structure I ethane would be negligible. We expect that potential experimental error would be contained within the 95% confidence interval of the regression, $-w_0 \pm 0.062$ kcal/mol and $r_s \pm 0.032$ Å; therefore, the regression confidence intervals are assumed to be a good representation of the overall uncertainty.

Rodger[55] suggested that temperature variations in the hydrate system could significantly alter the cavity potentials. This temperature dependent variation in cavity potentials would manifest itself in deviations from the van't Hoff behavior. These deviations were examined by Bazant and Trout[5] and would be evident in the confidence intervals of the cell potentials listed in Table 4.2 and Table 4.3. Based on the small confidence intervals found over a large range of temperatures (applicable to hydrate systems) the ideal van't Hoff behavior assumed in Equation (4.50) and the subsequently

derived cell potentials do indeed provide an accurate approximation of the temperature dependence of the Langmuir constants.

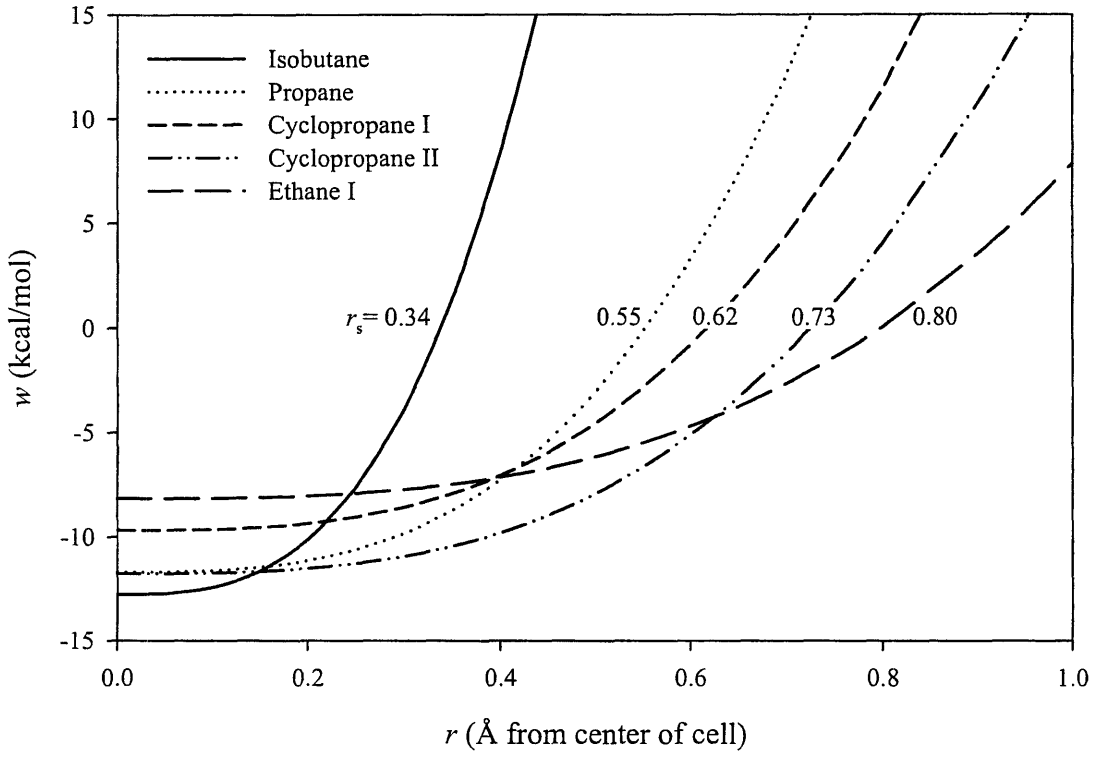

Figure 4.1: Cell potentials of single-cage hydrate occupying molecules calculated from pure guest experimental hydrate dissociation data.

Table 4.2: Calculated cell potential parameters w_0 and r_s with ±95% confidence intervals for structure I hydrates

Guest Molecule	Temperature range of exp. Data (K)	$-w_0$ (kcal/mol)	r_s (Å)
ethane	200-288[31-39]	8.152 ± 0.062	0.803 ± 0.032
cyclopropane	237-289[40]	9.677 ± 0.022	0.617 ± 0.009
methane, small cage(5^{12})	149-320[a]	5.645 ± 0.007	0.918 ± 0.004
methane, large cage ($5^{12}6^2$)	149-320[a]	5.665 ± 0.002	1.501 ± 0.002
argon, small cage(5^{12})	133-304[a]	4.947 ± 0.002	1.118 ± 0.001
argon, large cage ($5^{12}6^2$)	133-304[a]	4.463 ± 0.002	1.678 ± 0.003
chlorodifluoromethane (R-22)	267-289[41]	9.933 ± 0.156	0.492 ± 0.049

[a]cell potential calculated via *ab initio* potentials

Table 4.3: Calculated cell potential parameters w_0 and r_s with ±95% confidence intervals for structure II hydrates

Guest Molecule	Temperature range of exp. Data (K)	$-w_0$ (kcal/mol)	r_s (Å)
ethane	[b]	8.714 ± 0.068	1.474 ± 0.066
cyclopropane	258-274[40]	11.766 ± 0.089	0.726 ± 0.042
propane	247-278[32,33,42-49]	11.694 ± 0.173	0.552 ± 0.062
isobutane	241-275[46,48,50-52]	12.768 ± 0.130	0.338 ± 0.028
methane, small cage(5^{12})	149-320[a]	5.514 ± 0.006	0.911 ± 0.004
methane, large cage ($5^{12}6^4$)	149-320[a]	4.962 ± 0.005	2.389 ± 0.009
argon, small cage(5^{12})	133-304[a]	4.945 ± 0.001	1.106 ± 0.001
argon, large cage ($5^{12}6^4$)	133-304[a]	3.927 ± 0.008	2.408 ± 0.015
trichlorofluoromethane (R-11)	266-281[41]	15.973 ± 1.122	0.120 ± 0.092
dichlorodifluoromethane (R-12)	264-285[41,53]	11.089 ± 0.551	1.308 ± 0.467
bromotrifluoromethane (R-13B1)	266-280[41]	11.941 ± 0.493	0.589 ± 0.189
chloroform	272-274[54]	13.105 ± 3.375	0.686 ± 2.896
R-134a	275-283[53]	10.323 ± 0.288	1.794 ± 0.328

[a]cell potential calculated via *ab initio* potentials
[b]cell potential calculated via structure I cell potential

It should be noted that there is a strong inverse correlation between the size of the guest molecule and the resulting radius of negative energy, r_s. This correlation should be expected due to the nature of hydrate-guest interactions. Using the cell potentials listed in Table 4.2 and Table 4.3, we can reproduce the single component hydrate phase equilibria for the studied systems very accurately; however, this simply indicates that the

form of our potential is adequate and is not a test of the overall predictive ability of the method.

The predictive ability of our cell potential method can be tested against experimental structural changes that are known to occur. For example, cyclopropane undergoes a structural transition as a function of temperature[40], namely that between 257.1 K and 274.6 K cyclopropane forms a structure II hydrate, while outside that region it forms structure I. Using the cyclopropane cell potentials listed in Table 4.2 and Table 4.3 we predict these transitions to occur at 256.5 K and 274.6 K, respectively.

4.7.2 Using Ab Initio Potentials to Determine Cell Potentials

As explained in Section 4.4.2, site-site *ab initio* potentials were used to calculate Langmuir constants for methane and argon in both structures I and II over a wide range of temperatures and pressures. By incorporating accurate potentials and calculating the full 6-dimensional configurational integral, these Langmuir constants are independent of any fitting parameters. The resulting cell potentials are shown in Figure 4.2.

The central-well potentials for argon shown in Figure 4.2 are the simplest cell potentials that will reproduce the calculated Langmuir constants. However, Barrer and Edge[56] identified that the cell potential for argon exhibits a non-central minimum for the large cage of the structure I hydrate. Employing the non-central family of solutions discussed in Section 6.2.3 of Bazant and Trout[5], we can reproduce the non-central minimum; however, for hydrate equilibrium calculations the central-well solution accurately reproduces the Langmuir constants and therefore would provide a simpler model with no loss in accuracy.

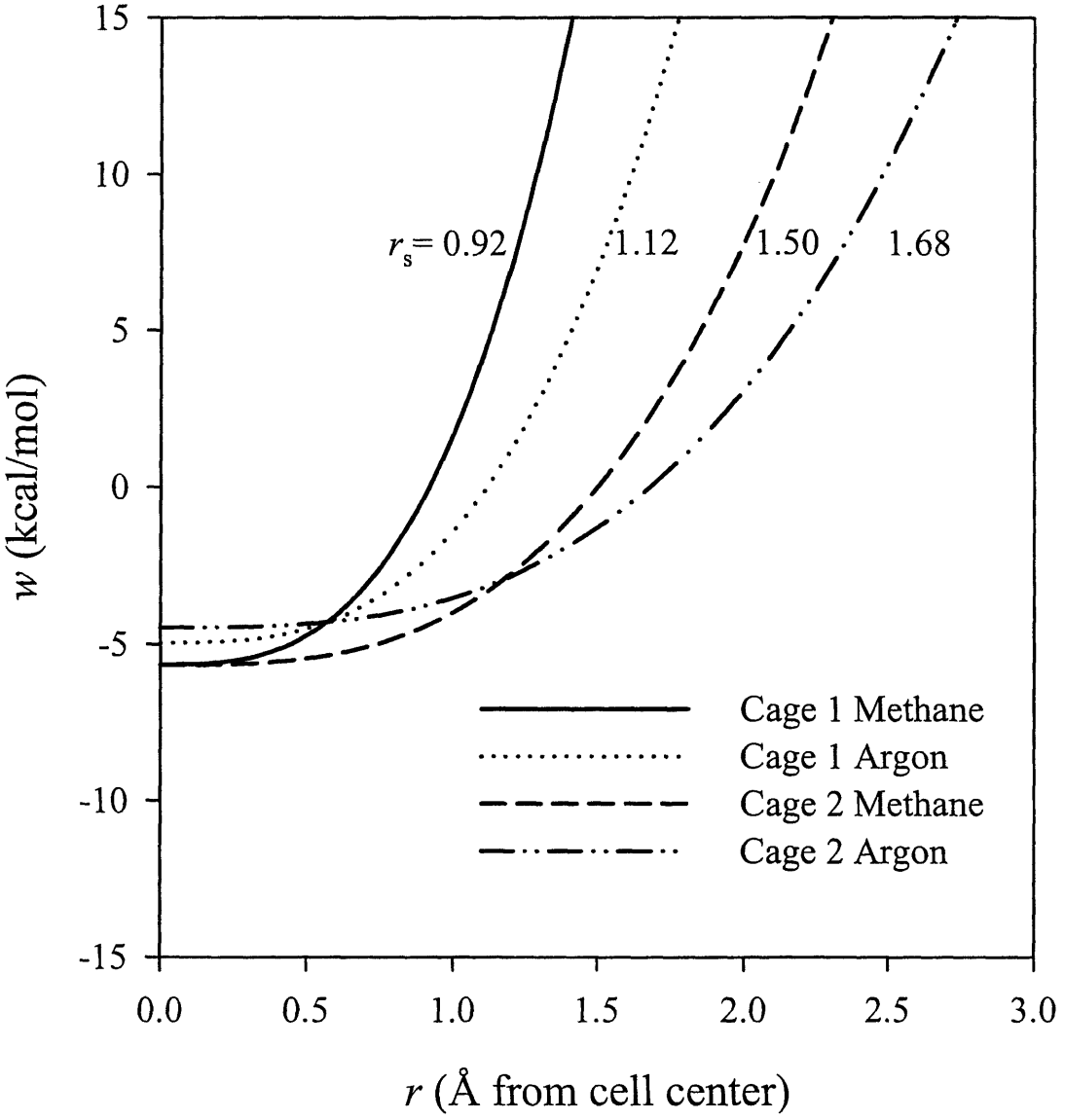

Figure 4.2a: Cell potentials of methane and argon in structure I lattices. Cell potentials were calculated using an *ab initio* site-site potential[4]

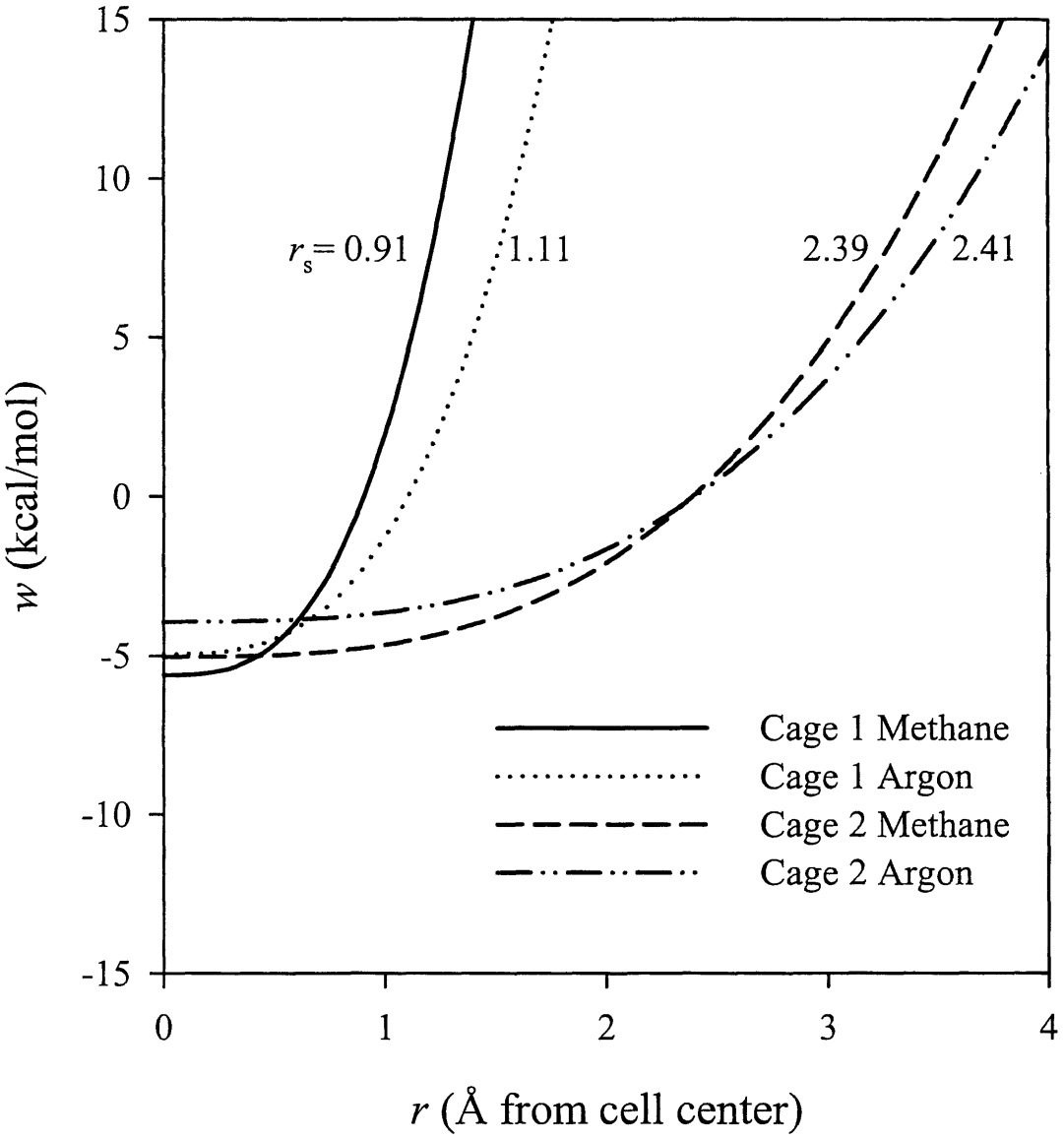

Figure 4.2b: Cell potentials of methane and argon in structure II lattices. Cell potentials were calculated using an *ab initio* site-site potential[4]

4.7.3 Extrapolating Known Cell Potentials from One Structure to Cell Potentials for Other Structures

Following the methodology described in Section 6, various potential forms were fit to the cell potentials previously calculated for methane. Figures 4.3 and 4.4 show the Kihara and Lennard-Jones 6-10 potentials fitted to the cell potentials and compared to spherically-averaged ab initio structure I cell potentials determined from the full six-dimensional configurational integral[4], reproducing the Langmuir constants as shown in Figure 4.5. It was found that a L-J 6-10 potential fit to the structure I cell potentials best reproduces the structure II potentials and the structure I and II Langmuir constants; therefore, a L-J 6-10 potential will be used for extrapolation of the ethane structure I cell potentials to find structure II for use in mixture predictions. The best-fit Kihara parameters are ε/k = 147.6 K, σ = 3.17 Å, with a = 0.3834 Å while the best fit L-J 6-10 parameters are ε/k = 192.82 K and σ = 3.441 Å.

As evident in Figure 4.4, the best-fit Kihara potential does not reproduce the attractive volume of the spherically-averaged ab initio potential as well as the L-J 6-10 potential. In fact, this is best illustrated in Figure 4.5 where the Kihara potential fails to reproduce the Langmuir constants for methane in a structure II lattice. The Kihara potential is inherently too strong in the repulsive region of the methane-water interaction in structure II cavities. It should be noted that all of the spherically-averaged pair-type potentials shown in Figure 4.4b (ab initio, Kihara, and L-J 6-10) exhibits the non-central minimum in the large cage of structure II discussed in the previous section. This non-central behavior is averaged into the cell potential.

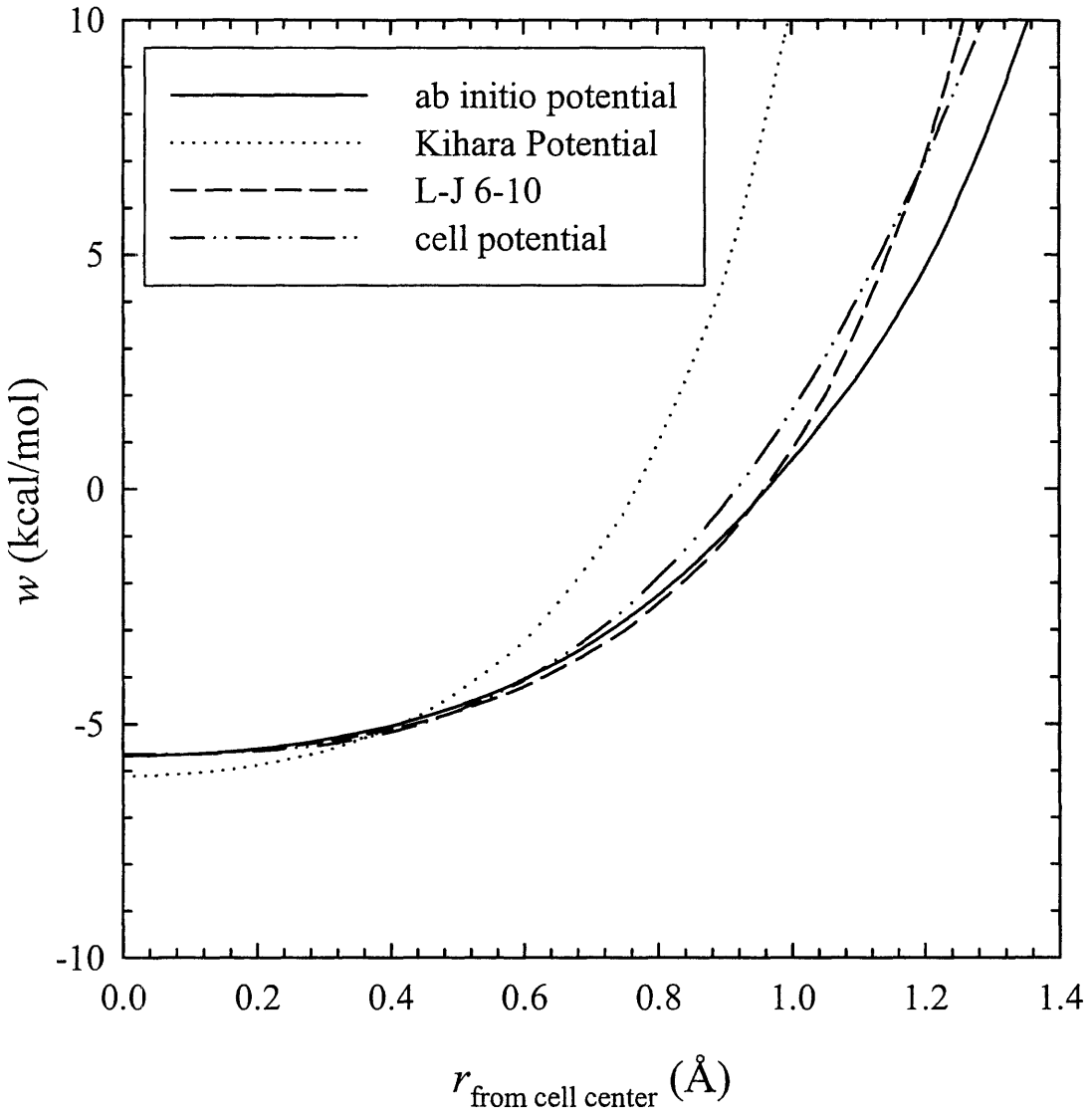

Figure 4.3a: Fit of common potential forms to spherically averaged ab initio potentials of methane in the small cage of structure I

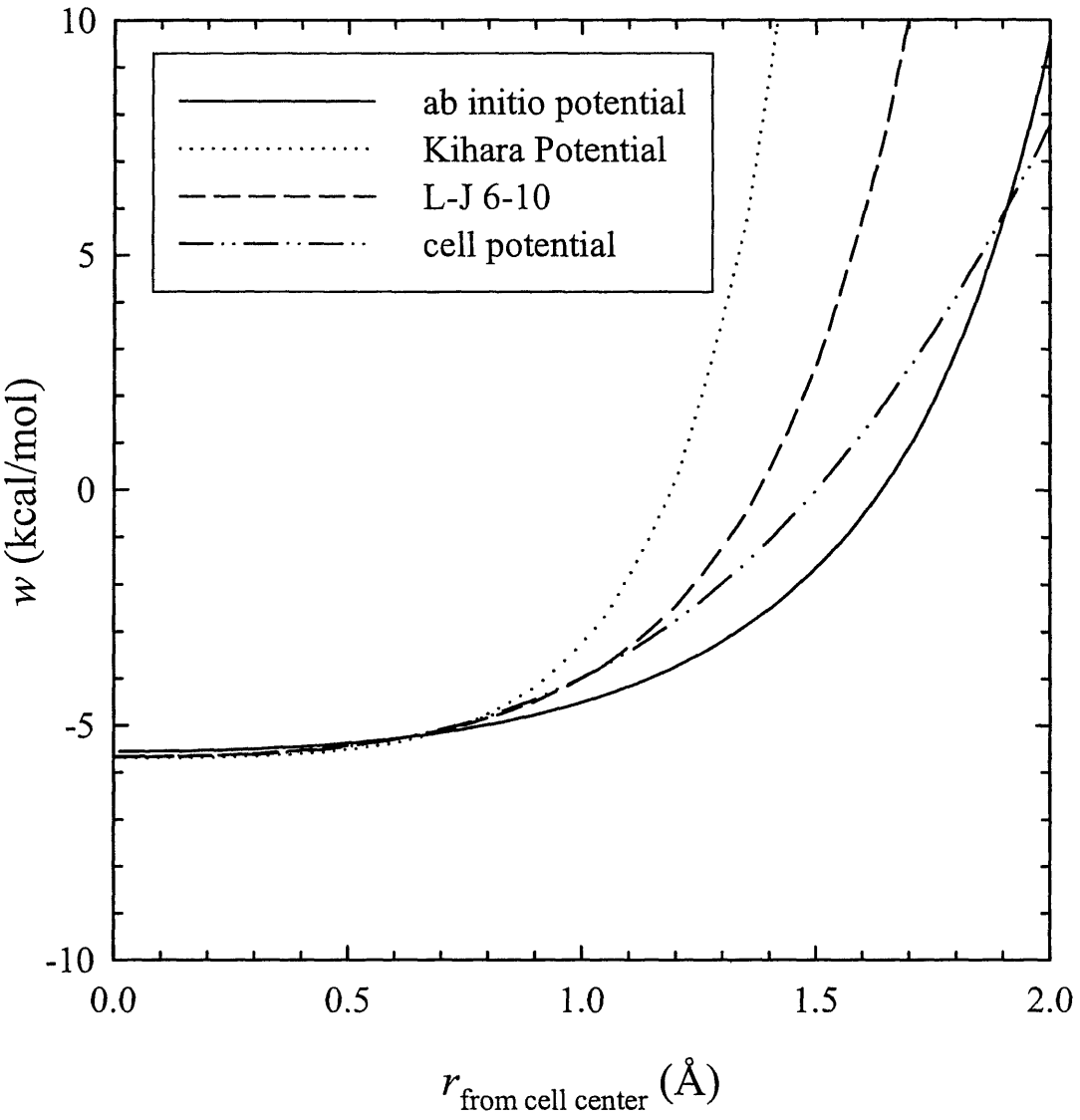

Figure 4.3b: Fit of common potential forms to spherically averaged ab initio potentials of methane in the large cage of structure I

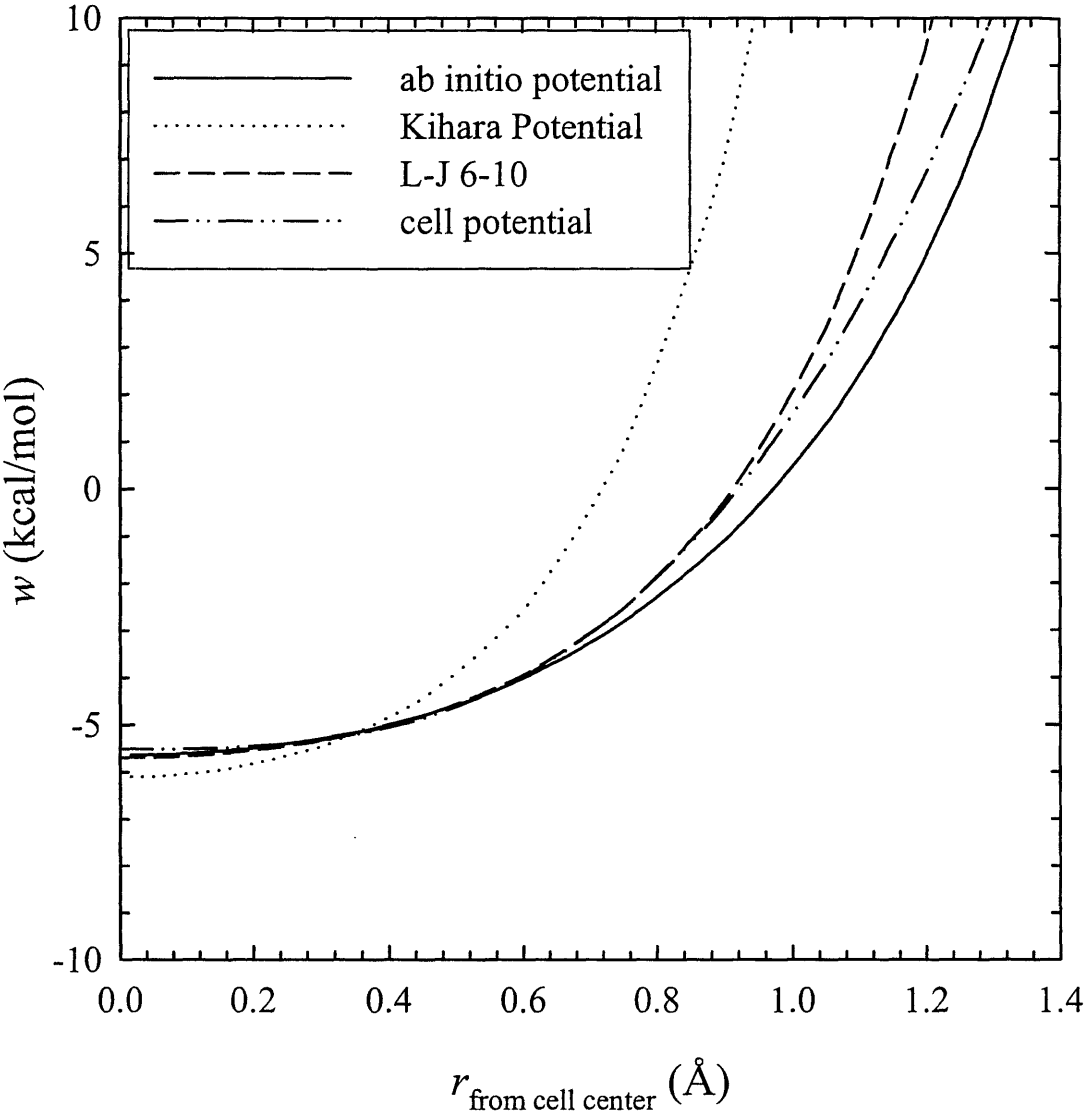

Figure 4.4a: Fit of common potential forms to spherically averaged ab initio potentials of methane in the small cage of structure II

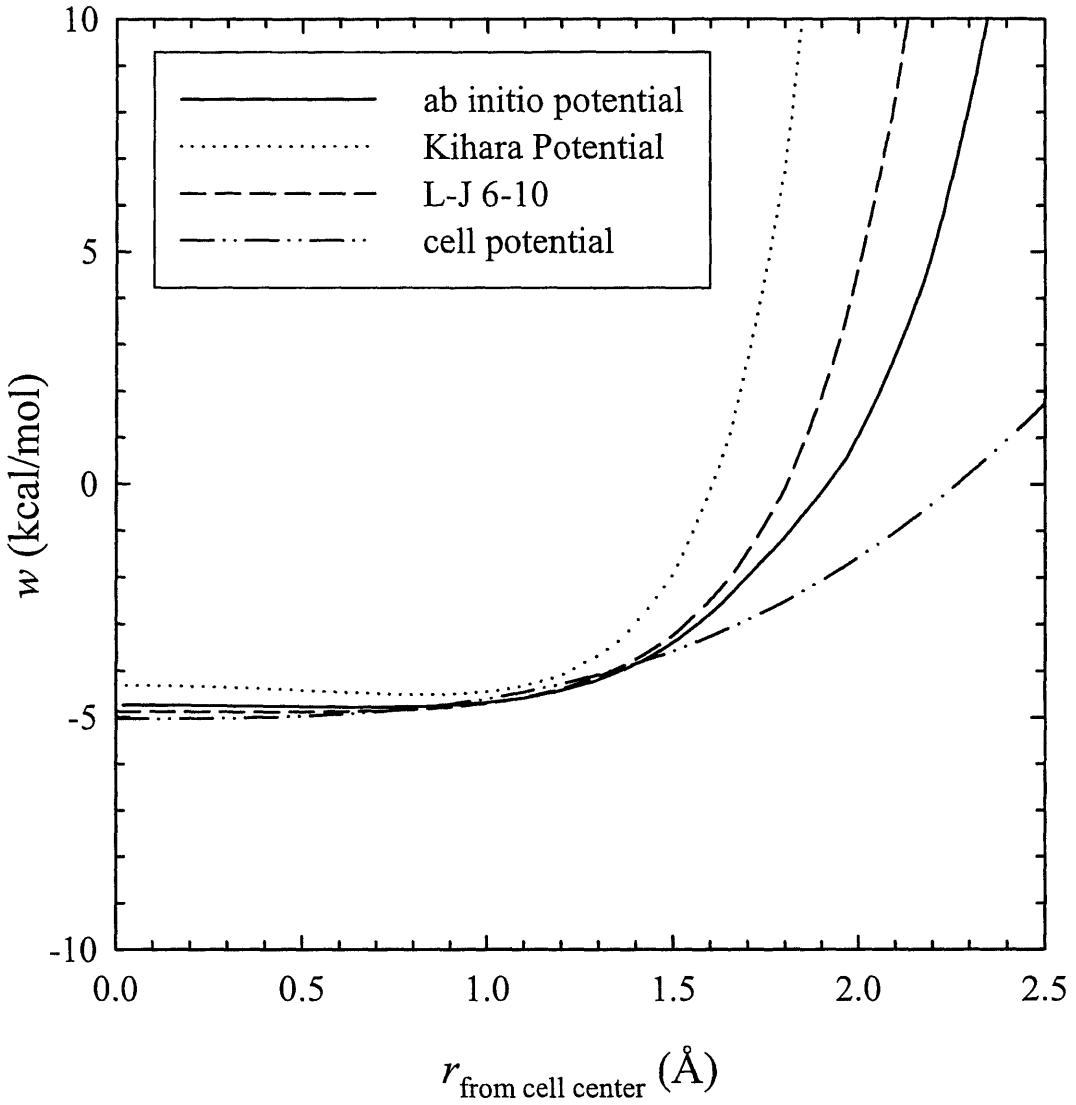

Figure 4.4b: Fit of common potential forms to spherically averaged ab initio potentials of methane in the large cage of structure II

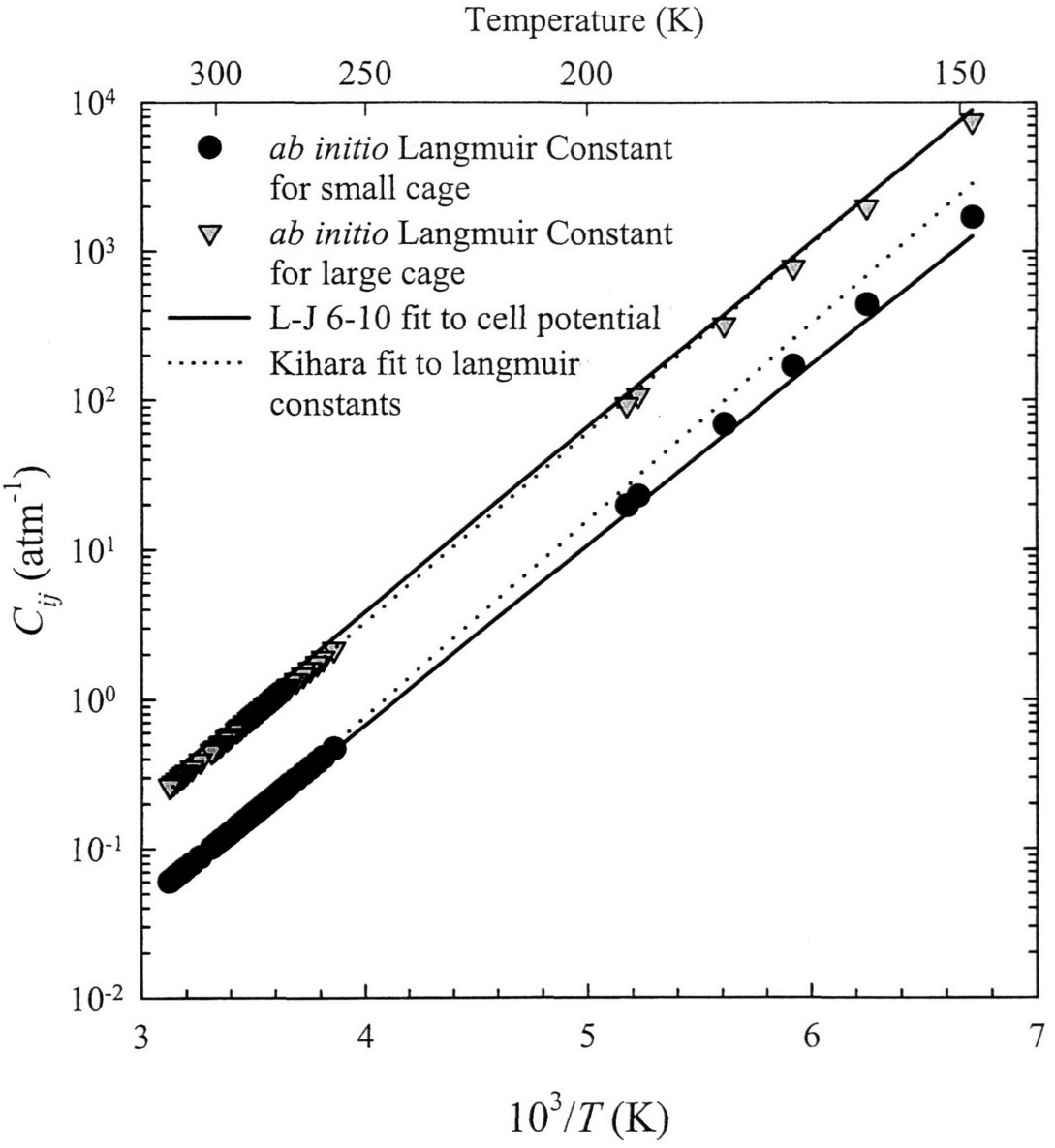

Figure 4.5a: Methane Langmuir Constants for structure I calculated using fit potential forms compared to values calculated via a site-site *ab initio* potential[4]

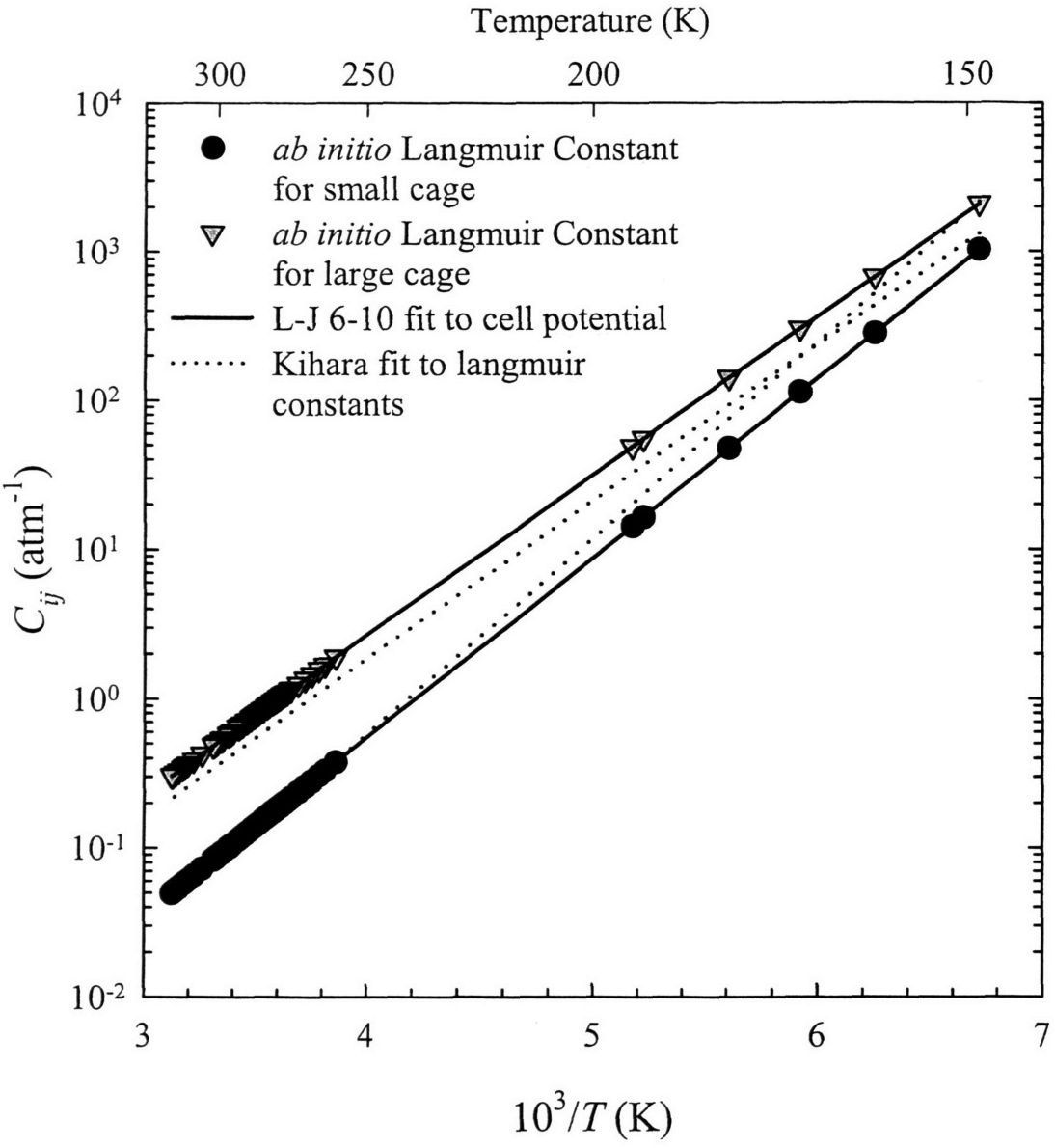

Figure 4.5b: Methane Langmuir Constants for structure II calculated using fit potential forms compared to values calculated via a site-site *ab initio* potential[4]

After validating the L-J 6-10 potential form for use in the hydrate lattice, it was used to fit the ethane structure I cell potential and calculate the cell potential for structure II ethane. The fit potential parameters are ε/k = 234.22 K and σ = 3.888 Å. Figure 4.6 shows the ethane cell potentials for structure I and II.

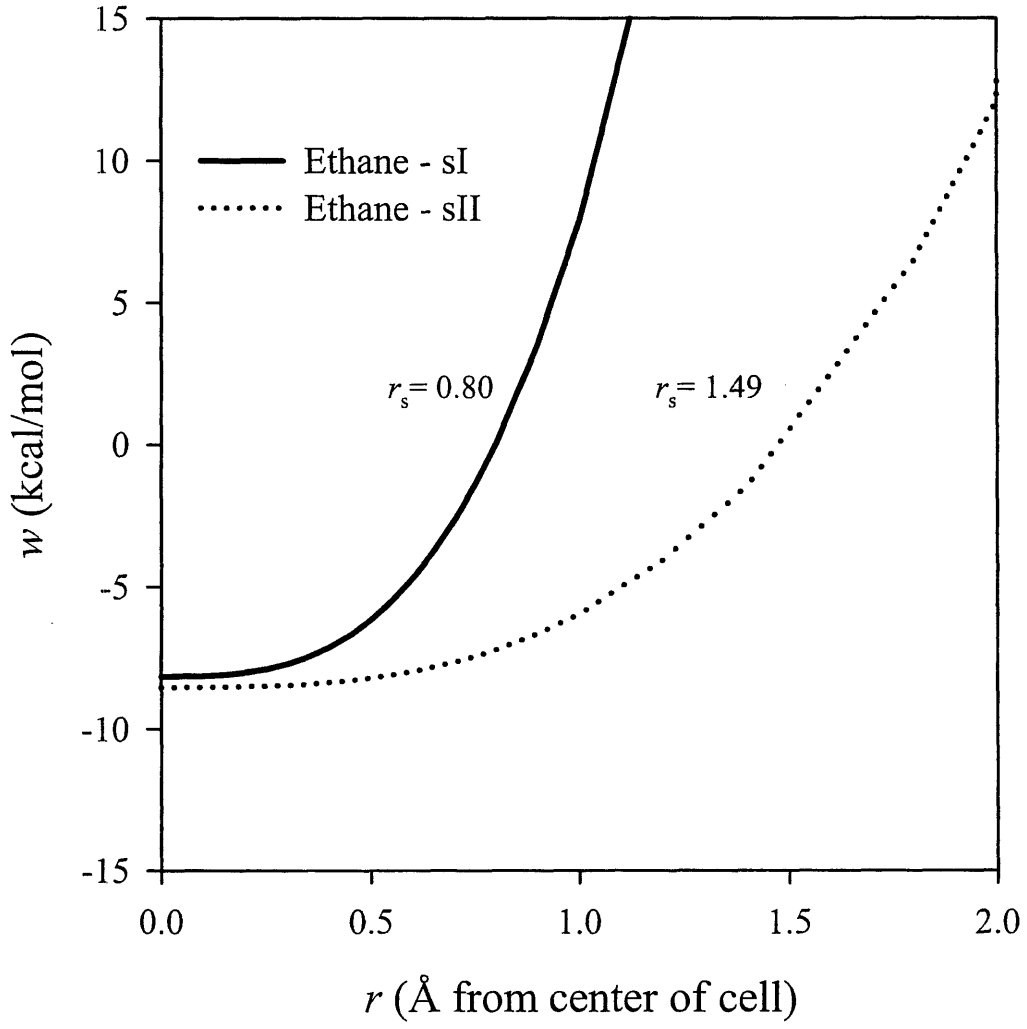

Figure 4.6: Cell potentials for ethane in the large cage of the structure I and structure II lattice

4.8 Phase Equilibrium Predictions

Because the cell potentials were extracted using single-component hydrate experimental equilibrium data, the best test of the applicability of the calculated cell potentials with the assumptions inherent in the van der Waals-Platteeuw model and the reference parameters is their ability to predict the phase behavior of mixed gas hydrate systems. Kvamme et al.[57] showed that guest-guest interactions have a significant effect on Langmuir constants of guest molecules. This energy would be incorporated in the mean field way in the fitting of parameters for pure hydrate systems. For mixed hydrate systems, deviations from this mean field energy could be important over certain composition ranges. Predicting phase equilibria data for mixed hydrate systems provides a test of the generality of the reference parameters used as well as the assumption in the van der Waals-Platteeuw model that the guest-guest interactions can be adequately treated via mean field energies.

In many instances, these predictions can be validated using existing experimental data, in others, predictions await experimental confirmation. In these predictions the cell potentials were fitted only to the single component hydrate equilibria data and the reference parameters were calculated from methane and argon single component hydrate data[4]. No parameter fitting to any data from mixed guest hydrate systems was performed.

4.8.1 Methane Mixtures

Accurate predictions for the mixed methane-ethane hydrate system are of great importance in the production and pipeline transmission of natural gas where hydrate forming temperatures and pressures exist. Figure 4.7 shows predictions using the

methane and ethane cell potentials compared to predictions from the CSMHYD program[1], along with experimental data[32,36,58]. The average absolute deviation (AAD) for the cell potential method is 6.2% compared to 11.9% for the CSMHYD. Using the model parameters optimized for the methane-ethane mixture by Ballard and Sloan[2] the AAD is 10.8%. Similar predictions using the cell potentials in Table 4.3 for methane-isobutane mixtures result in an AAD of 6.7% compared to 13.2% for CSMHYD.

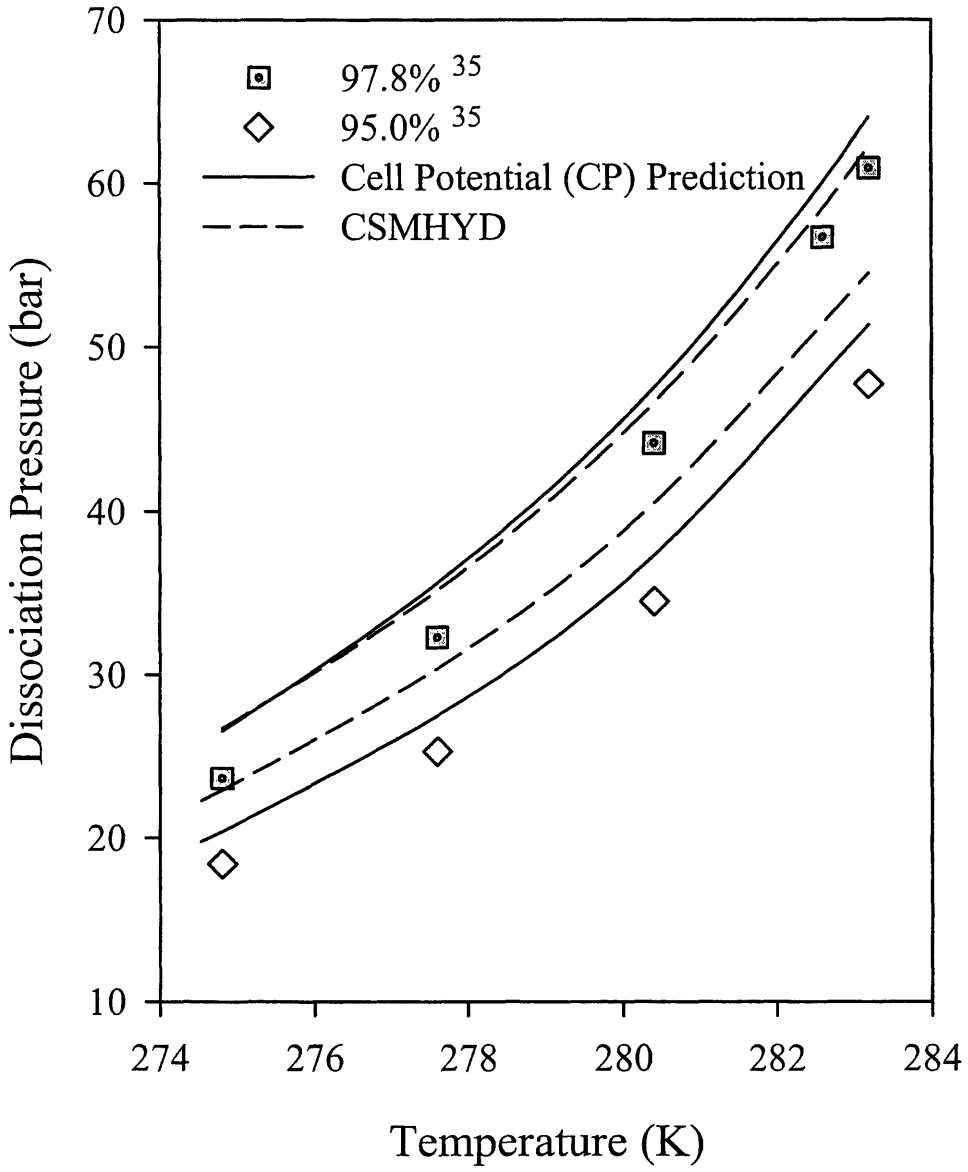

Figure 4.7a: Predicted dissociation pressures for various methane-ethane mixture compared to experimental data[32,36,58]

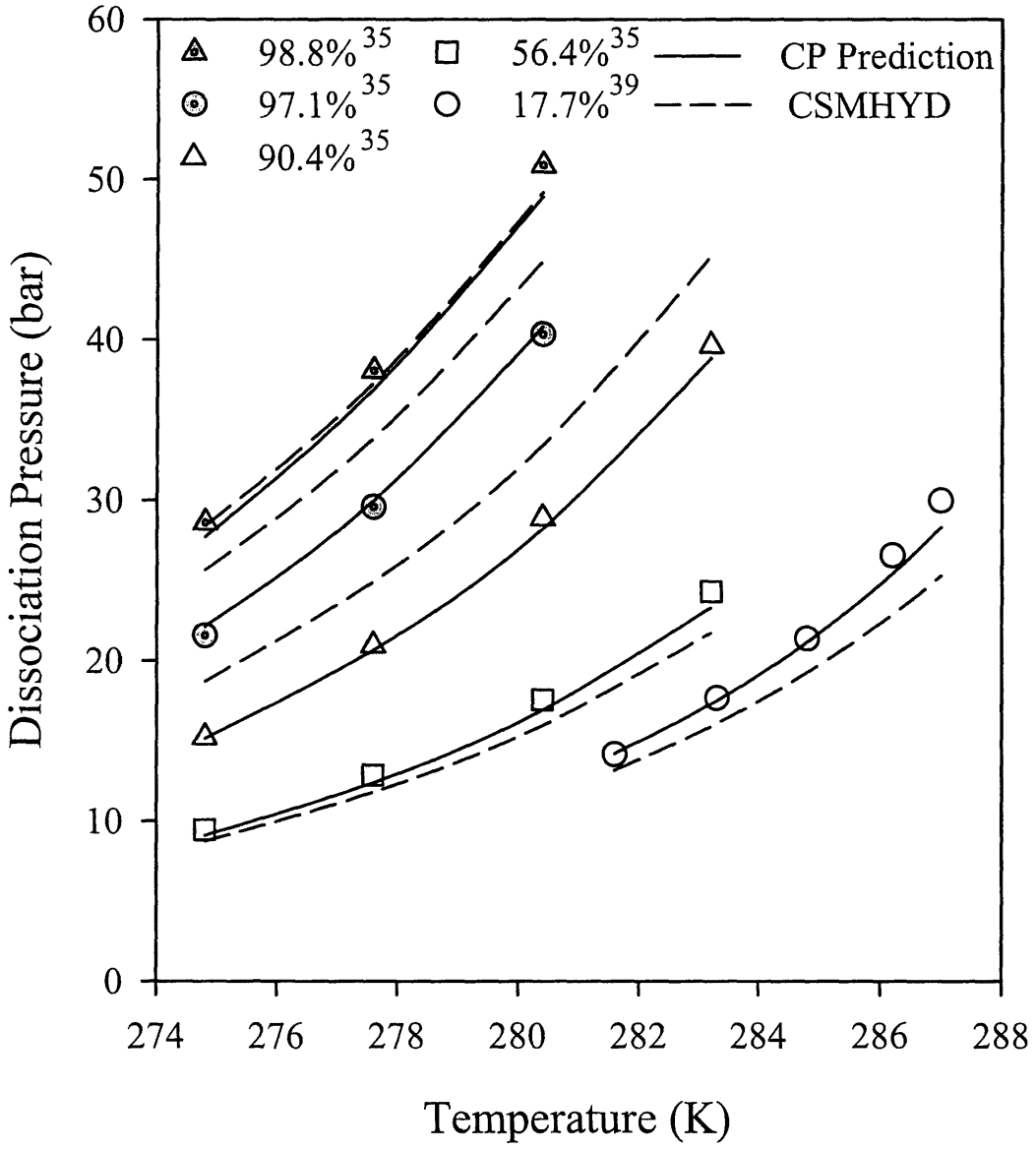

Figure 4.7b: Predicted dissociation pressures for various methane-ethane mixture compared to experimental data[32,36,58]

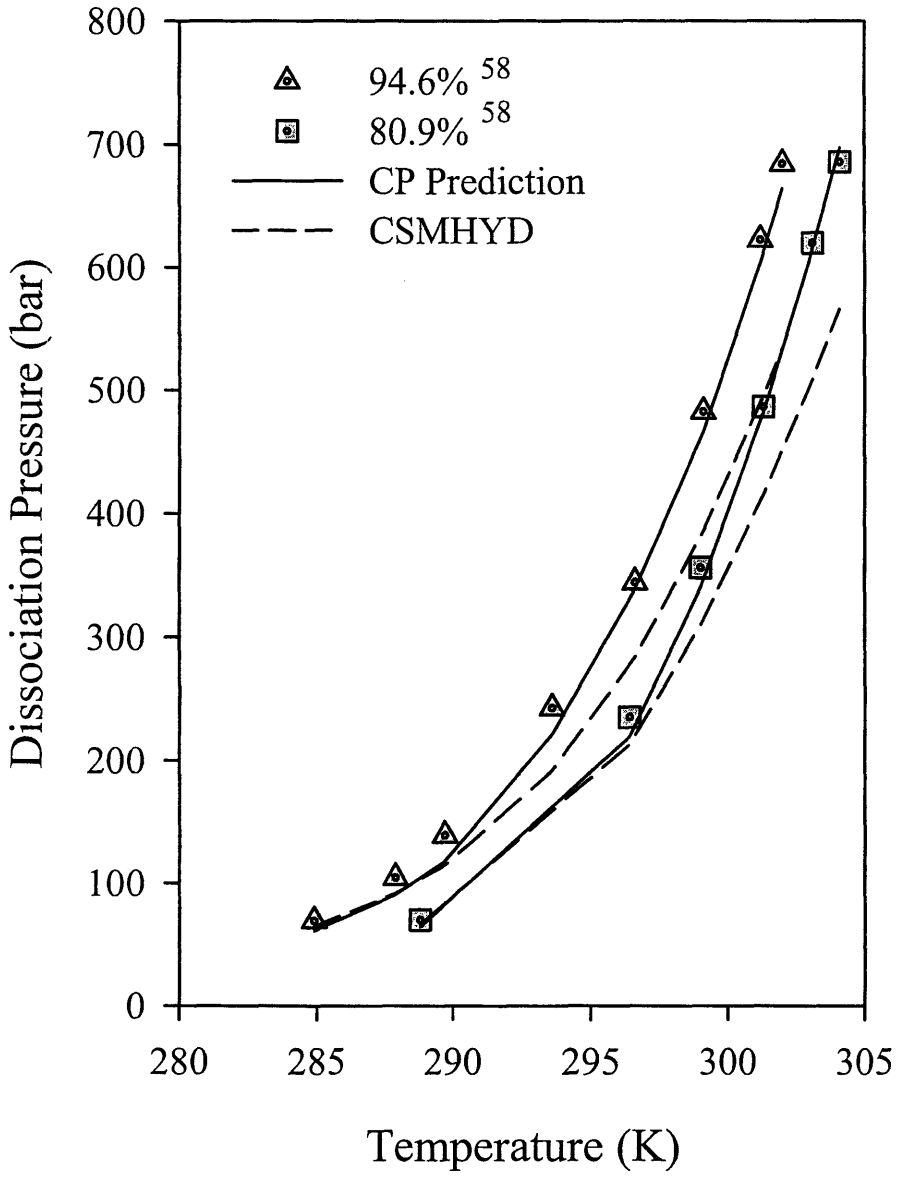

Figure 4.7c: Predicted dissociation pressures for various methane-ethane mixture compared to experimental data[32,36,58]

The methane-ethane mixture undergoes a transition from structure I with pure methane to structure II at a methane mole fraction between 0.72 and 0.75[23,25] at 274.2 K, although both guests form structure I as simple hydrates. Using the cell potentials calculated using the pure methane and ethane clathrate data, this method predicts that this structural change will occur at $x_{CH_4} = 0.74$, within the range of the experimental measurements. Using the Kihara potential, this transition is predicted to occur at a mole fraction of 0.52 methane[2]. However, other groups[2,26] have modified the methane and ethane parameters to reproduce the experimental mole fraction for this transition. Our predicted phase diagram, with no adjustment of parameters, was in agreement with experimental data from Deaton and Frost[32] and Jhaveri and Robinson[59] for a methane-ethane-water mixture at 277.6 K as shown in Figure 4.8. Our predicted lines directly overlap the measured points within expected experimental uncertainty.

The predicted equilibrium lines shown in Figure 4.8 and the similar figures that follow were calculated using the mixture form of the Peng-Robinson equation of state[8] to calculate the fugacity of the gas and liquid phases of the guests on a water-free basis. The hydrate-water-guest equilibrium and the composition of the hydrate phase were computed using the cell potential method. The phases present represent the phases with the lowest free energy. For systems with liquid guest (L_{hc}) hydrate equilibia, the fugacity of the liquid guest mixture is used in the van der Waals-Platteeuw model to calculate the equilibrium pressure. These equilibrium lines are nearly vertical due to the small compressibility of the liquid guest mixture. For the three-component, isothermal systems presented, i.e. water-methane-ethane in Figure 4.8, a constant pressure lever rule tie line is to be applied whenever there are three phases present at a given composition and

pressure. From the Gibbs Phase Rule, $f = n + 2 - \pi - r = 2 - r$ where n = number of components = 3, π = number of phases = 3, r = number of restrictions or constraints. With P and T specified, $r = 2$ and $f = 0$ as expected, so the phase compositions are given by the tie line.

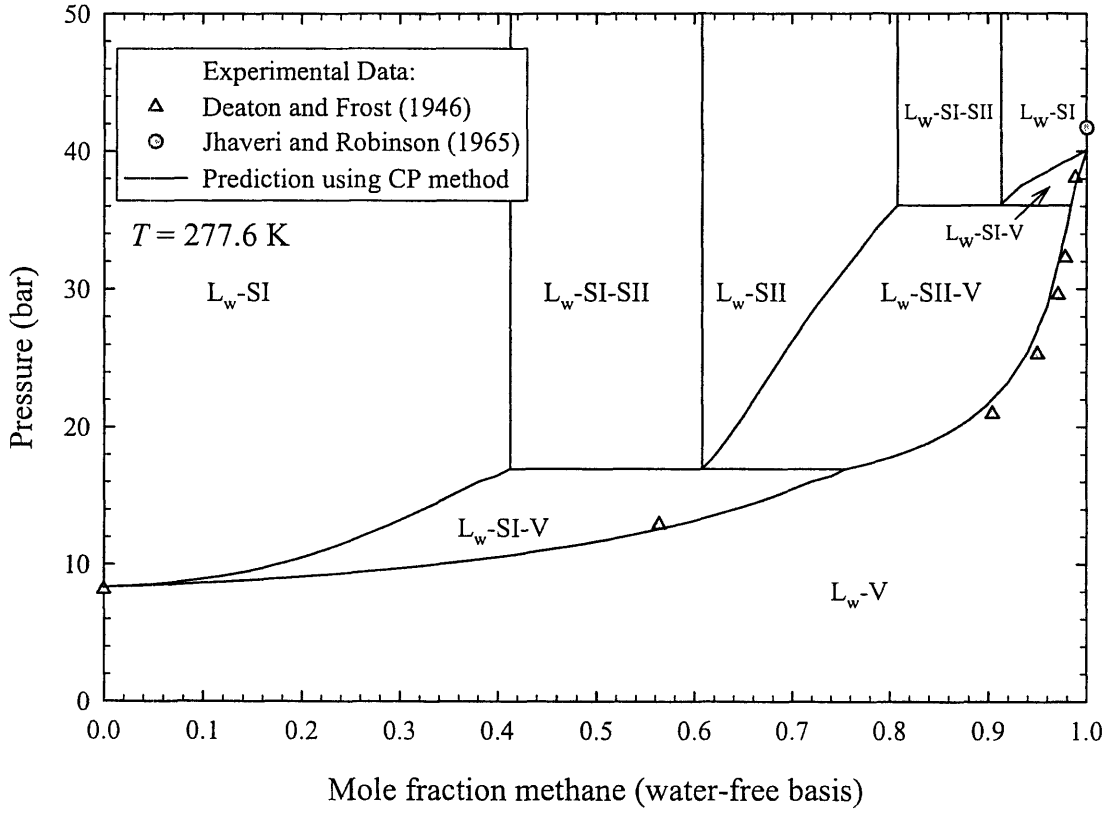

Figure 4.8: Predicted hydrate phase diagram for methane and ethane at 277.6 K. Experimental data from Deaton and Frost[32] and Jhaveri and Robinson[59]

Figure 4.9 is the pressure vs. composition (on a water-free basis) phase diagram for the methane-propane-water system. One may notice that at a propane mole fraction composition of 0.001, a structure II hydrate is predicted to form. This compares to a value of 0.0005 predicted by Ballard and Sloan[26] using methane Kihara parameters optimized to the methane ethane mixture. The structure I to II transition point has not been determined experimentally.

Figure 4.10 is the pressure versus water-free composition isothermal phase diagram for a methane-cyclopropane-water mixture at 277.15 K. Although these P and T conditions are outside the structure II region for pure cyclopropane, as methane is added to pure cyclopropane, we predict that the structure I hydrate changes to a structure II hydrate because methane serves to stabilize the small cage of structure II, while cyclopropane fills the large cage. This structural change is predicted to occur at a methane mole fraction of 0.38. Because the methane simple hydrate exists as structure I, an upper transition from structure II back to structure I occurs at 0.9996 mole fraction methane. Figure 4.11 is the pressure vs. water-free composition phase diagram for a methane-cyclopropane-water mixture at 281.15 K. Similar to the phenomena predicted at 277.15 K, we predict that between 0.566 and 0.9994 mol fraction methane the methane-cyclopropane-water system forms a structure II hydrate.

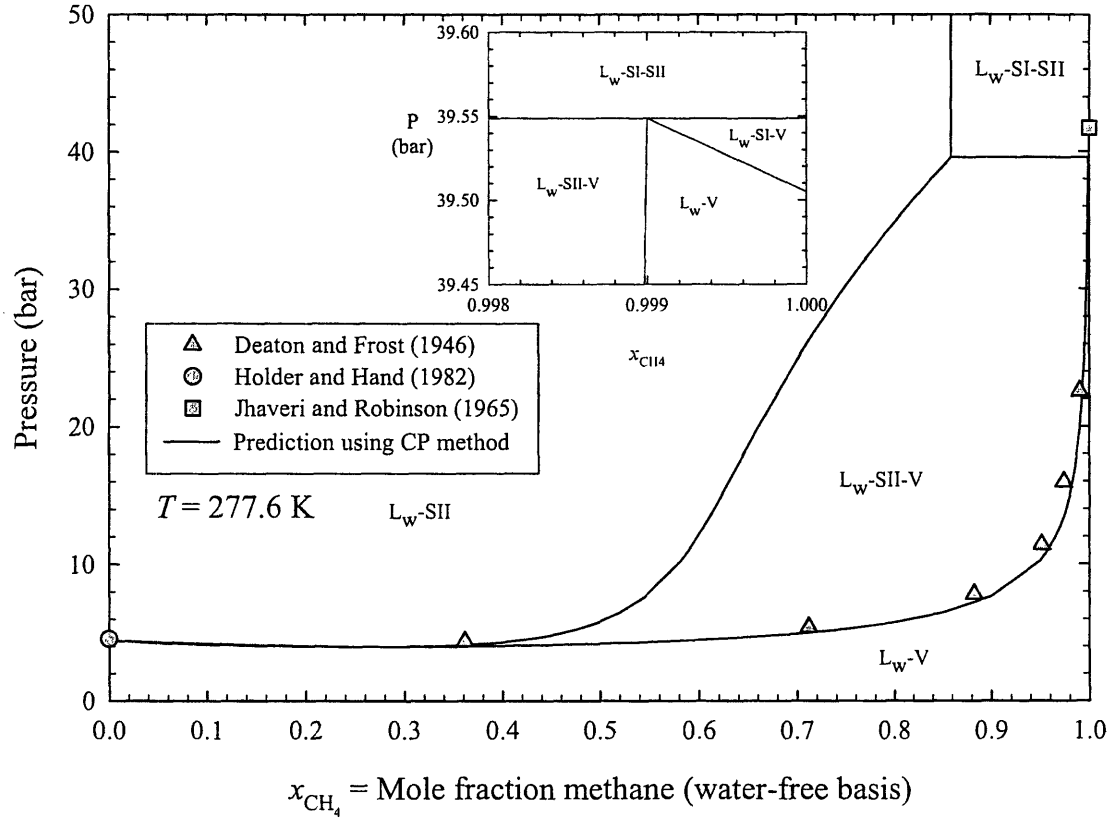

Figure 4.9: Predicted isothermal hydrate phase diagram for methane and propane at 277.6 K. Experimental data from Deaton and Frost[32], Holder and Hand[37], and Jhaveri and Robinson[59]

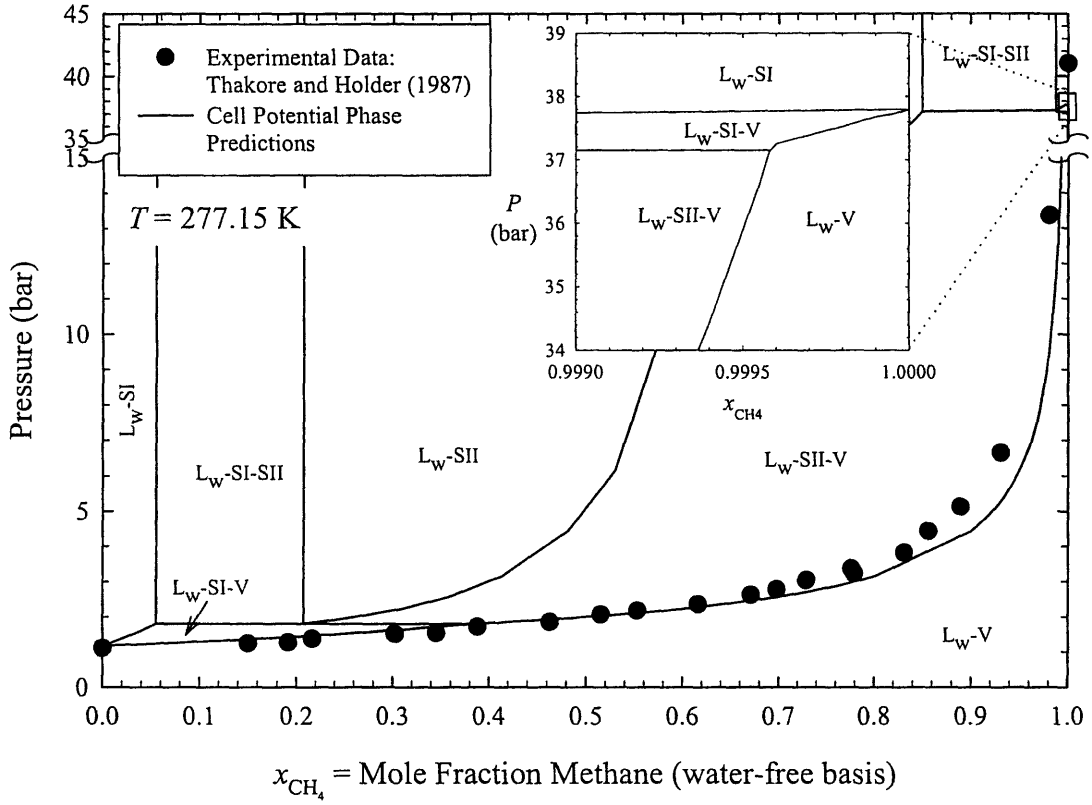

Figure 4.10: Predicted isothermal hydrate phase diagram for methane and cyclopropane at 277.15 K compared with experimental data from Thakore and Holder[48]

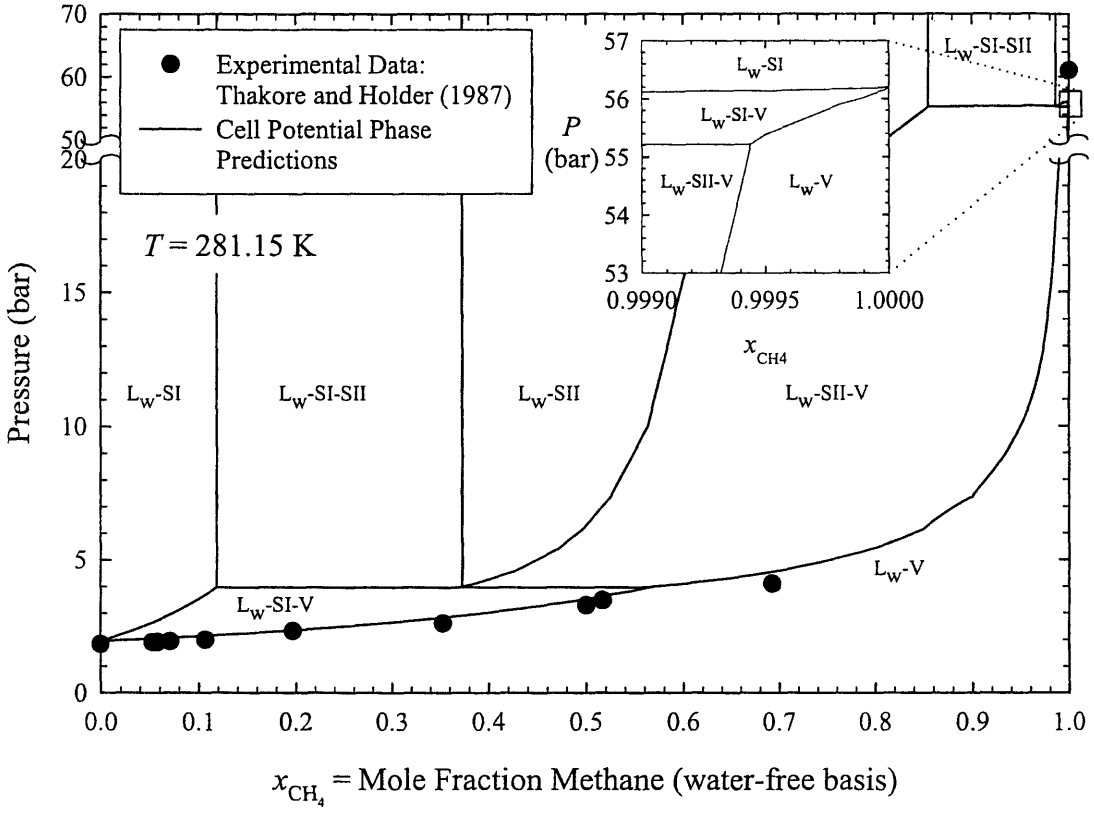

Figure 4.11: Predicted isothermal hydrate phase diagram for methane and cyclopropane at 281.15 K compared with experimental data from Thakore and Holder[48]

4.8.2 Other Hydrocarbon Mixtures

Figure 4.12 shows the results of using the cell potentials for propane and isobutane for the prediction of the hydrate phase equilibrium for the mixture. It is clearly evident that the cell potentials found using only pure component hydrate data is applicable to mixtures. Ballard et al.[60] show experimental evidence as well as predictions that a methane-propane-water mixture undergoes a "pseudo-retrograde" decomposition near 278 K. That is, the hydrate will actually decompose upon pressurization. Figure 4.13 shows the predicted hydrate phase diagram for an ethane-propane-water mixture at 277.6 K. One can see that the cell potentials predict the experimental data of Holder and Hand[37] well and that we also predict this "pseudo-retrograde" decomposition to occur between 0.60 and 0.685 mol fraction ethane. The cell potential method also predicts the 60 known data points for ethane-propane mixtures with an AAD of 5.9% compared to previous studies by Klauda and Sandler[61] (8.86%) and Sloan[1] (10.5%) and the refit by Ballard and Sloan[26] (5.72%).

If the mixture presented in Figure 4.13 is cooled, the L_w-V-L_{hc} envelope, within which "pseudo-retrograde" decomposition occurs, disappears. The hydrate dissociation pressure decreases at a faster rate than the dew point pressure curve and therefore we predict the "pseudo-retrograde" phenomena to cease at 277.3 K. At this temperature there will be a quintuple point with five phases (L_w-V-L_{hc}-SII-SI) in equilibrium. For this system, $f = n + 2 - \pi = 3 + 2 - 5 = 0$. This invariant point is predicted to occur at T = 277.3 K, P = 12.28 bar, y_{eth} = 0.676 and is shown in Figure 4.14.

Another mixture that is expected to undergo "pseudo-retrograde" decomposition is the ethane-isobutane-water system[60]. Therefore, it should be expected that a L_w-V-L_{hc}-

sII-sI quintuple point should exist. Figure 4.15 is the predicted hydrate phase diagram for an ethane-isobutane-water mixture at 274.7 K. The quintuple point is predicted to occur at $T = 274.7$ K, $P = 7.18$ bar, and $y_{eth} = 0.81$.

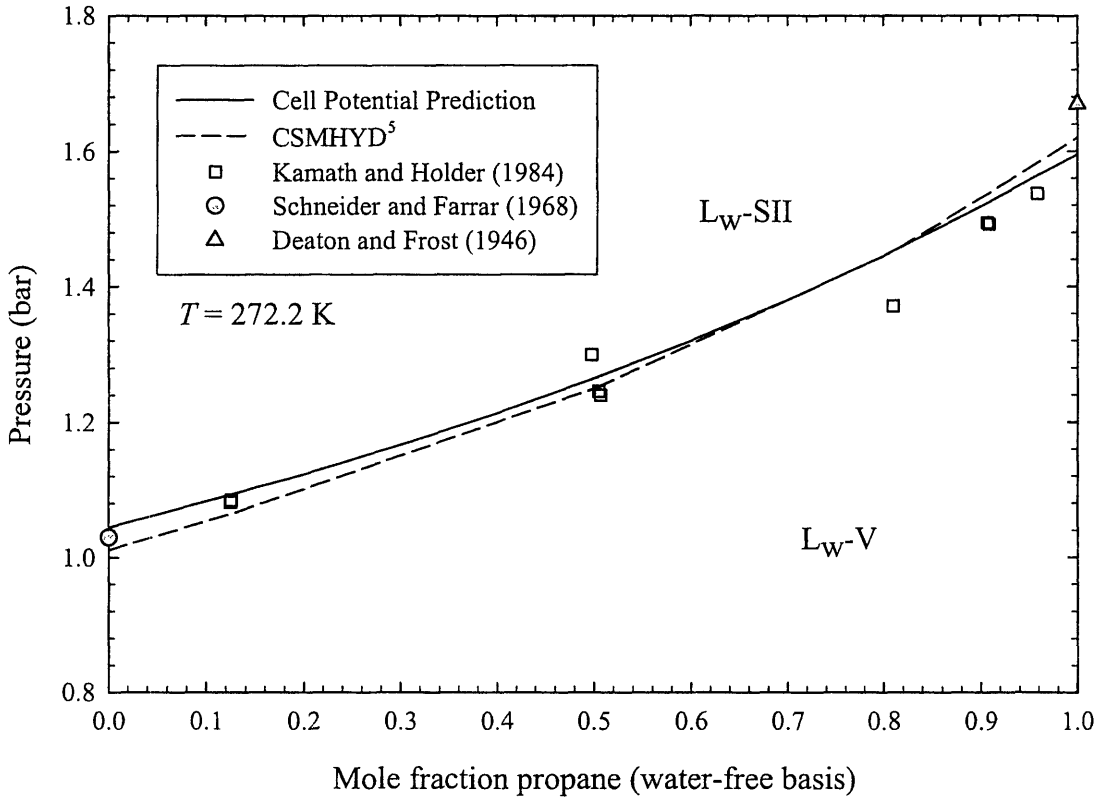

Figure 4.12: Predicted isothermal hydrate phase equilibrium for propane and isobutane at 272.2 K with experimental data from Kamath and Holder[62], Schneider et al.[50], and Deaton and Frost[32]

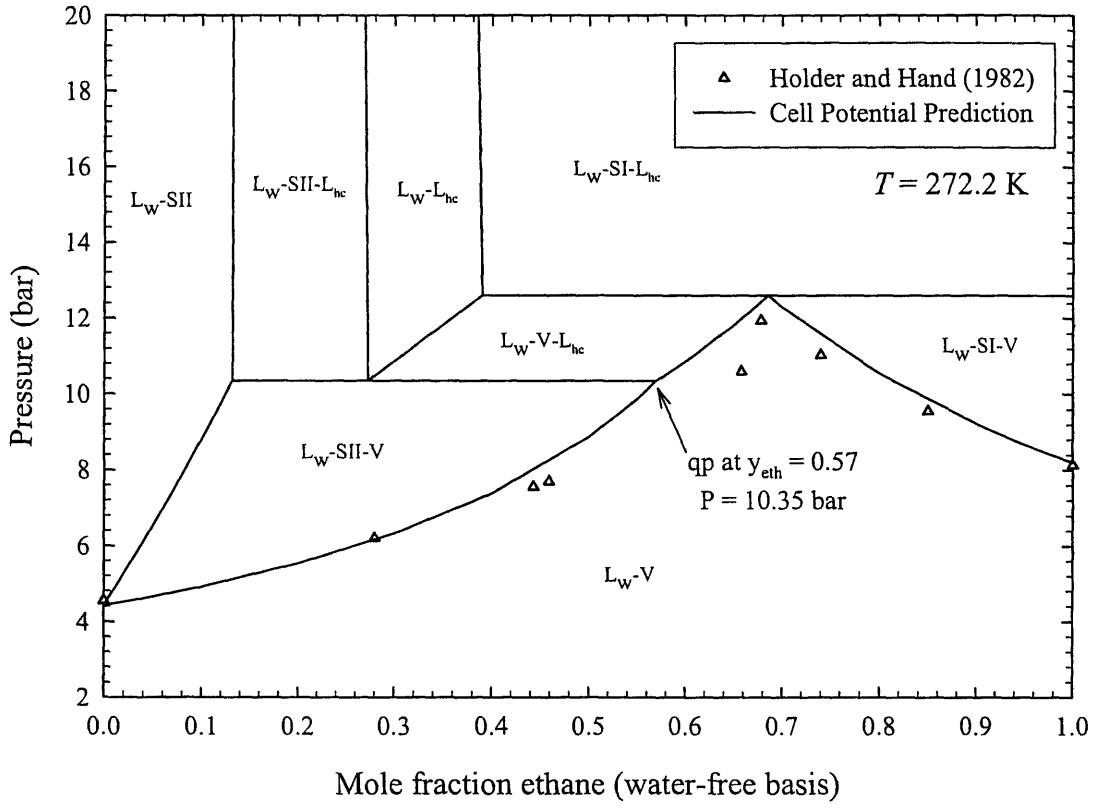

Figure 4.13: Predicted isothermal hydrate phase diagram for ethane and propane at 277.6 K with experimental data from Holder and Hand[37]

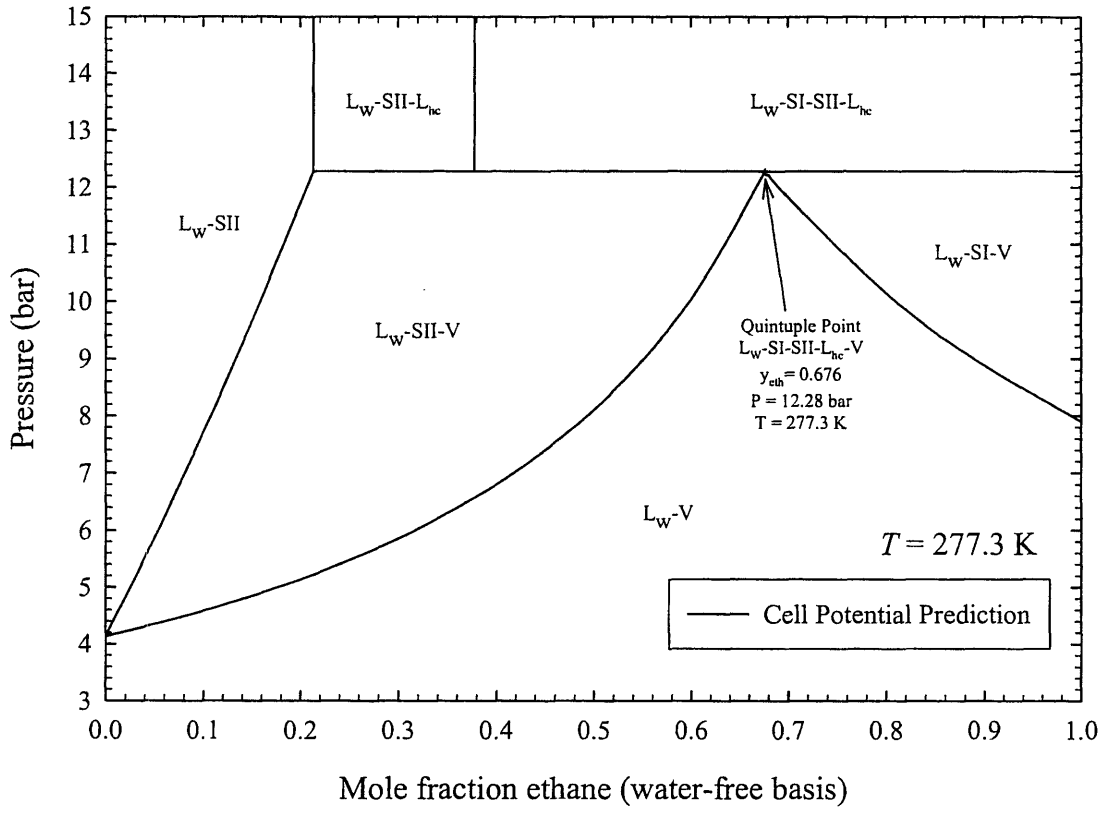

Figure 4.14: Predicted isothermal hydrate phase diagram for ethane and propane at 277.3 K with a five-phase quintuple point indicated.

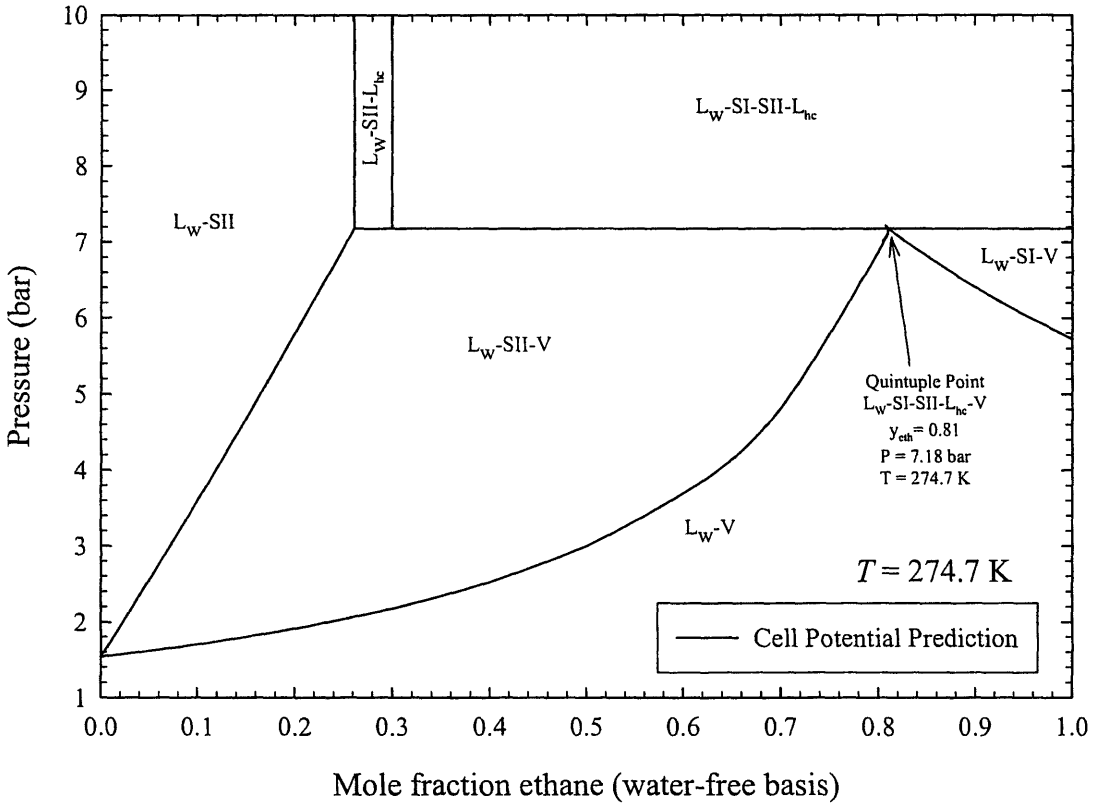

Figure 4.15: Predicted isothermal hydrate phase diagram for ethane and isobutane at 274.7 K with a five-phase quintuple point indicated.

4.9 Conclusions

We have presented the application of our cell potential method in which the form of the guest–host interaction potential in clathrate hydrates is determined analytically. Our approach was validated by making numerous predictions of multi-component phase data without fitting mixture data to experiments. The spherically averaged Kihara potential form is adequate in representing the overall guest-host interaction in structure I; however, guest-host interactions in the large cage of structure II are not effectively reproduced, thus leading to inaccurate reference parameters which have commonly appeared in the literature. The reference parameters used in this paper were further validated by their successful utilization in predicting mixed gas hydrate phase equilibrium data. All mixture predictions in this work are performed without fitting to any mixture data and nonetheless predict the experimental data accurately.

Overall, the cell potential method developed in this work has demonstrated its effectiveness and applicability to successfully model mixed hydrate systems without any adjustable parameters. For example, the structure I to structure II transition for methane-ethane gas mixtures was predicted to occur at 0.75 mol fraction methane at 274.2 K, within the experimental range measured to be 0.72-0.75 mol fraction methane. In addition, we were able to extrapolate the results of the calculated cell potentials to other systems. The cell potential that is calculated for ethane in a structure I hydrate lattice provides sufficient quantitative insight into the interaction between ethane and the water surrounding it in the hydrate that we have been able to model the ethane-water interaction in a structure II lattice. Several predictions were also developed that await experimental testing. For example, structure I to structure II phase transitions have been predicted for

methane-cyclopropane gas mixtures outside the temperature range of the pure cyclopropane structure II envelope. Quintuple (L_w-SI-SII-L_{hc}-V) points have been predicted for the ethane-propane-water (277.3 K, 12.28 bar, and $x_{eth,waterfree} = 0.676$) and ethane-isobutane-water (274.7 K, 7.18 bar, and $x_{eth,waterfree} = 0.81$) systems.

We conclude by commenting on why it might be that our simple, cubic cell potentials outperform more complicated, fitted potentials when predicting clathrate phase equilibria. In atomistic modeling, potential parameters are usually fit to reproduce the energies of ideal structures, at low (or zero) temperature, which can be calculated using *ab initio* methods or taken from experiment. Phase behavior, however, depends on high temperature configurations, which involve complicated deformations of ideal structures. By starting directly from thermodynamic data at finite temperature, and by using a Boltzmann-weighting scheme over a large configuration space when calculating our *ab initio* potential[4], our method easily determines an appropriate cell potential, which accounts for statistical averaging of configurations over a wide range of temperatures. The basic idea of solving an inverse problem for an "exact" thermodynamic potential may find further successful applications in other areas of materials modeling, where *ad hoc* fitting ideal structures remains the standard theoretical approach.

4.10 References

(1) Sloan, E. D., Jr. *Clathrate hydrates of natural gases - 2nd ed., rev. and expanded*; Marcel Dekker, Inc.: Monticello, 1998.
(2) Ballard, A. L.; Sloan, E. D. *Gas Hydrates: Challenges for the Future* **2000**, *912*, 702.
(3) Handa, Y. P.; Tse, J. S. *Journal of Physical Chemistry* **1986**, *90*, 5917.
(4) Anderson, B. J.; Tester, J. W.; Trout, B. L. *Journal of Physical Chemistry B* **2004**, *108*, 18705.
(5) Bazant, M. Z.; Trout, B. L. *Physica A* **2001**, *300*, 139.
(6) van der Waals, J. H.; Platteeuw, J. C. *Adv. Chem. Phys.* **1959**, *2*, 1.
(7) Anderson, B. J.; Bazant, M. Z.; Tester, J. W.; Trout, B. L. *Journal of Physical Chemistry B* **2005**, *109*, 8153.
(8) Peng, D.-Y.; Robinson, D. B. *Ind. Eng. Chem. Fund.* **1976**, *15*, 59.
(9) Sparks, K. A.; Tester, J. W. *Journal of Physical Chemistry* **1992**, *96*, 11022.
(10) Sparks, K. A.; Tester, J. W.; Cao, Z. T.; Trout, B. L. *Journal of Physical Chemistry B* **1999**, *103*, 6300.
(11) John, V. T.; Papadopoulos, K. D.; Holder, G. D. *AIChE J* **1985**, *31*, 252.
(12) John, V. T.; Holder, G. D. *J. Phys. Chem.* **1985**, *89*, 3279.
(13) Cao, Z. T.; Tester, J. W.; Sparks, K. A.; Trout, B. L. *J. Phys. Chem. B.* **2001**, *105*, 10950.
(14) Stackelberg, M. v.; Müller, H. R. *Zeitschrift für Elektrochemie* **1954**, *58*, 25.
(15) Holder, G. D.; Corbin, G.; Papadopoulos, K. D. *Industrial & Engineering Chemistry Fundamentals* **1980**, *19*, 282.
(16) Lennard-Jones, J. E.; Devonshire, A. F. *Proc. Roy. Soc.* **1938**, *165*, 1.
(17) Kihara, T. *Reviews of Mod. Phys.* **1953**, *25*, 831.
(18) Parrish, W. R.; Prausnitz, J. M. *Industrial & Engineering Chemistry Process Design and Development* **1972**, *11*, 26.
(19) Cao, Z.; Tester, J. W.; Trout, B. L. *J. Chem. Phys.* **2001**, *115*, 2550.
(20) Cao, Z.; Tester, J. W.; Sparks, K. A.; Trout, B. L. *J. Phys. Chem. submitted* **2001**.
(21) Cao, Z. T.; Tester, J. W.; Trout, B. L. *J. Chem. Phys.* **2001**, *115*, 2550.
(22) Cao, Z. T.; Tester, J. W.; Trout, B. L. *Journal of Physical Chemistry B* **2002**, *106*, 7681.
(23) Subramanian, S.; Kini, R. A.; Dec, S. F.; Sloan, E. D. *Chemical Engineering Science* **2000**, *55*, 1981.
(24) Subramanian, S.; Kini, R. A.; Dec, S. F.; Sloan, E. D. *Gas Hydrates: Challenges for the Future* **2000**, *912*, 873.
(25) Subramanian, S.; Ballard, A. L.; Kini, R. A.; Dec, S. F.; Sloan, E. D. *Chemical Engineering Science* **2000**, *55*, 5763.
(26) Ballard, A. L.; Sloan, E. D. *Chemical Engineering Science* **2001**, *56*, 6883.
(27) Tester, J. W.; Modell, M. *Thermodynamics and its applications*, 3rd ed.; Prentice-Hall, Inc.: New Jersey, 1997.
(28) Ballard, A. L.; Sloan, E. D. *Chemical Engineering Science* **2000**, *55*, 5773.
(29) Rodger, P. M. *International Conference on Natural Gas Hydrates* **1994**, *715*, 207.
(30) Tse, J. S. *International Conference on Natural Gas Hydrates* **1994**, *715*, 187.

(31) Roberts, O. L.; Brownscombe, E. R.; Howe, L. S. *Oil & Gas Journal* **1940**, *39*, 37.
(32) Deaton, W. M.; Frost, E. M. *Gas hydrates and their relation to the operation of natural-gas pipe lines*, 1946.
(33) Reamer, H. H.; Selleck, F. T.; Sage, B. H. *J Petrol Technol* **1952**, *4*, 197.
(34) Galloway, T. J.; Ruska, W.; Chappelear, P. S.; Kobayashi, R. *Industrial & Engineering Chemistry Fundamentals* **1970**, *9*, 237.
(35) Falabella, B. J.; Vanpee, M. *Industrial & Engineering Chemistry Fundamentals* **1974**, *13*, 228.
(36) Holder, G. D.; Grigoriou, G. C. *Journal of Chemical Thermodynamics* **1980**, *12*, 1093.
(37) Holder, G. D.; Hand, J. H. *AIChE Journal* **1982**, *28*, 440.
(38) Ng, H. J.; Robinson, D. B. *Fluid Phase Equilibria* **1985**, *21*, 145.
(39) Avlonitis, D. Multiphase Equilibria in Oil-Water Hydrate Forming Systems. M.Sc. Thesis, Heriot-Watt University, 1988.
(40) Hafemann, D. R.; Miller, S. L. *J. Phys. Chem.* **1969**, *73*, 1392.
(41) Wittstruck, T.; Brey, W., Jr.; Buswell, A. M.; Rodebush, W. H. *Journal of Chemical and Engineering Data* **1961**, *6*, 343.
(42) Wilcox, W. I.; Carson, D. B.; Katz, D. L. *Journal of Industrial and Engineering Chemistry* **1941**, *33*, 662.
(43) Miller, B.; Strong, E. R., Jr. *American Gas Association Monthly* **1946**, *28*, 63.
(44) Robinson, D. B.; Mehta, B. R. *Journal of Canadian Petroleum Technology* **1971**, *10*, 33.
(45) Verma, V. K. Gas Hydrates from Liquid Hydrocarbon-Water Systems. Ph.D. Thesis, University of Michigan, 1974.
(46) Holder, G. D.; Godbole, S. P. *AIChE Journal* **1982**, *28*, 930.
(47) Kubota, H.; Shimizu, K.; Tanaka, Y.; Makita, T. *Journal of Chemical Engineering of Japan* **1984**, *17*, 423.
(48) Thakore, J. L.; Holder, G. D. *Industrial & Engineering Chemistry Research* **1987**, *26*, 462.
(49) Patil, S. L. Measurements of Multiphase Gas Hydrates Phase Equilibria: Effect of Inhibitors and Heavier Hydrocarbon Components. M.S. Thesis, University of Alaska, 1987.
(50) Schneider, G. R.; Farar, J.; Hunter, J. A.; Gillam, W. S.; Johnson, S. *U. S. Dep. Interior, Office Saline Water Res. Develop. Progr. Rep.* **1968**, *No. 292*, 37.
(51) Rouher, O. S.; Barduhn, A. J. *Desalination* **1969**, *6*, 57.
(52) Wu, B. J.; Robinson, D. B.; Ng, H. J. *Journal of Chemical Thermodynamics* **1976**, *8*, 461.
(53) Dorstewitz, F.; Mewes, D. *Chemie Ingenieur Technik* **1992**, *64*, 466.
(54) Tester, J. W.; Wiegandt, H. F. *AIChE Journal* **1969**, *15*, 239.
(55) Rodger, P. M. *J. Phys. Chem.* **1989**, *93*, 6850.
(56) Barrer, R. M.; Edge, A. V. J. *Proc. Roy. Soc.* **1967**, *London A300*, 1.
(57) Kvamme, B.; Lund, A.; Hertzberg, T. *Fluid Phase Equilibria* **1993**, *90*, 15.
(58) McLeod, H. O., Jr.; Campbell, J. M. *J. Petrol. Technol.* **1961**, *13*, 590.
(59) Jhaveri, J.; Robinson, D. B. *Canadian Journal of Chemical Engineering* **1965**, *43*, 75.

(60) Ballard, A. L.; Jager, M. D.; Nasrifar, K.; Mooijer-van den Heuvel, M. M.; Peters, C. J.; Sloan, E. D. *Fluid Phase Equilibria* **2001**, *185*, 77.
(61) Klauda, J. B.; Sandler, S. I. *Chemical Engineering Science* **2003**, *58*, 27.
(62) Holder, G. D.; Kamath, V. A. *Journal of Chemical Thermodynamics* **1984**, *16*, 399.

Chapter 5. Properties of Inhibitors of Methane Hydrate Formation via Molecular Dynamics Simulations

5.1 Introduction

Natural gas water clathrates or gas hydrates are systems of polyhedral cells formed by hydrogen-bonded water molecules and stabilized by encaged guest molecules, such as methane and/or carbon dioxide (Figures 5.1 and 5.2). They are of tremendous relevance in diverse areas such as energy, the environment, astrophysics, geology, and marine ecosystems[1-4]. The existence of clathrate hydrates was first documented by Sir Humphrey Davy[5] in 1811, who observed that a solution of chlorine gas in water freezes more readily than pure water. Since 1939, when Hammerschmidt[6] concluded that natural gas hydrates were blocking gas transmission lines, the susceptibility of forming solid hydrates in gas transmission lines under normal operating conditions has led to many investigations aimed at understanding and avoiding hydrate formation, an area of ongoing research. The optimization of natural gas production and transmission operations depends on the ability to make quantitative predictions of the rates of formation of solid hydrates as a function of temperature, pressure, and composition, including the effects of additives designed to inhibit the formation of hydrates.

Annually, oil and gas companies spend over 500 million US dollars on hydrate prevention via methanol injection. Typically, large amounts (up to 50 vol %) of methanol are used to help avoid hydrate plugging by lowering the formation temperature, with significant economic costs and potential environmental effects. The lowering of the hydrate formation temperature in the presence of methanol reflects the thermodynamic

effect of methanol on reducing the chemical potential of water in the liquid phase mixture, resulting in a freezing point depression of the solid hydrate phase.

In the last 15 years or so, many research efforts have been focused on developing what are termed "low-dosage hydrate inhibitors", or LDHIs, that can kinetically inhibit hydrate formation.[7] LDHIs operate much differently than thermodynamic inhibitors such as methanol. They are often effective at concentrations as low as 0.5 wt%[7] and act by delaying the onset of hydrate formation, while thermodynamic inhibitors are effective only at much higher concentrations and act by changing the conditions of hydrate thermodynamic stability.

Understanding the nucleation and growth of hydrates is a challenge that is just starting to be met and has tremendous scientific and technological ramifications. Noting that current experimental technology is not able to capture the nucleation process of clathrate-hydrates, we developed a molecular simulation approach based on sophisticated methods from theoretical chemistry to do so[8-10]. Recently, Rodger's group at Warwick[11,12] used molecular simulations and found that LDHIs (specifically tributylammoniumpropylsulfonate [TBAPS], poly-vinylpyrollidone [PVP], poly-vinylcaprolactam [PVCap], and poly-dimethylaminoethyl methacrylate [PDMAEMA]) reduce the degree of structure in the surrounding water which would presumably increase the barrier to hydrate nucleation. This study focuses on the action of LDHIs on ensuing crystallites of hydrates within a reasonable framework of nucleation and crystallization.

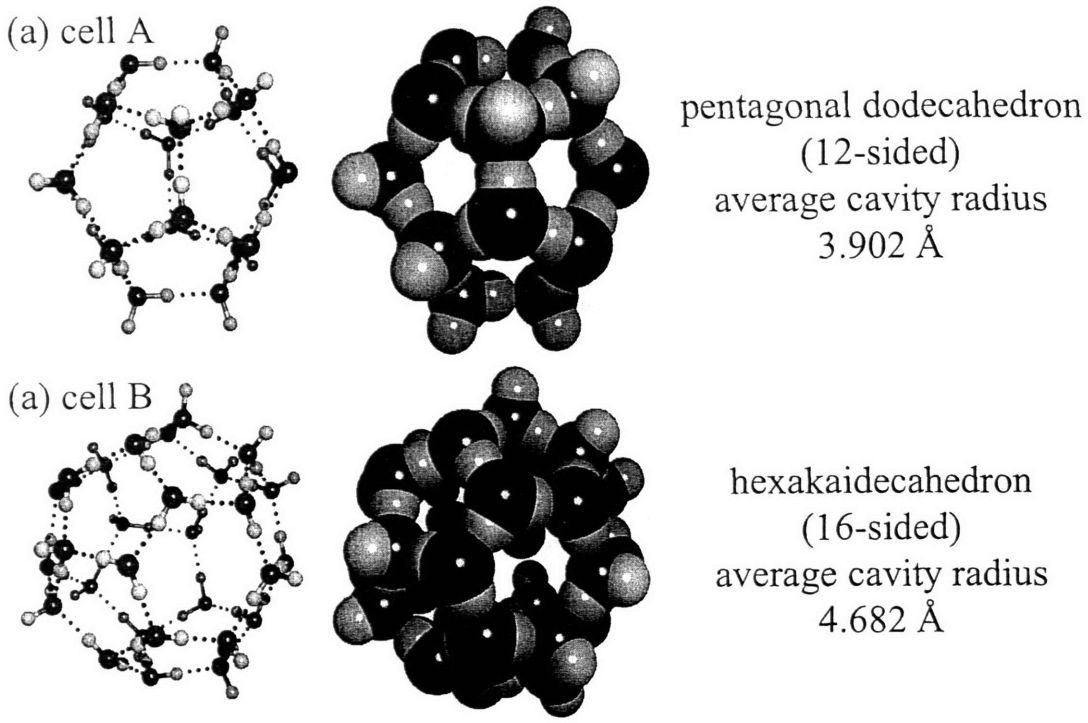

Figure 5.1: Cavities of Structure II Clathrates: This study focuses on the structure II hydrate as that is the form formed by natural gas which are typically mixtures of roughly 95% CH_4, 2.5% C_2H_6, 1.5% N_2, and the balance C_3H_8 and trace gases.

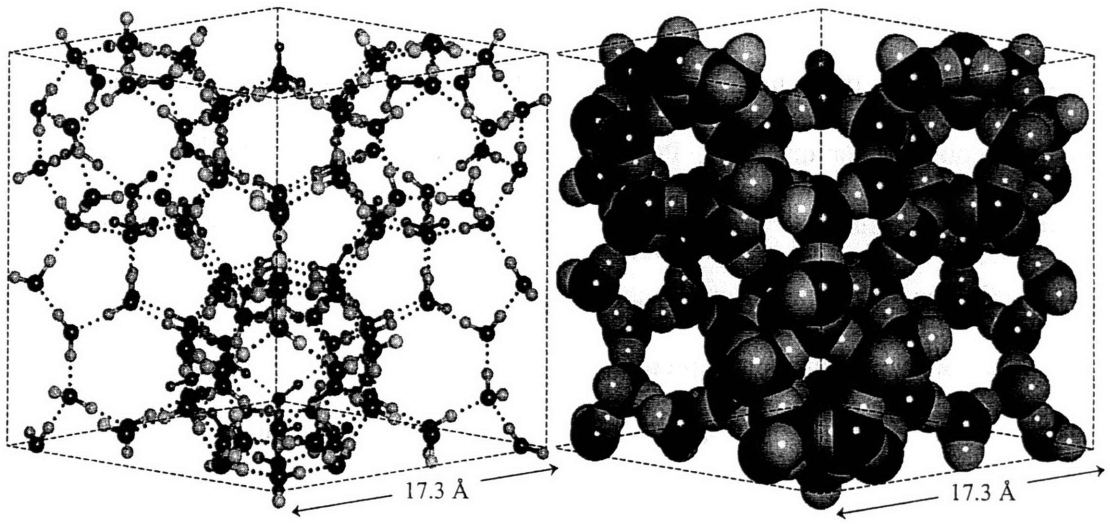

Figure 5.2: Ball and stick and space filling models of a unit cell of the structure II clathrate with a lattice constant of 17.3 Å. Consists of 136 water molecules that form 16 pentagonal dodecahedral cavities (cell A) and 8 hexakaidecahedral cavities (cell B), thus for a completely occupied system, the ideal stoichiometry would be (16 A, 8B)•136 H_2O.

5.2 Proposed Inhibition Mechanism

There has been much discussion and disagreement regarding the mechanism by which LDHIs inhibit hydrate formation[11,13-17]. Furthermore, no proposed mechanism fully explains all of the phenomena associated with hydrate kinetic inhibition such as increased induction time with sudden growth coupled with the crystal morphology changes observed in inhibited growth conditions.[11,18-20] The following section outlines a proposed mechanism that will act as a framework for our study of the factors that control hydrate inhibition properties.

The formation of natural gas hydrates begins with either a heterogeneous or homogeneous nucleation event. Previous work in our group at MIT[8] concluded that nucleation proceeds via "the local structuring mechanism," i.e., a thermal fluctuation causing the local ordering of guest molecules leads to the nucleation of the clathrate, and not by the previous conceptual picture, called "the labile cluster hypothesis" proposed by Sloan and others[1,21-23]. Our statistical approach is also contrasted with classical nucleation theory, in which macroscopic properties are assumed to describe systems of dimensions on the order of Ångstroms.

Similar to the classical theory of nucleation, our approach treats nucleation as an activated event, which is more or less irreversible. Once the system surpasses the free energy barrier to nucleation, crystal growth occurs. Within that context, the sizes of nuclei are on the order of 10s of Ångstroms.[8,24] On the other hand, the distance between inhibitor molecules is much larger than that. We can illustrate this using poly(N-vinyl-2-caprolactam), called PVCap, with a molecular weight of ~100,000. PVCap at approximately this molecular weight has been measured using small-angle neutron

scattering to have a radius of gyration, R_g, of 155 Å[25] and is highly miscible in water at temperatures of interest (T_{cloud} ~ 30° C). If PVCap is added to water at 0.5 wt %, its approximate volume fraction is 0.4 %. Assuming that the PVCap polymers are evenly dispersed throughout the water phase, then their approximate average separation would be 300 Å. Thus, nuclei could still form.

Given the information summarized briefly above, we propose that hydrate inhibition occurs via a two-step mechanism. (1) Inhibitor molecules disrupt the local organization of the water and guest molecules, increasing the barrier to nucleation and nuclei propagation. (2) Once nucleation occurs, the inhibitor binds to the surface of the hydrate nanocrystal and retards further growth along the bound growth plane.

In the first step, the disruption of newly forming nuclei occurs as proposed by Storr et al.[11] who used simulations and demonstrated that localized structure inconsistent with hydrate formation was induced by tributylammoniumpropylsulfonate (TBAPS) over several solvation shells. This element of the mechanism hitherto has not been verified experimentally. Our work focuses on step (2) and, as we will demonstrate, step (2) is consistent with several qualitative experimental results.

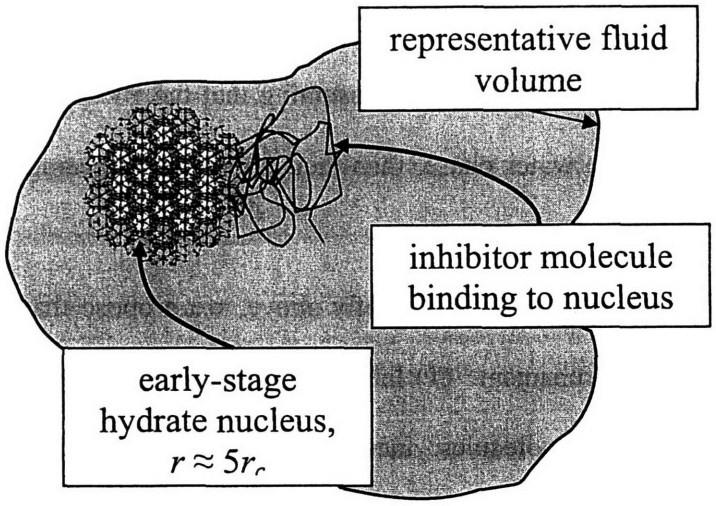

Figure 5.3: Conceptual model for inhibitor binding and crystal growth inhibition. Shown is step one of the two-step mechanism for hydrate inhibition. Inhibitor molecules disrupt the local organization of water and guest molecules and attach to forming hydrate nuclei, transferring enthalpy locally into the nuclei.

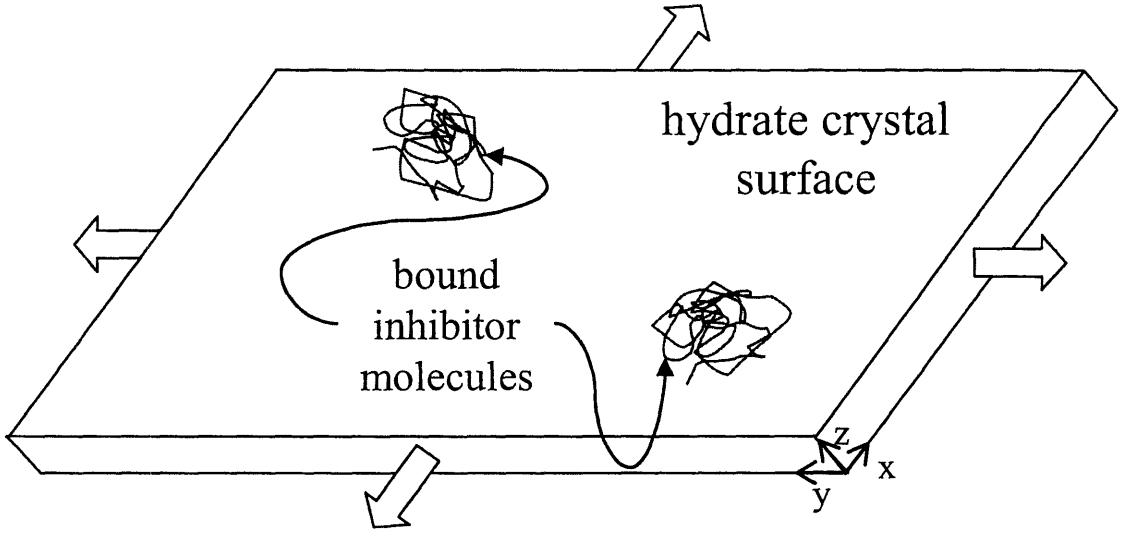

(a)

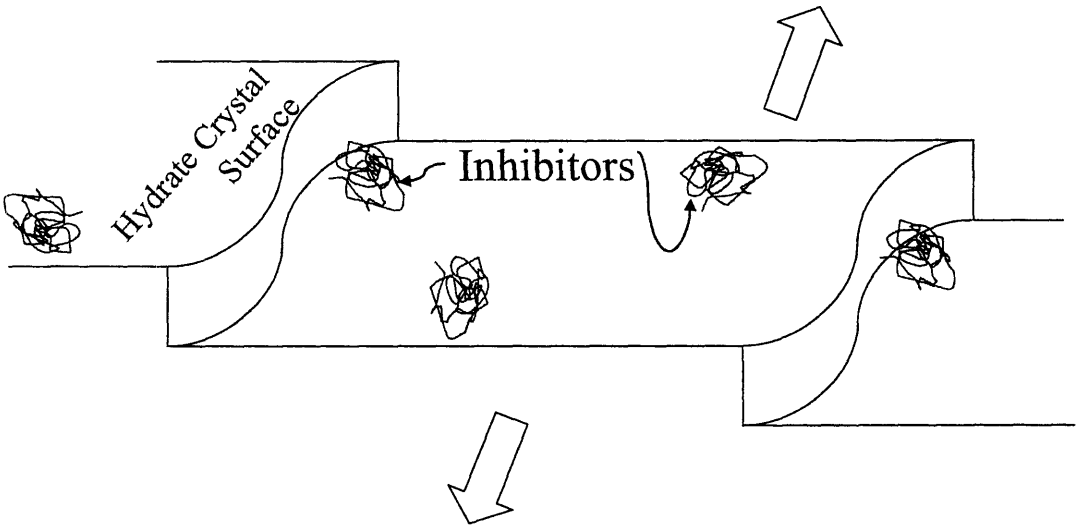

(b)

Figure 5.4: Conceptual model for inhibitor binding and crystal growth inhibition. Shown is step two of the two-step mechanism for hydrate inhibition. (a) Once the crystal has nucleated and crystal growth begins, the inhibitor binds to the surface and retards growth in the z-direction by hindering step growth through the process of step-pinning (b).

While TBAPS was shown to have an inhibition activity comparable to poly(N-vinyl-2-pyrrolidone), known as PVP, the resulting crystal morphology was quite different. PVP and PVCap have been shown to result in plate-like hydrate crystals upon crystallization[11,18-20], consistent with part (2) of the proposed mechanism while the hydrate crystals grown in the presence of TBAPS have been observed to be deformed, and particularly elongated, octahedra.

Once an inhibitor molecule such as PVP binds to one face of the hydrate nanocrystal, growth along that face is slowed significantly. King et al[25] have shown that in the presence of a hydrate-crystal/liquid slurry three active inhibitors, PVP, PVCap, and N-methyl, N-vinylacetamide/N-vinyl-2-caprolactam copolymer (VIMA/PVCap), are adsorbed to the hydrate-crystal surface while a non-inhibiting polymer, poly(ethylene oxide) was not adsorbed further supporting the surface binding hypothesis. Given these initial results, *we hypothesize that the stronger its binding to the hydrate surface, the more disruptive an inhibitor is to the structure of forming hydrate nuclei.* The rest of this paper presents the test of this hypothesis using qualitative experimental results from the literature and new quantitative molecular computational results.

5.3 Methodology

Our approach is different from previous studies[11,12,26-30] with four key variations, the use of a liquid water phase in equilibrium with the hydrate crystal, the quantitative analysis of the energetics of inhibitor binding, the use of fully dynamic water molecules in the hydrate crystal, and the placement of the water-soluble inhibitor in the liquid water phase as opposed to in the gas or vacuum phase. Previous computational studies focused on the morphologic effects[11], the topology[26-29] of the hydrate–inhibitor interaction, or the

structural behavior of inhibitor molecules in solution[30], all structural studies. This project focuses on estimating the binding energy of the inhibitor on the hydrate crystal surface.

5.3.1 Development of molecular-interaction parameters

Hydrate-clathrates cannot be modeled quantitatively on a molecular level without incorporating accurate guest–host interactions. Our guest-host potentials are derived from *ab initio* calculations and are directly connected to molecular force interactions and sizes and proven to reproduce experimental data for the hydrate-clathrate system[31-33]. In this study, we have developed and parameterized an accurate potential for methane–water interactions that can be used with the CHARMM® molecular dynamics package. This was developed using our *ab initio* methane-water potential energy surface developed earlier[31,34]. The 18,000 methane–water *ab initio* energies were fit to the CHARMM® potential minimizing the Boltzmann-weighted square error χ between the *ab initio* potential energy surface and the CHARMM® potential energy surface.

$$\chi = \sum_{i}^{\#\text{ of QM points}} \left[\exp\left(\frac{-\Delta E_{cp,i}}{kT} \right)_{QM} - \exp\left(\frac{-\Phi_i^{tot}}{kT} \right)_{model} \right]^2 \qquad (5.60)$$

$$\text{with: } \Phi^{tot} = \sum_{k}^{\#\text{ of sites}} \Phi_{CH_4\text{-}k}$$

The adjustable parameters in the CHARMM® potential are the characteristic energy, ε, and the soft core radius, σ, of the L-J 6-12 potential for both the $H_4\mathbf{C}$–$\mathbf{O}H_2$ and the $H_3C\mathbf{H}$–$\mathbf{O}H_2$ interactions as shown in Figure 5.5. (The atoms marked in bold indicate the location of the interaction site for use in a site-site potential.) Interaction parameters

given in Table 5.1 and Table 5.2 were found by applying traditional Lorentz-Berthelot mixing rules:

$$\varepsilon_{ij} = \sqrt{\varepsilon_i \varepsilon_j}$$
$$\sigma_{ij} = \frac{\sigma_i + \sigma_j}{2} \tag{5.61}$$

Table 5.1: CHARMM Potential Parameters Determined for the Methane–Water Interaction (atoms marked in bold indicate interaction site)

interaction	$\varepsilon_{C,H-O}$	$\sigma_{C,H-O}$	$Q_{C,H,O}$	Q_M
H_4**C**–**X**	0.18	3.5	-0.24	
H_3C**H**–**X**	0.03	2.5	0.06	
TIP4P[35,36] H_2**O**–**O**H_2	0.155	3.154	0.52	-1.04

Table 5.2: OPLS[37,38] Potential Parameters Commonly Used for Methane (atoms marked in bold indicate interaction site)

site	ε_{ij}	$\sigma_{C,H-O}$	$Q_{C,H}$
H_4**C**–**X**	0.066	3.5	-0.24
H_3C**H**–**X**	0.030	2.5	0.06

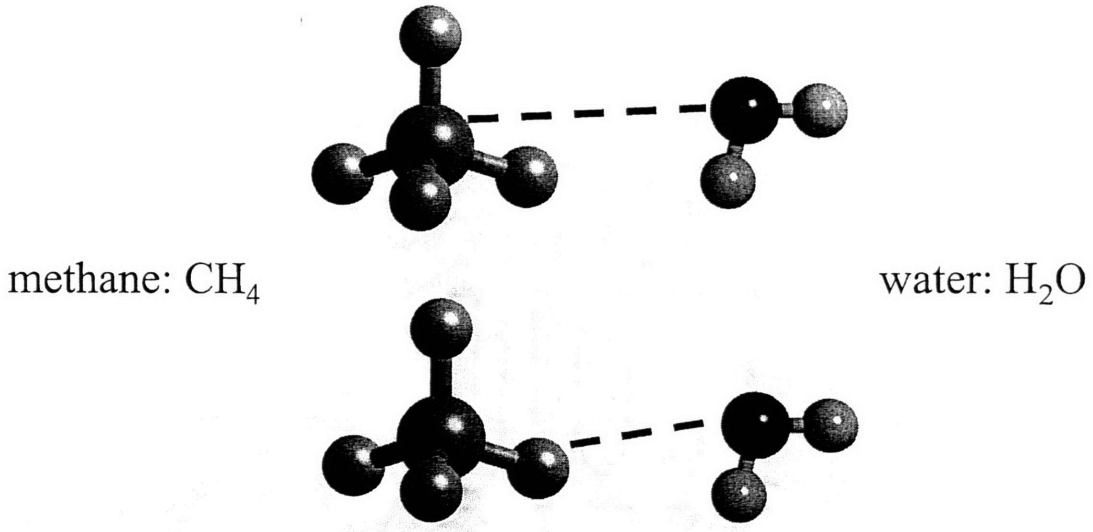

Figure 5.5: Site-Site Interactions between Methane (C=blue, H=grey) and Water (O=red, H=Grey) Accounted for in the Developed CHARMM Potential

The CHARMM® model with this set of intermolecular potential parameters was then verified by simulation of a 34.6 Å cubic volume consisting of 8 structure II unit cells (2×2×2) with full methane occupancy (see Figure 5.6). This scale results in a simulation with 1088 water and 192 methane molecules. The TIP4P model was used for water in the development of the methane potential and in the dynamic simulations. The sII crystal was then simulated using CHARMM® until the simulation reached equilibrium and then molecular dynamics were run for 100 ps. During the sII hydrate simulation the lattice parameter of the sII hydrate unit cell ranged from 17.16–17.45 Å with an average of 17.31 Å and a standard deviation of 0.022 Å. This result compares favorably to the experimental lattice parameter of 17.3 Å and serves as a validation of the use of our

developed methane–water potential in these dynamic simulations.

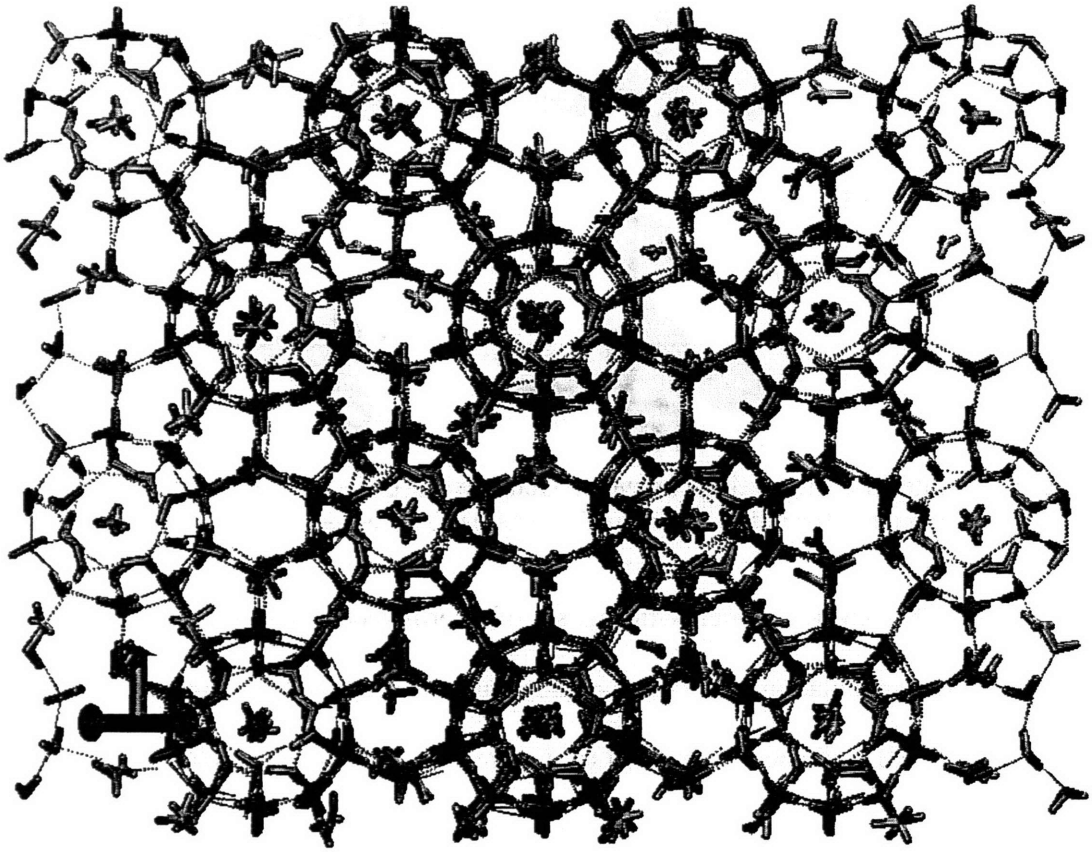

Figure 5.6: 34.6 Å × 34.6 Å × 34.6 Å box Consisting of eight Structure II Unit Cells with Methane Guest Molecules

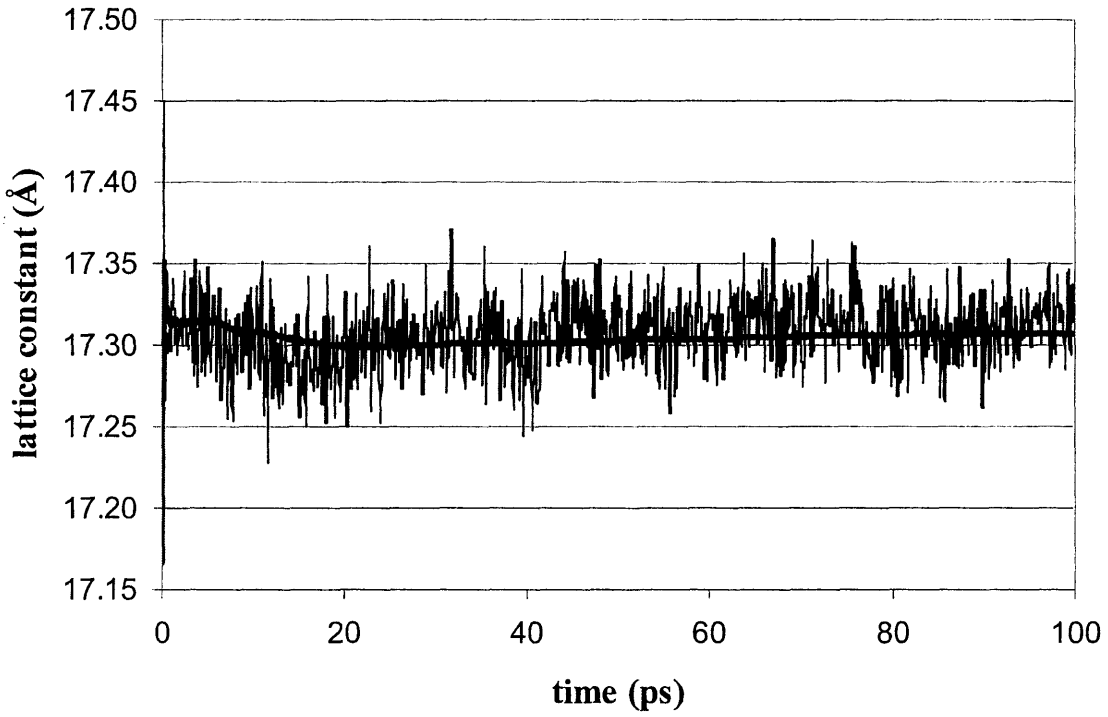

Figure 5.7: Equilibration of the Lattice Constant of Eight Structure II Unit Cells

5.3.2 Structure II hydrate surface

A molecular-scale slab model was used in surface interaction calculations involving the sII hydrate molecules and inhibition molecules. The hydrate molecules are embedded in a particular crystallographic plane that spans 4 sII unit cells were placed in a 34.6 Å × 34.6 Å × 17.3 Å box. On top of the solid layer of crystalline hydrate is placed a layer of liquid water another 17.3 Å thick. To replicate conditions occurring in gas transmission line hydrate crystal growth, the liquid layer serves as the water condensate layer that solubilizes the inhibitor molecules. Figure 5.8 shows the resulting 34.6 Å cubic simulation box. Periodic boundary conditions were incorporated to model the solid-liquid system dynamically and to simulate a stable hydrate crystal surface at 200 K and 4 bar.

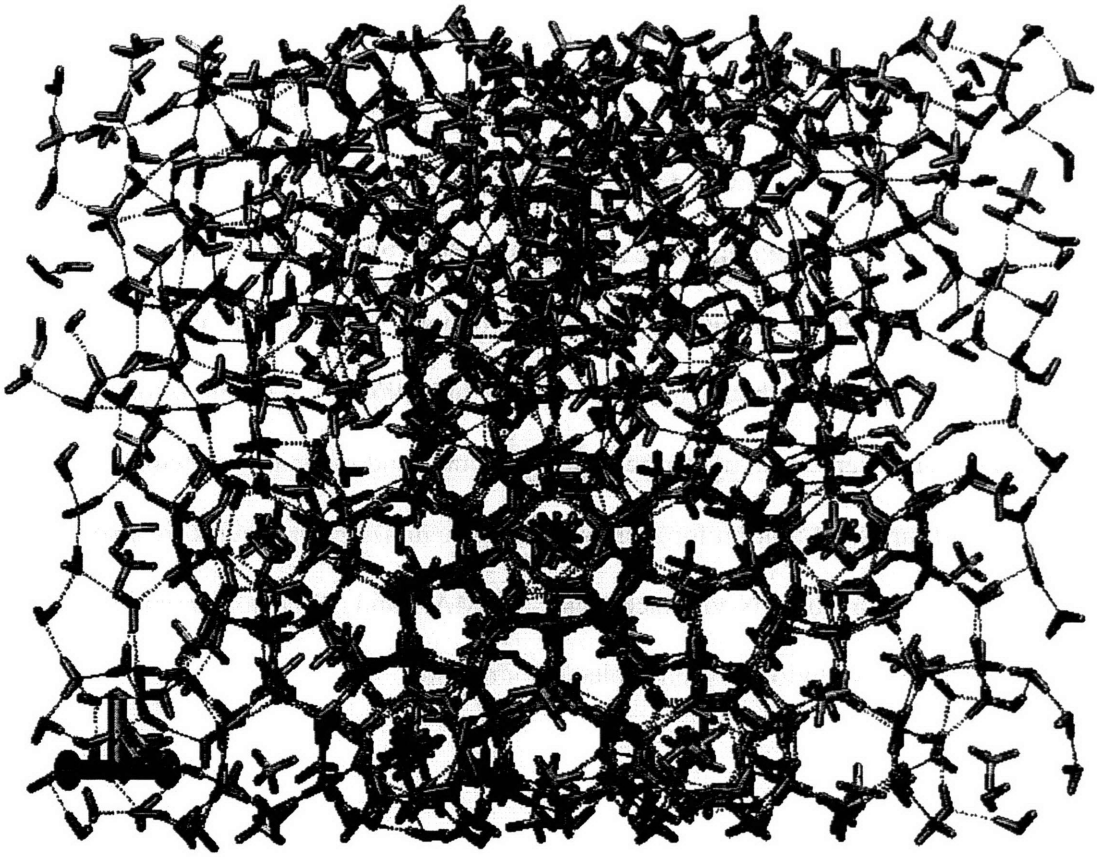

Figure 5.8: Hydrate Slab with Liquid Water in the Fluid Phase

5.3.3 Determination of inhibitor binding energy

Once the hydrate crystal–liquid water slab model described above was constructed, a monomer unit of inhibitor was placed in either the middle of the liquid phase or near hydrate solid surface. We define the surface adsorption energy as the difference between the energy of the entire simulation with the monomer bound to the crystal minus the energy of the system with the monomer in the bulk liquid. NPT molecular dynamic simulation runs were then performed on the bound and unbound systems for 6-7 ns allowing full ranges of motion for all molecules. The inhibitor molecules we studied were PVP, PVCap, N-methyl, N-vinylacetamide (VIMA), and PEO, a non-inhibitor[25], see Figure 5.9 for a description of their molecular structures.

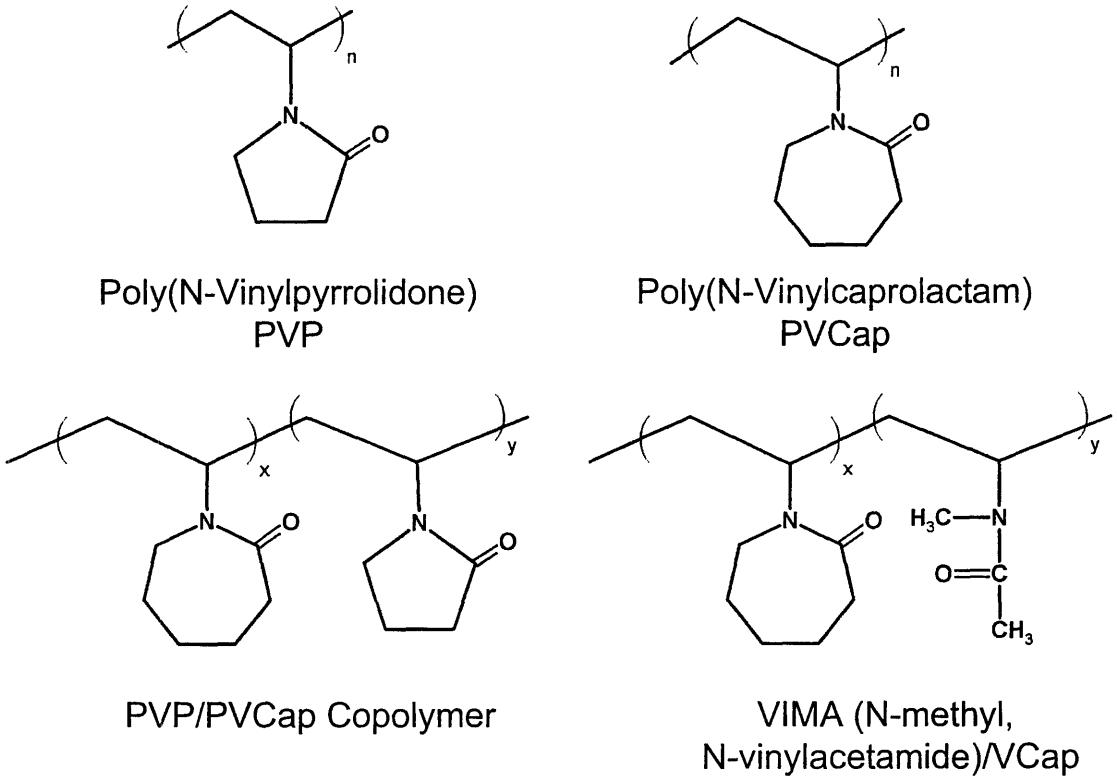

Figure 5.9: Structure of four common kinetic hydrate inhibitors comprised of the monomer units studied in this project

5.3.4 Inhibitor molecules studied

The partial atomic charges for PVP, PVCap, N-methyl, N-vinylacetamide, and PEO were calculated using Gaussian 03® and the nonbonded interaction parameters were chosen from the parameters optimized for alkanes found in CHARMM®. In this study we assumed that the binding energy of the monomer was independent of the chain length and was linearly additive. Therefore, the PVP/PVCap copolymer is analyzed by considering both the PVP and PVCap monomer units as well as the VIMA/VCap polymer examined by King et al[25]. This assumption is justified in the work by Lederhos et al.[7] which showed that PVP/PVCap copolymers exhibited induction times for hydrate formation between that of the two homopolymers.

5.3.5 Free energy of binding

The Gibbs free energy of binding is calculated using Kirkwood's coupling parameter method[39]. Specifically, it is the difference in the Gibbs free energy of inserting an inhibitor molecule on the surface of the hydrate and in the liquid water phase. Because binding energy is a thermodynamic property, the insertion of an inhibitor can be performed along a fictitious pathway λ, in which λ = fraction of insertion. To be able to evaluate a relatively smooth energy profile from an unincorporated (ghost) inhibition molecule (invisible to other molecules) at $\lambda = 0$ to a fully incorporated inhibition molecule at $\lambda = 1$, have used ten evenly spaced values of λ over λ [0,1] in our energy simulations. λ is used as a multiplier on the ε value in the nonbonded energy terms between any atom on the inhibitor and the other molecules in the simulation, effectively turning on and off the inhibitor–water and inhibitor–methane interactions. To calculate

the free energy, the Hamiltonian, H, is calculated for each value of λ and integrated from $\lambda = 0$ to $\lambda = 1$ as shown below[40]:

$$G(\lambda=1)-G(\lambda=0)=\int_0^1\left\langle\frac{d\mathsf{H}(\lambda)}{d\lambda}\right\rangle_\lambda d\lambda \cong \int_0^1\left\langle \mathsf{H}_1-\mathsf{H}_0\right\rangle_\lambda d\lambda \tag{5.62}$$

where $\mathsf{H}(\lambda) = \mathsf{H}_0 + \lambda(\mathsf{H}_1 - \mathsf{H}_0)$, and G is the Gibbs free energy.

5.3.6 Estimation of statistical error

Determination of the variances of the ensemble averages of the system energy not only allows us to calculate potential error in the values for system energy but also provides a metric for determining the length of simulation required to calculate accurate statistical quantities.

The reported error bars for the energy calculations are the standard deviations of the ensemble average energy and were calculated using both the method described by Frenkel and Smit[40] in Appendix D and the method developed by Flyvbjerg and Petersen[41] as follows. The ensemble average is estimated from

$$\langle E\rangle \approx \bar{E} \equiv \frac{1}{L}\sum_{i=1}^{L} E_i \tag{5.63}$$

where $E_1, E_2, \ldots, E_L$ are consecutive values of the energy of the system over windows of simulation with length L, assuming all discrete E_i values have been taken after the system reaches equilibrium. The variance is estimated by

$$\sigma^2(E)=\left\langle E^2\right\rangle-\langle E\rangle^2 \approx \frac{1}{L}\sum_{i=1}^{L}\left[E_i-\bar{E}\right]^2 \tag{5.64}$$

One now needs to eliminate correlation effects due to the consecutive nature of molecular dynamic simulations. To do this, the energy is grouped into consecutive blocks,

computing the average along the way. The block averages will exhibit less correlation as the blocking continues.

$$E_i' = 0.5\left(E_{2i-1} + E_{2i}\right) \tag{5.65}$$

So now $L' = 0.5L$ and the variance of the new set is

$$\sigma^2\left(E'\right) = \left\langle E'^2 \right\rangle - \left\langle E' \right\rangle^2 \approx \frac{1}{L'}\sum_{i=1}^{L'} E_i'^2 - \bar{E}'^2 \tag{5.66}$$

As the blocking procedure is followed we can find our estimate of the variance as

$$\sigma^2\left(E\right) \approx \frac{\sigma^2\left(E'\right)}{L'-1} \approx \text{constant} \tag{5.67}$$

5.4 Results/Discussion

5.4.1 Energetics of Binding

The optimal binding site for both the PVP and PVCap monomers on the hydrate surface was found to be a partially formed 16-sided hexakaidecahedron ($5^{12}6^4$) as shown in Figure 5.10(a) and (c). On the plane chosen to create the surface of the hydrate, the hexakaidecahedron is cleaved in half leaving the open top side exposed to the liquid phase. The PVP monomer binds in this half-cavity on the hydrate surface with an energy of binding of -20.6 ± 2.5 kcal/mol. The ensemble averaged energy of PVP on and off the hydrate surface resulting from the MD simulation is shown in Figure 5.11. The system equilibrated in about 2.5 ns and then statistics were accumulated for another 3-4 ns where each timestep was 0.001 ps. Similarly, as illustrated in Figure 5.12 the energy of binding of PVCap was found to be -37.5 ± 3.4 kcal/mol. PVCap, therefore, is clearly the stronger

binder to the hydrate crystal surface. The energy of binding to the hydrate surface for PVCap is about 20 kcal/mol stronger than the energy of binding of PVP.

The free energy calculation for PVCap is shown in Figure 5.13. The free energy of binding for PVCap is calculated to be -9.4 ± 3.8 kcal/mol while the free energy of binding of PVP is found to be 0.5 ± 3.7 kcal/mol. The free energy of binding of PVP is effectively zero while the equilibrium reaction for PVCap binding favors the inhibitor bound to the hydrate surface as opposed to in solution. In the case of PVP, the negative binding energy coupled with the neutral (zero) binding free energy can be interpreted as an exothermic phase adsorption reaction in which an equal number of PVP species bind to and dissociate from the hydrate surface at equilibrium.

The PVCap binding event is also exothermic ($\Delta E < 0$); however, in the case of PVCap binding, the equilibrium is shifted toward "products" (bound species) by the negative free energy of binding. Therefore, a higher fraction of PVCap monomers are bound to the surface compared to PVP. This is consistent with the relative effectiveness of these two inhibitors found experimentally, our proposed mechanism, and with the low fraction of bound PVP species found by Hutter et al.[17]

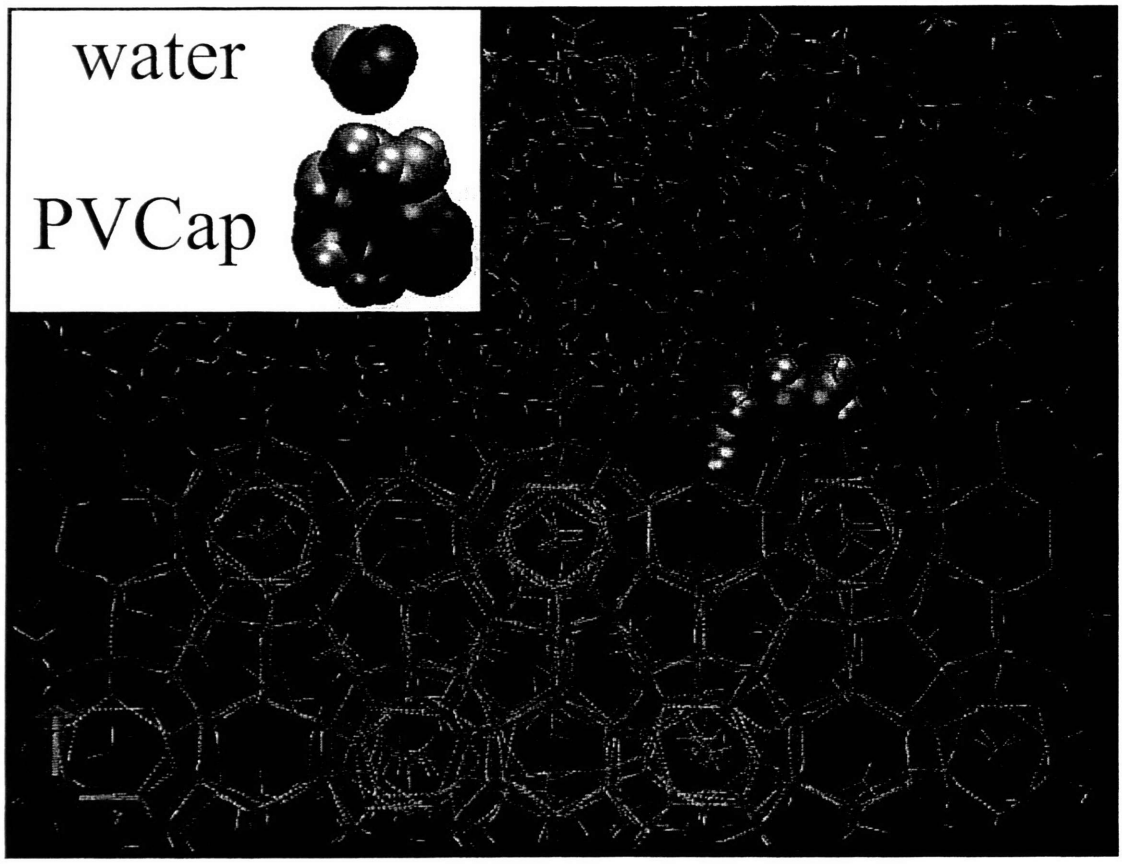

Figure 5.10a: Snapshots from the simulation of PVCap in the presence of a hydrate surface. PVCap monomer is adsorbed into the open face of a hexakaidecahedron. Hydrogen bonds are shown in white to illustrate the hydrate lattice.

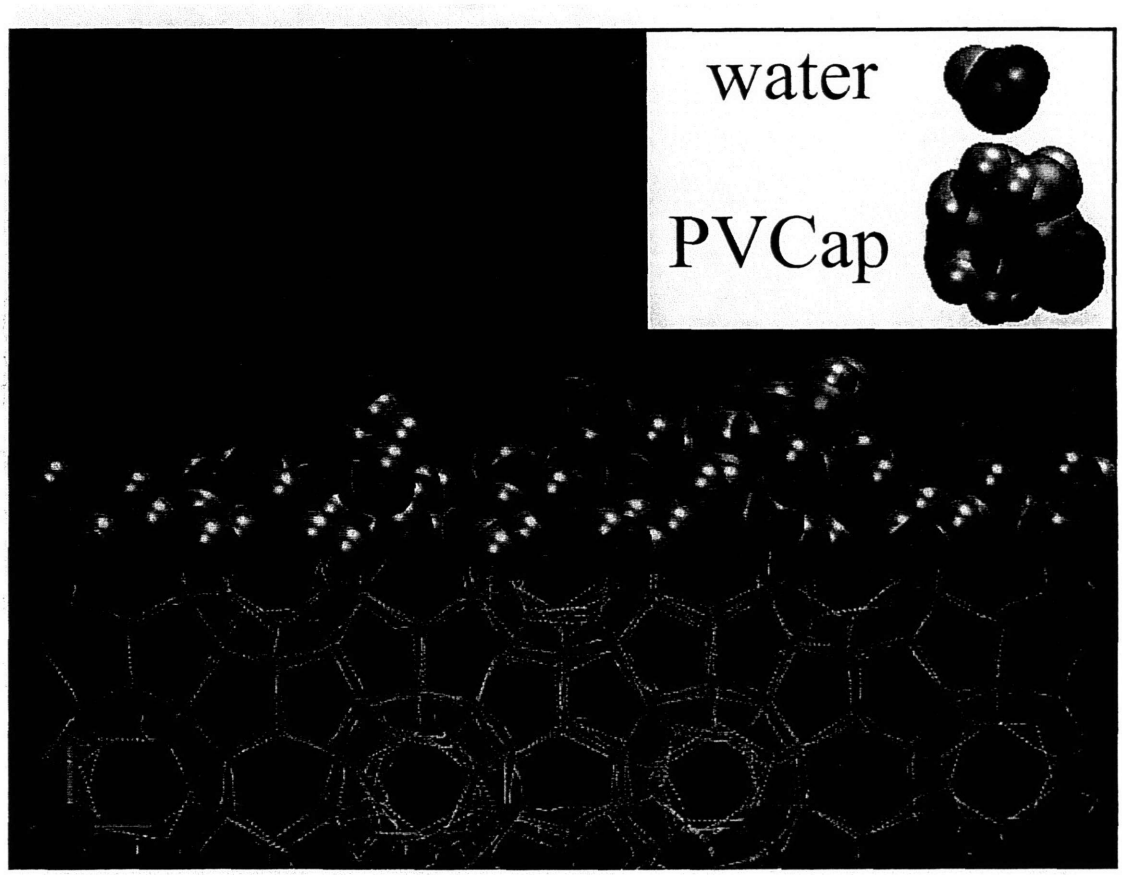

Figure 5.10b: Snapshots from the simulation of PVCap in the presence of a hydrate surface. The liquid waters found in Figure 5.10 are now invisible and the waters on the surface of the hydrate crystal are expanded to a van der Waals representation to illustrate the surface structure.

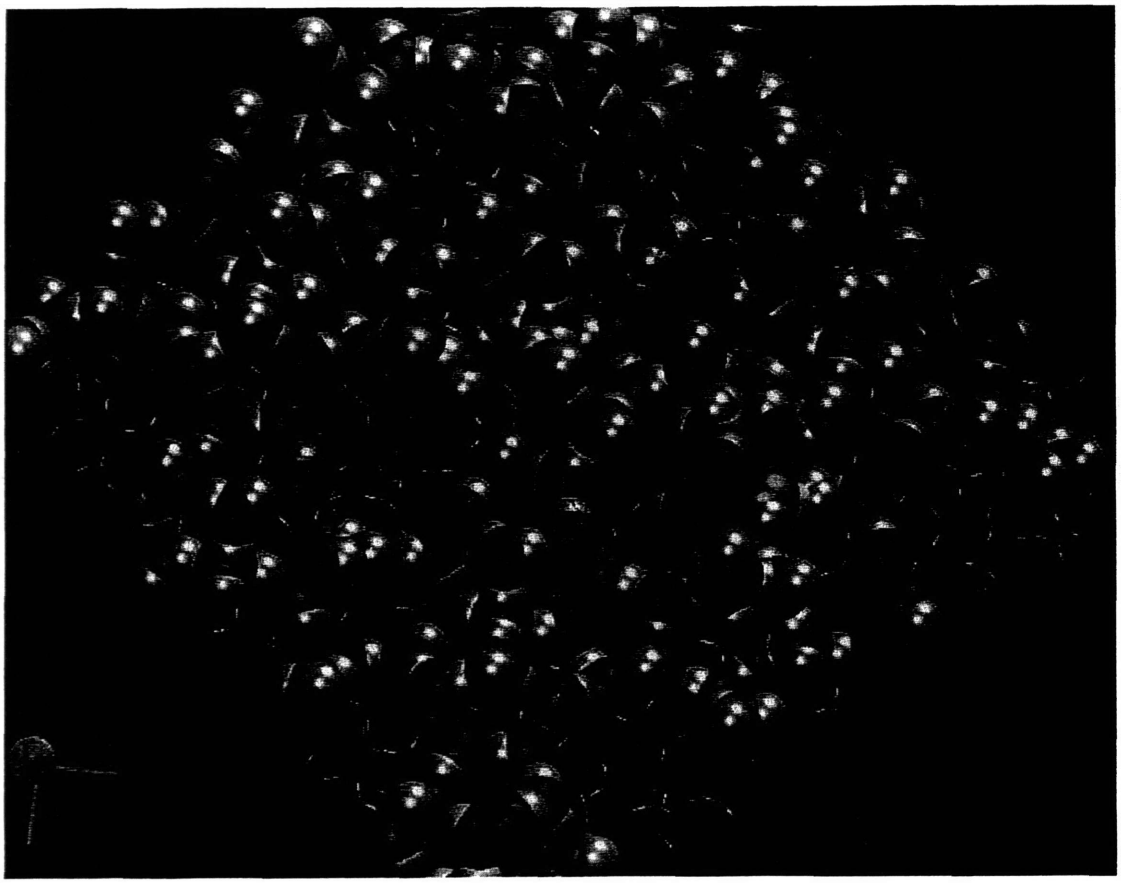

Figure 5.10c: Snapshots from the simulation of PVCap in the presence of a hydrate surface. The hydrate surface is rotated toward the reader to show the binding site of the PVCap monomer.

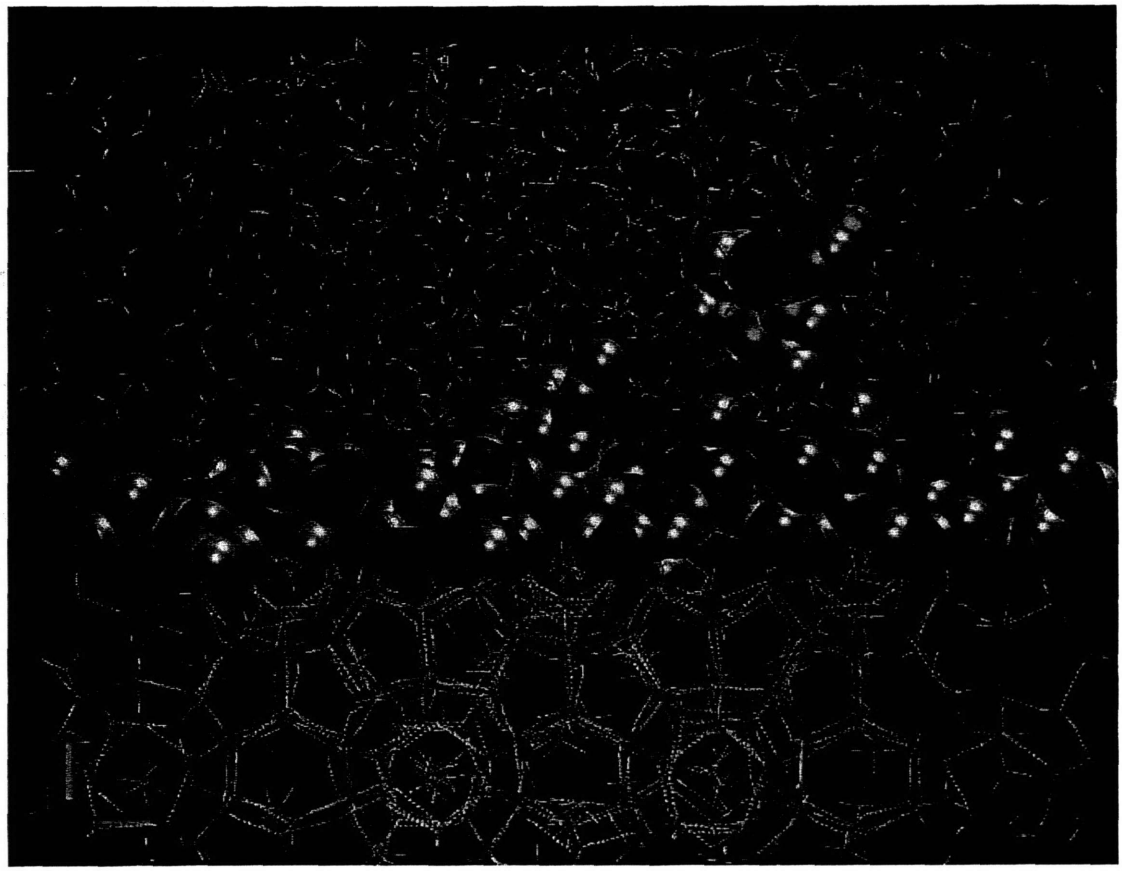

Figure 5.10d: Snapshots from the simulation of PVCap in the presence of a hydrate surface. The PVCap monomer is away from the surface of the hydrate.

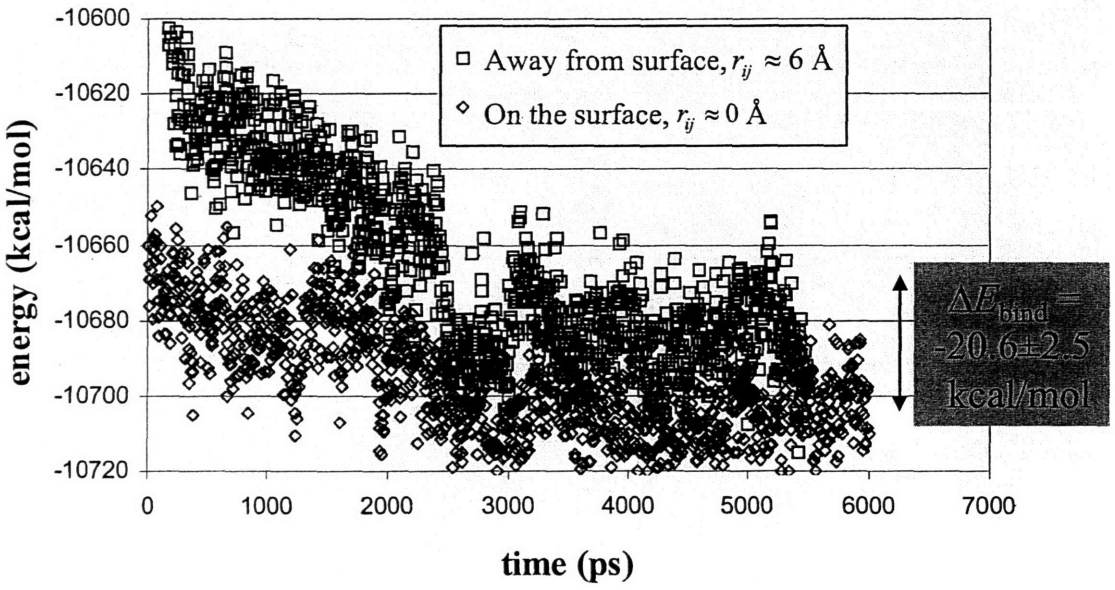

Figure 5.11: Dynamic energy of the PVP-hydrate surface

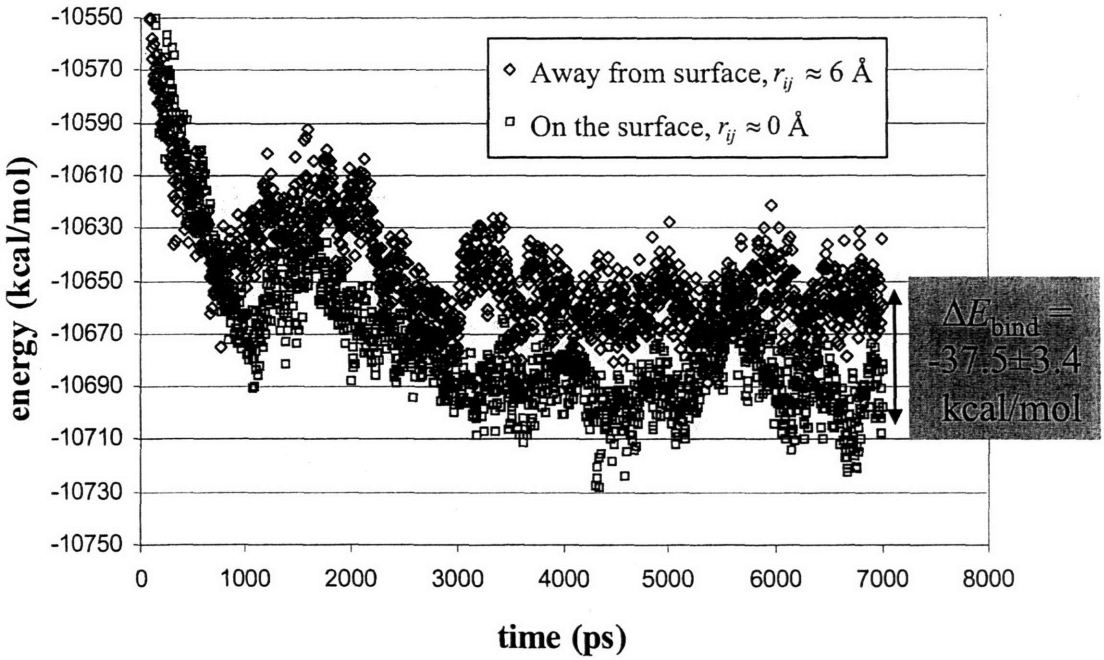

Figure 5.12: Dynamic energy of the PVCap-hydrate surface

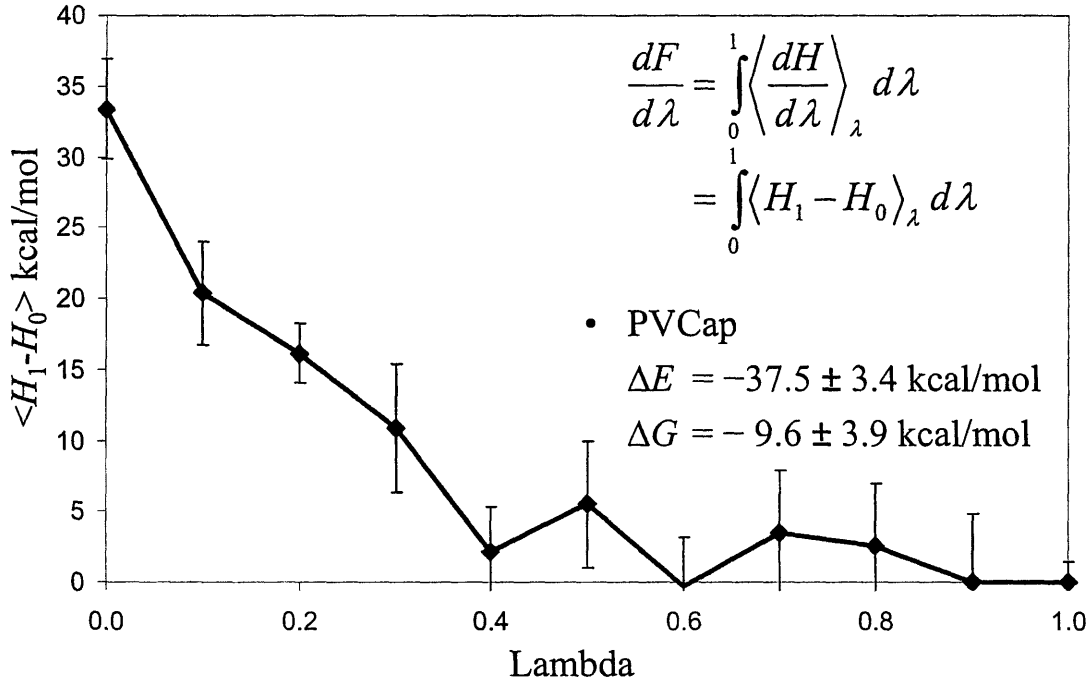

Figure 5.13: Differential Hamiltonion plot for PVCap

The lowest-energy binding site for the VIMA monomer is significantly different than that for the two previous inhibitor monomers, PVP and PVCap. As shown in Figure 5.14, in contrast to the binding site found for PVP and PVCap (in the half-formed hexakaidecahedron cavity) the VIMA monomer binds to what one might call a "bridge" site between two adjacent cavities. In the MD simulation, the VIMA monomer jumped from the higher energy binding site inside the open cavity to the bridge site, thus lowering its total energy. This transition corresponds to the second drop in ensemble energy occurring around 1400 ps as seen in Figure 5.15. The resulting binding energy for the VIMA monomer is -45.8 ± 4.5 while the binding free energy is -15.1 ± 4.6, both significantly lower than the binding energy and free energy for the PVP and PVCap monomers.

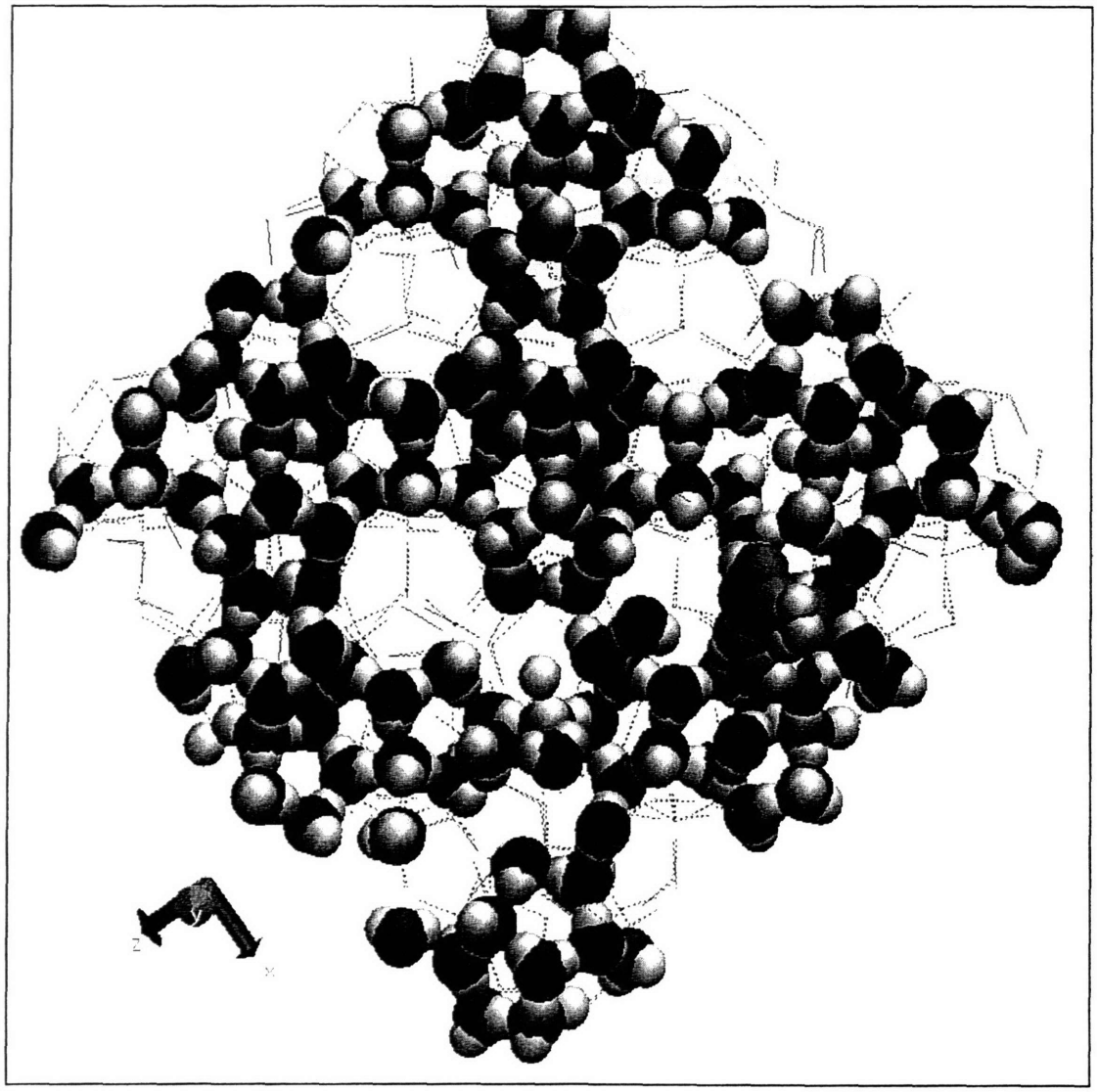

Figure 5.14:VIMA bound to the sII hydrate surface in the minimum-energy binding site

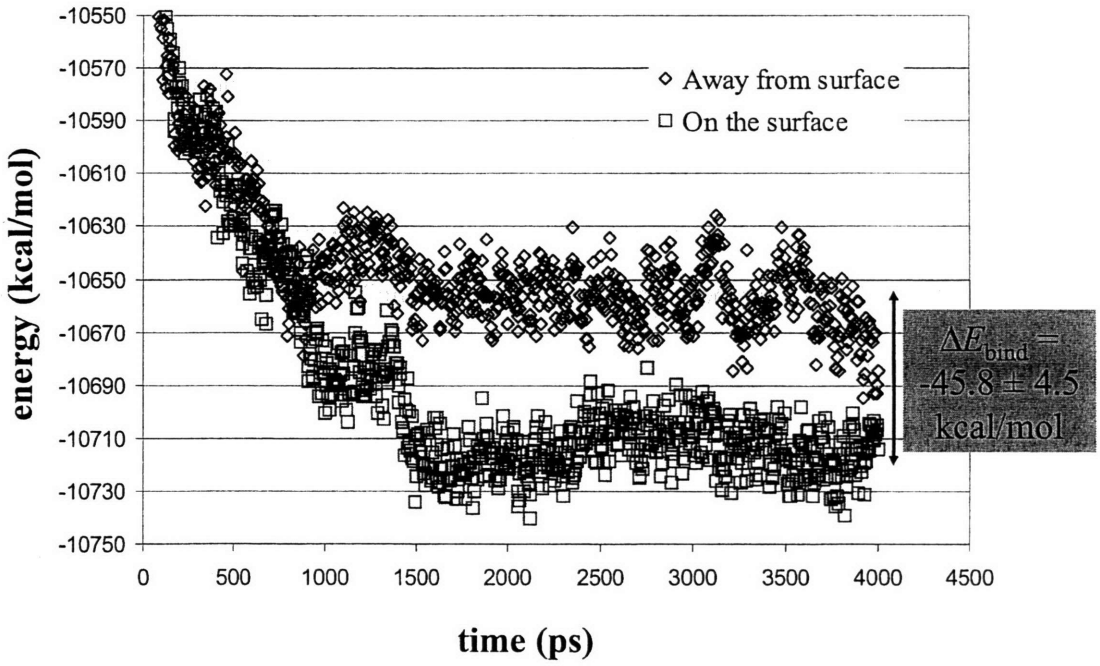

Figure 5.15: Dynamic energy of the VIMA-hydrate surface

The binding energy and free energy for PEO was calculated as a control experiment. King et al.[25] concluded from their small-angle neutron scattering (SANS) study that "there is no evidence of an adsorbed layer" of PEO in the presence of hydrate surfaces. This result is consistent with our proposed mechanism in that since if there is no polymer adsorption on the hydrate surfaces then there would be no hydrate formation inhibition. In our MD simulations, we also observe adsorption of PEO to the surface of hydrate crystals. The resulting "binding energy" for PEO is -0.2 ± 2.8 (Figure 5.16) and the binding free energy (Figure 5.17) is +0.4 ± 3.9, indicating that the binding event is not thermodynamically favorable. Table 5.3 summarizes the binding energy study for the four molecules examined and compares the binding energy and free energy to reported effectiveness of the inhibitors. The rightmost column in Table 5.3 shows the order of increasing inhibitor effectiveness as described by a number of different research and engineering groups[7,25,42,43]. Inhibitor effectiveness ranges from inactive (PEO) to very active (VIMA/VCap) [25].

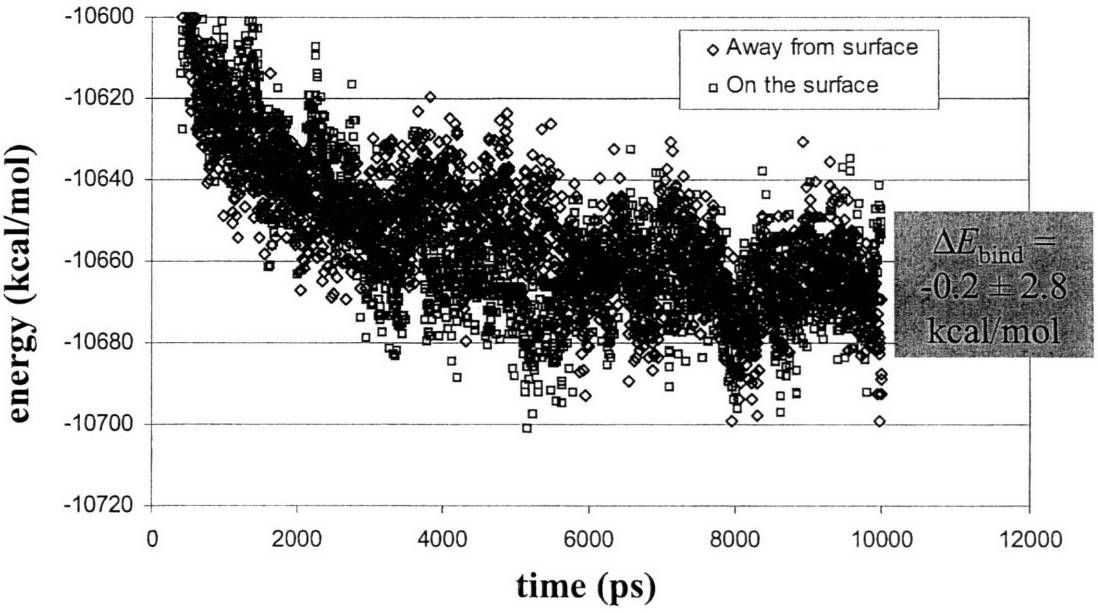

Figure 5.16: Dynamic energy of the PEO-hydrate surface

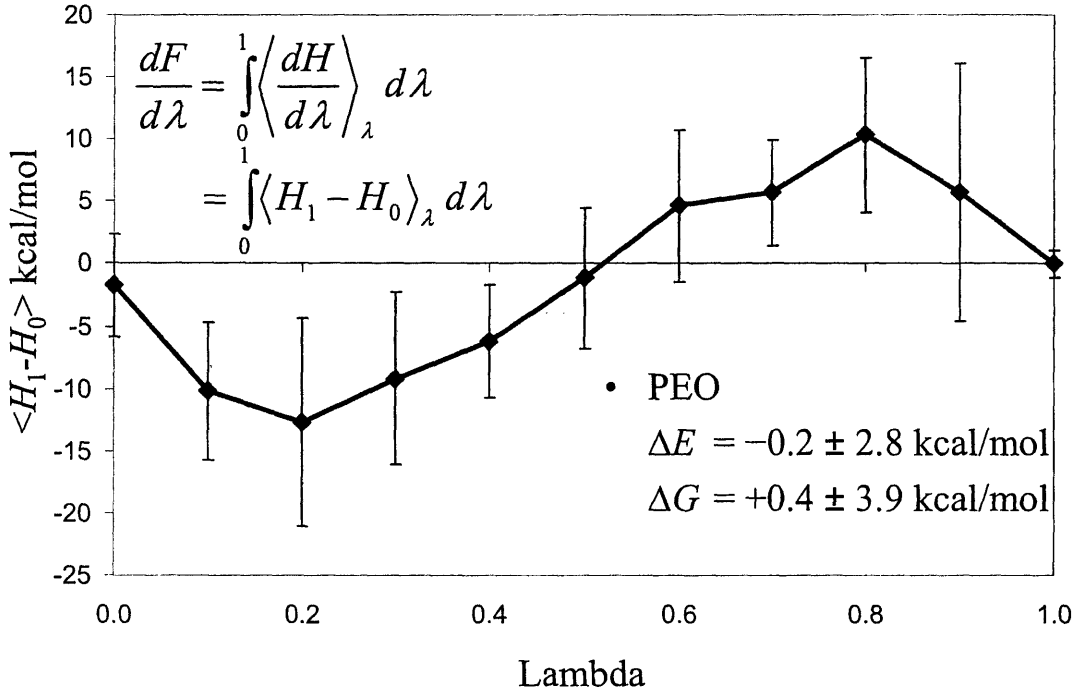

Figure 5.17: Differential Hamiltonion plot for PEO

Table 5.3: Summary of Binding Energies for Four Monomers Studied

Molecule	ΔE (kcal/mol)	ΔF (kcal/mol)	$T\Delta S$ (kcal/mol)	excess low-q scattering[25] (cm^{-1})[a]	Increasing inhibitor effectiveness[7,25,42,43]
PEO	-0.2 ± 2.8	+0.4 ± 3.9	-0.6	0	
PVP	-20.6 ± 2.5	+0.5 ± 3.7	-21.1	3	
PVCap	-37.5 ± 3.4	-9.4 ± 3.8	-28.1	10	
VIMA	-45.8 ± 4.5	-15.1 ± 4.6	-30.7	37[b]	

[a] Excess low-q scattering used as a measure of the change in polymer confirmation due to the introduction of hydrate surfaces for binding. This value is interpreted as a measure of the degree of polymer binding on the hydrate surfaces.

[b] Excess low-q scattering measured for VIMA/PVCap copolymer. King et al.[25] state that VIMA/PVCap is most effective inhibitor

5.4.2 Binding and Surrounding Water Morphology

Structural effects were examined by calculating the radial distribution functions, $g(r)$, of the double-bonded oxygen on the inhibitor molecules with the oxygen of water in either the hydrate phase (bound inhibitor) or the liquid phase (unbound).

$$g(r_{ij}) = \frac{V}{N^2}\left\langle \delta\left(r - r_{ij}\right)\right\rangle \tag{5.68}$$

where i is the oxygen on the inhibitor molecule and j is the oxygen in water in either the hydrate or liquid phase (indicated on plots). V/N^2 normalizes the $g(r)$ relative to an ideal gas of the same density. Figure 5.18 shows the radial distribution functions, RDFs, between the oxygen on the monomer and the oxygen on the surrounding water molecules for monomers both on and off the hydrate surface. One can clearly see in Figure 5.18a that the hydrate surface has little effect on the PEO monomer since the $g(r)$ does not change significantly. One should expect this result both from the SANS results[25] and the

energetic results from our simulation. One can also see a noticeable increase in the interaction between the monomer and the hydrate surface in Figure 5.18b-d. PVP, Figure 5.18b, is affected slightly while PVCap and VIMA, Figure 5.18c-d, are strongly affected. Note that there is a strong oxygen-oxygen correlation for both PVCap and VIMA on and off the surface.

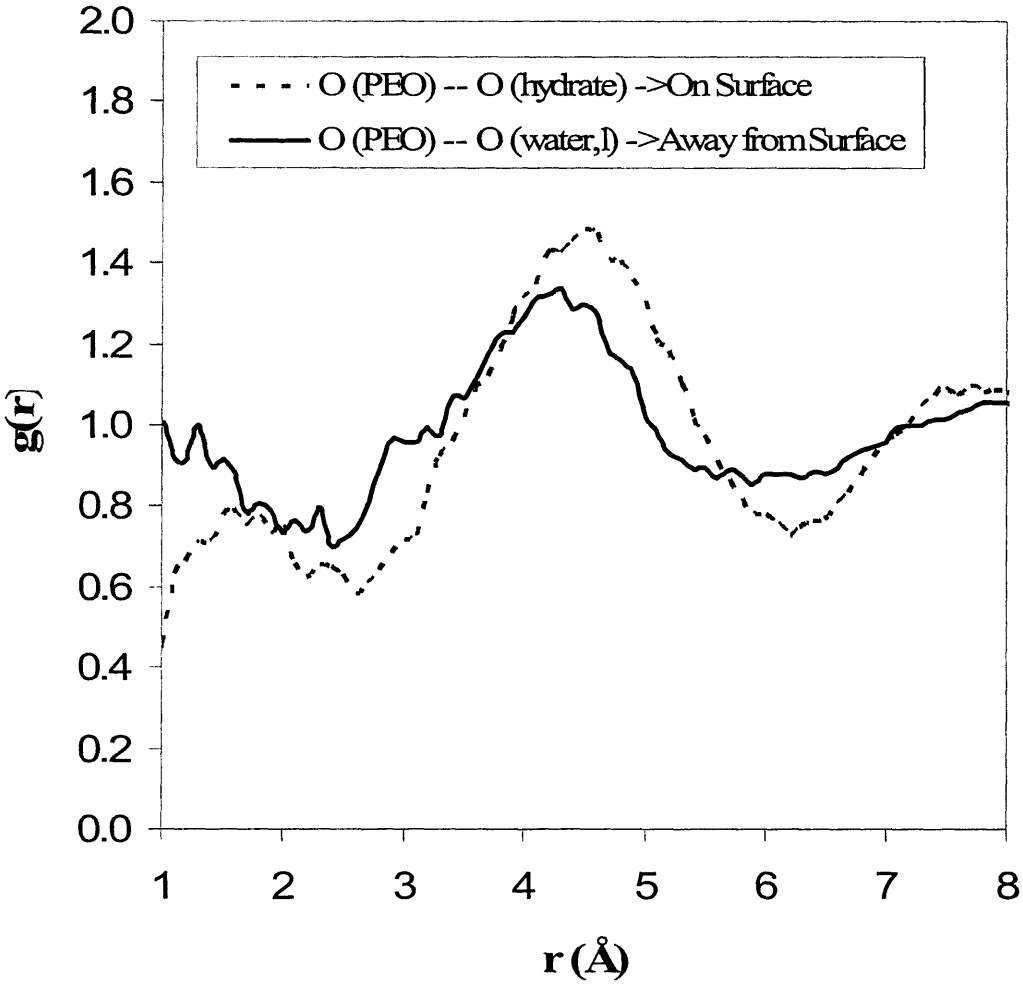

Figure 5.18a: Radial distribution functions between the double-bonded oxygen on PEO and the oxygen on water when the PEO is bound to the hydrate surface and away from the surface. Difference illustrates the effect of the hydrate surface on the morphology of the monomer and surrounding waters.

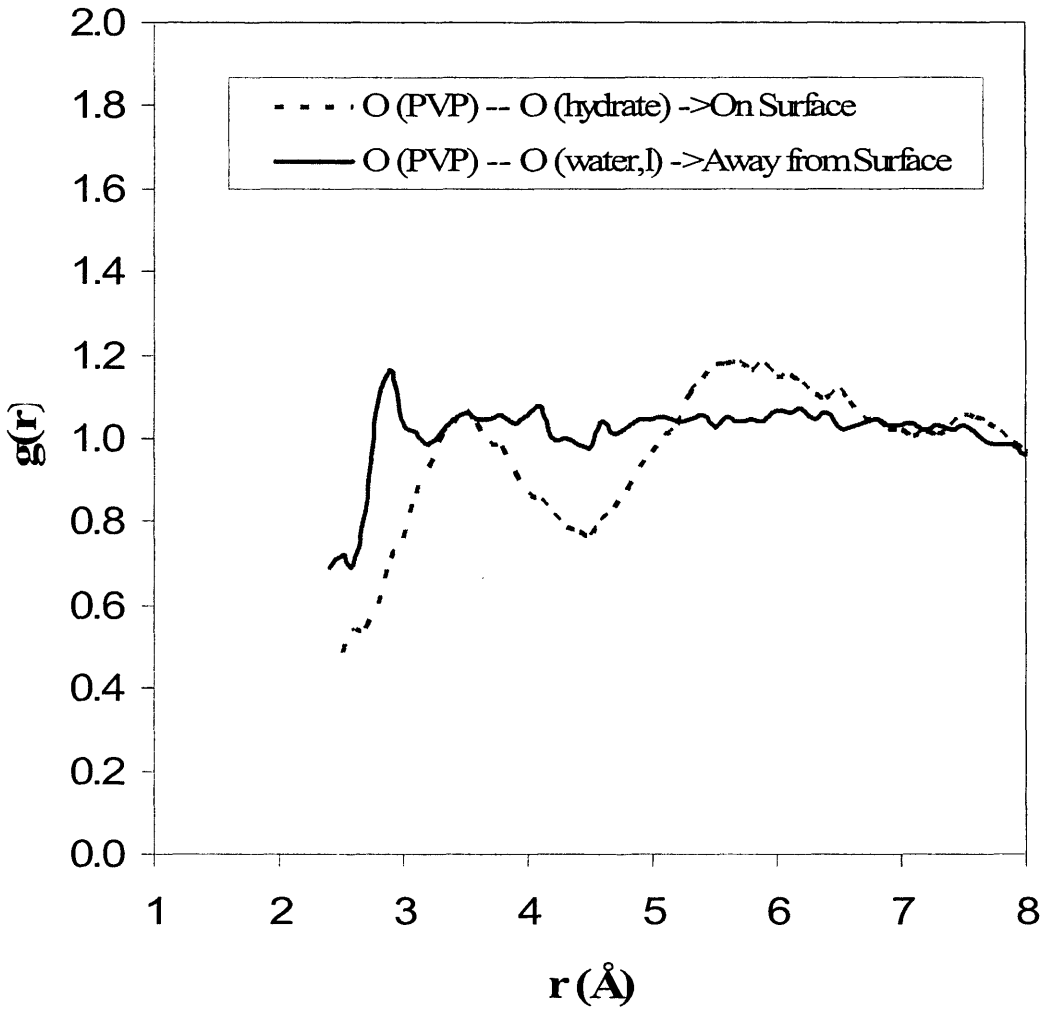

Figure 5.18b: Radial distribution functions between the double-bonded oxygen on PVP and the oxygen on water when the PVP is bound to the hydrate surface and away from the surface. Difference illustrates the effect of the hydrate surface on the morphology of the monomer and surrounding waters.

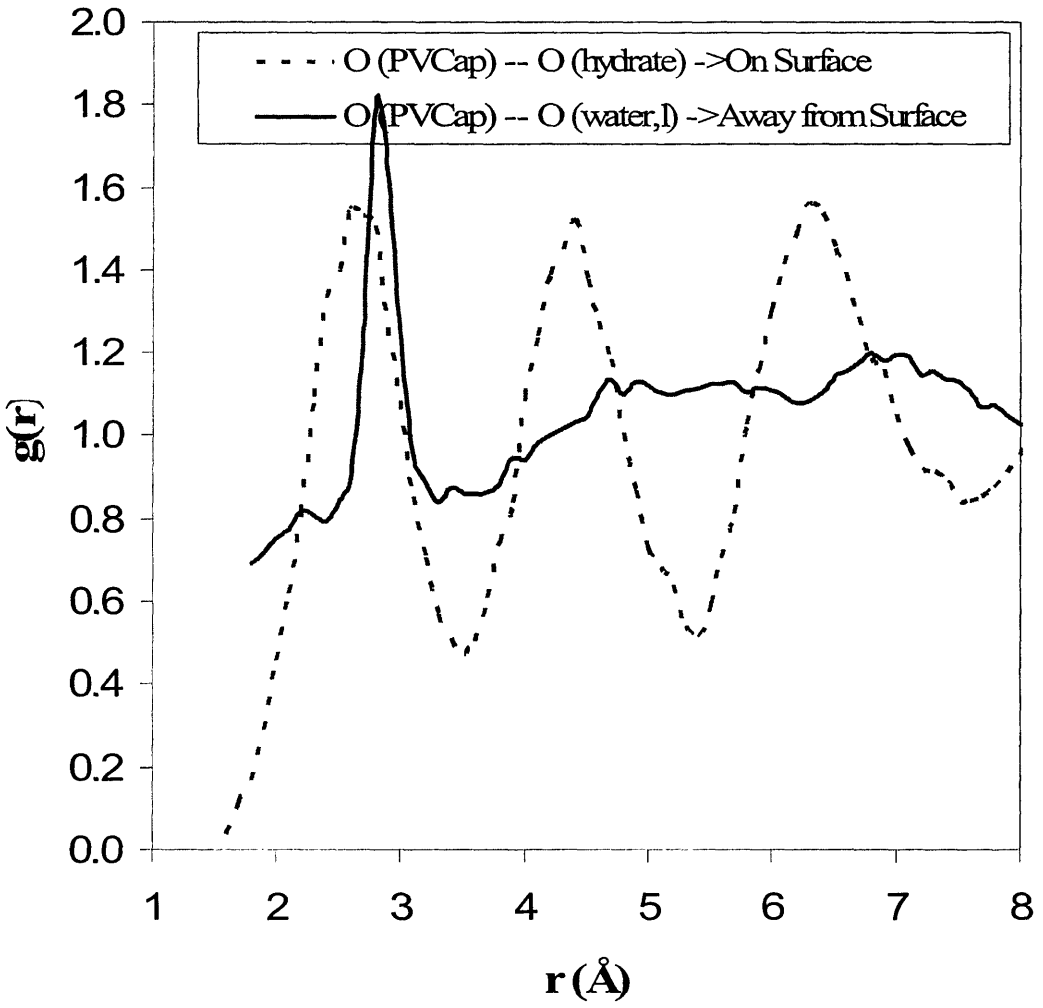

Figure 5.18c: Radial distribution functions between the double-bonded oxygen on PVCap and the oxygen on water when the PVCap is bound to the hydrate surface and away from the surface. Difference illustrates the effect of the hydrate surface on the morphology of the monomer and surrounding waters.

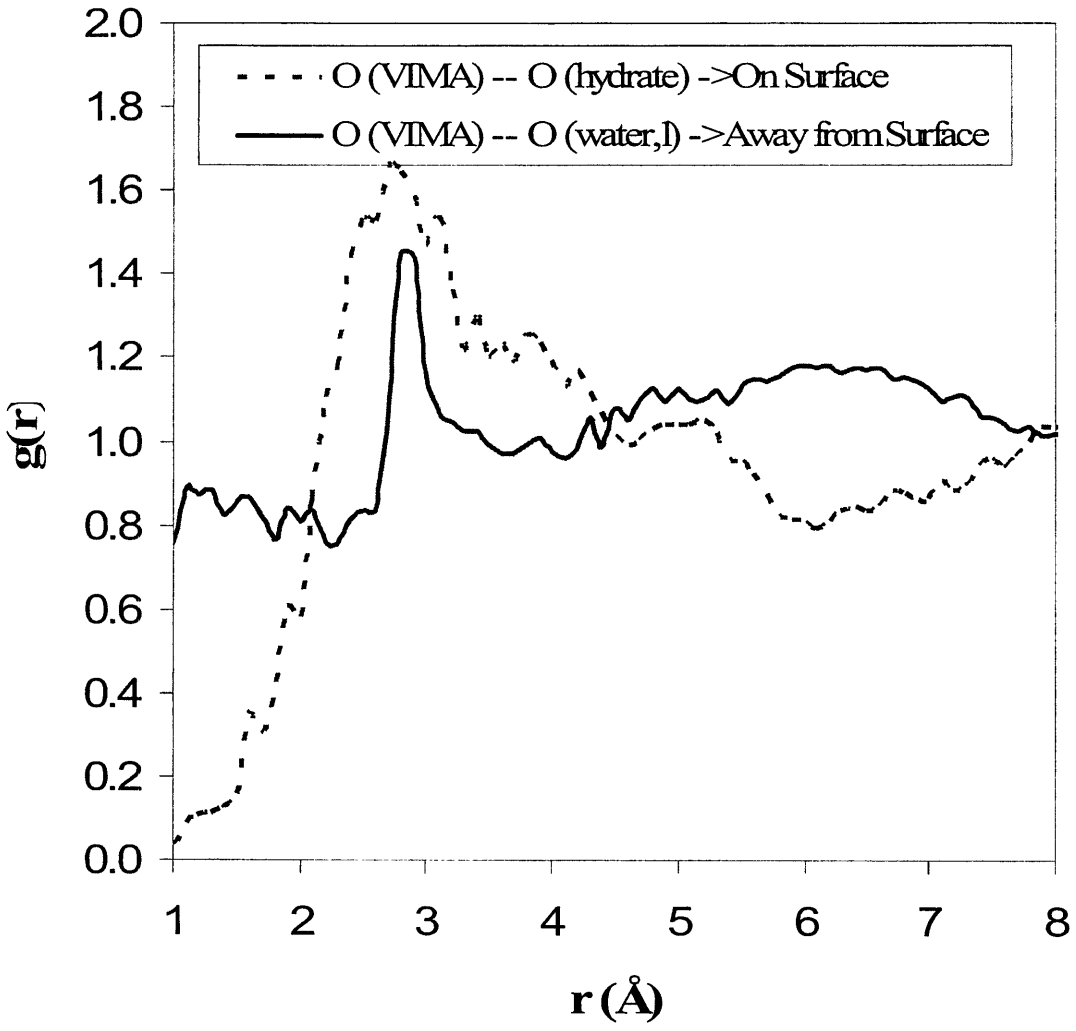

Figure 5.18d: Radial distribution functions between the double-bonded oxygen on VIMA and the oxygen on water when the VIMA is bound to the hydrate surface and away from the surface. Difference illustrates the effect of the hydrate surface on the morphology of the monomer and surrounding waters.

To examine more closely the water-inhibitor interaction, we look at these same RDFs for the oxygen on the monomer with the oxygen on water and compare them to $H_2O - OH_2$ RDFs. This way one can examine both how the monomer fits into the water structure and how it affects the water structure. The g(r) of PVCap, Figure 5.19, shows a great deal of correlation between the oxygen on the PVCap and the oxygen on the hydrate and liquid waters. The double-bonded oxygen falls into a lattice position typically occupied by a water molecule, thus leading to the strong energy of binding and the favorable free energy of reaction. In the liquid water phase, this =O is also coordinated in such a manner as to act like a water molecule.

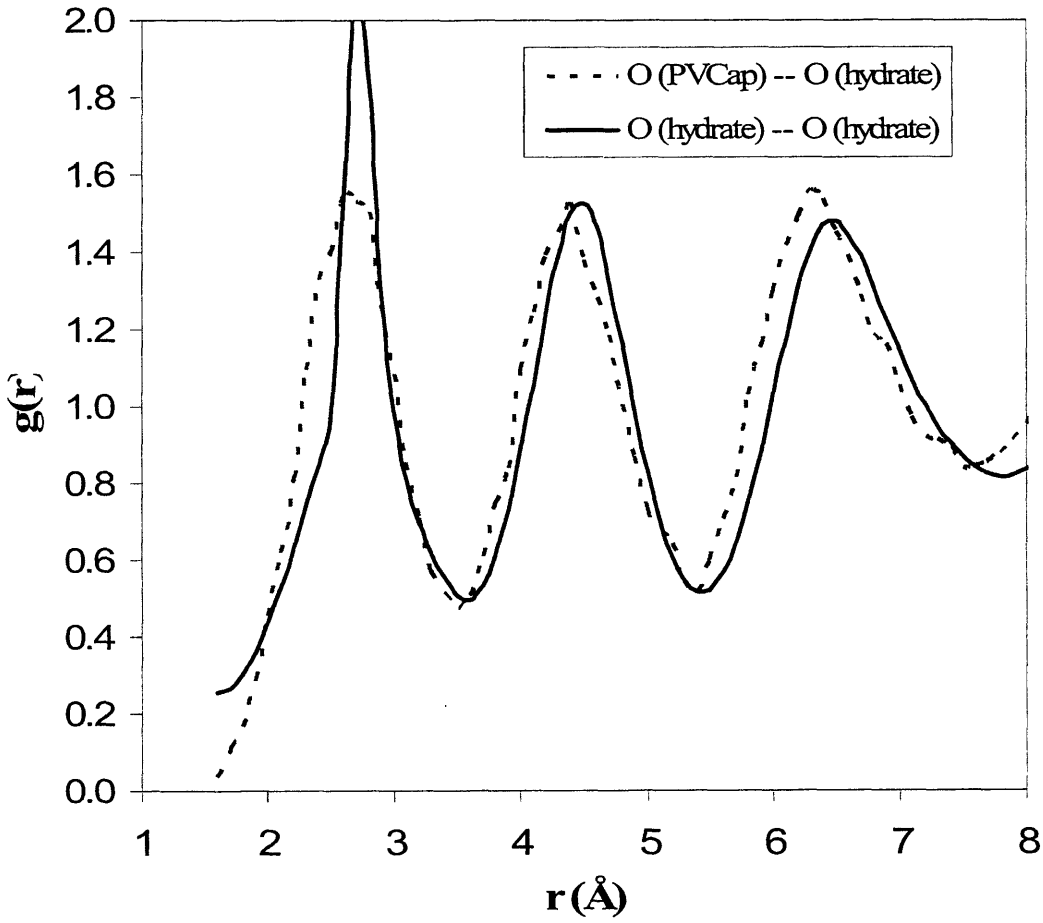

Figure 5.19a: Radial distribution functions between the double-bonded oxygen on PVCap and the oxygen on water when the PVCap is bound to the hydrate surface.

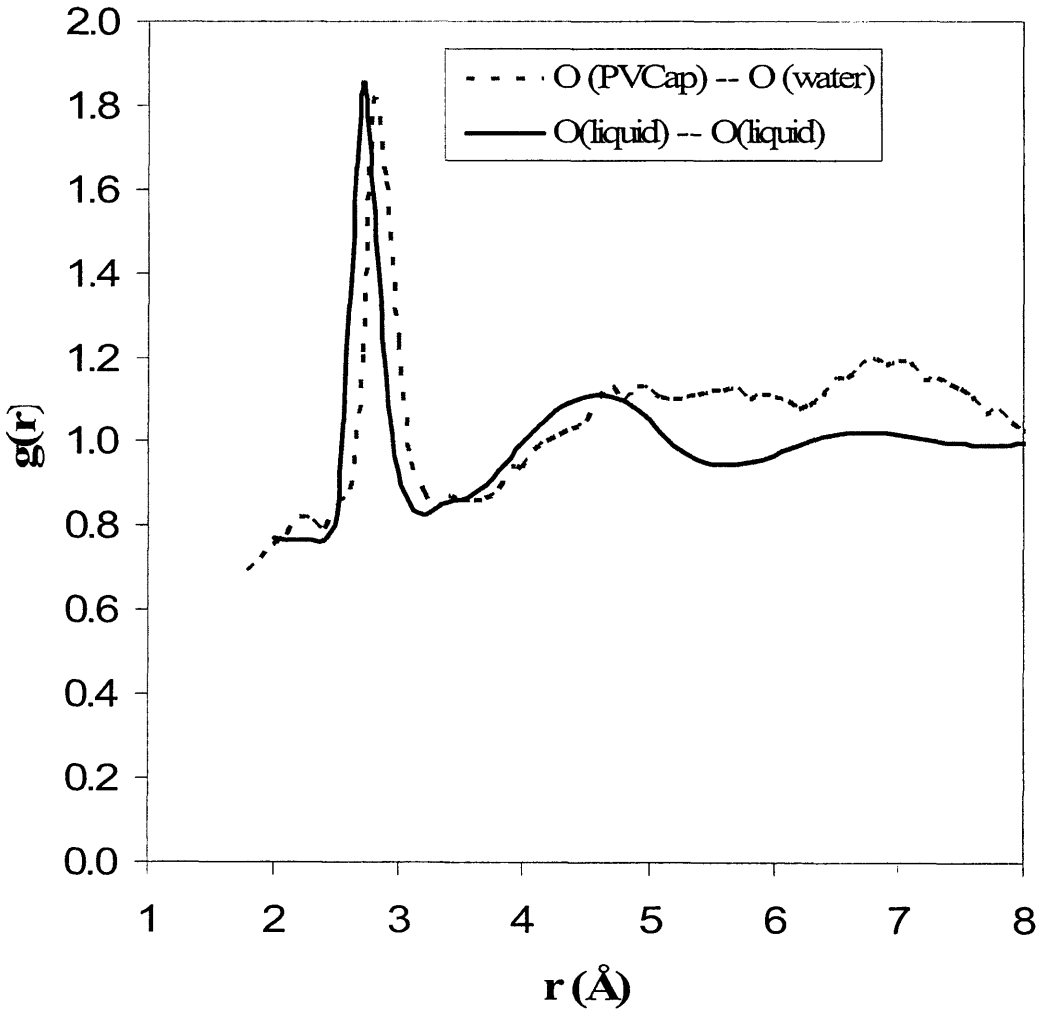

Figure 5.19b: Radial distribution functions between the double-bonded oxygen on PVCap and the oxygen on water when the PVCap is in solution away from the hydrate surface.

The calculated $g(r)$ of PVP, Figure 5.20, does not show the strong correlation with the hydrate crystal that the $g(r)$ of PVCap does. In fact, the first water oxygen neighbor is shifted away from the double-bonded oxygen in both the surface bound (a) and liquid water (b) cases. As evident in Figure 5.20b, the PVP monomer has little effect on the structure of water in the surrounding area. Finally, one can see from the $g(r)$ of VIMA, Figure 5.21a, that there is strong correlation in the first water shell both on and off the hydrate surface; however, unlike PVCap, the subsequent shells do not exhibit strong correlation. This is due to the double binding site nature of the VIMA monomer discussed in more detail in the next section. VIMA has two possible binding sites, between which the monomer frequently switches. These binding sites are not identical when bound to the hydrate surface (only one is bound at a time) and therefore the O–O $g(r)$ is averaged between these two distances, widening the first coordination shell and smoothing out the subsequent shells. Furthermore, as evident in Figure 5.21b, VIMA interacts strongly with the water in the liquid solution, where liquid water molecules surround the monomer, making the oxygen sites appear more similar.

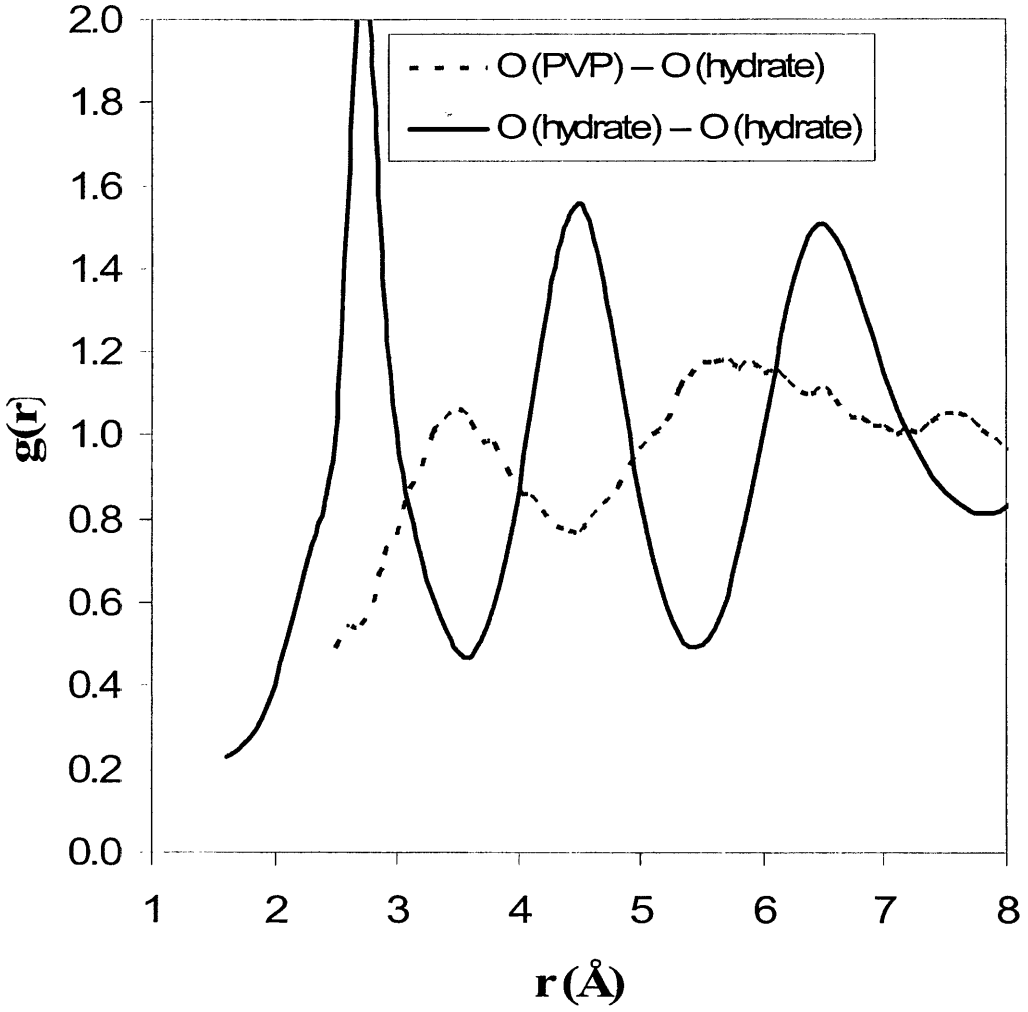

Figure 5.20a: Radial distribution functions between the double-bonded oxygen on PVP and the oxygen on water when the PVP is bound to the hydrate surface.

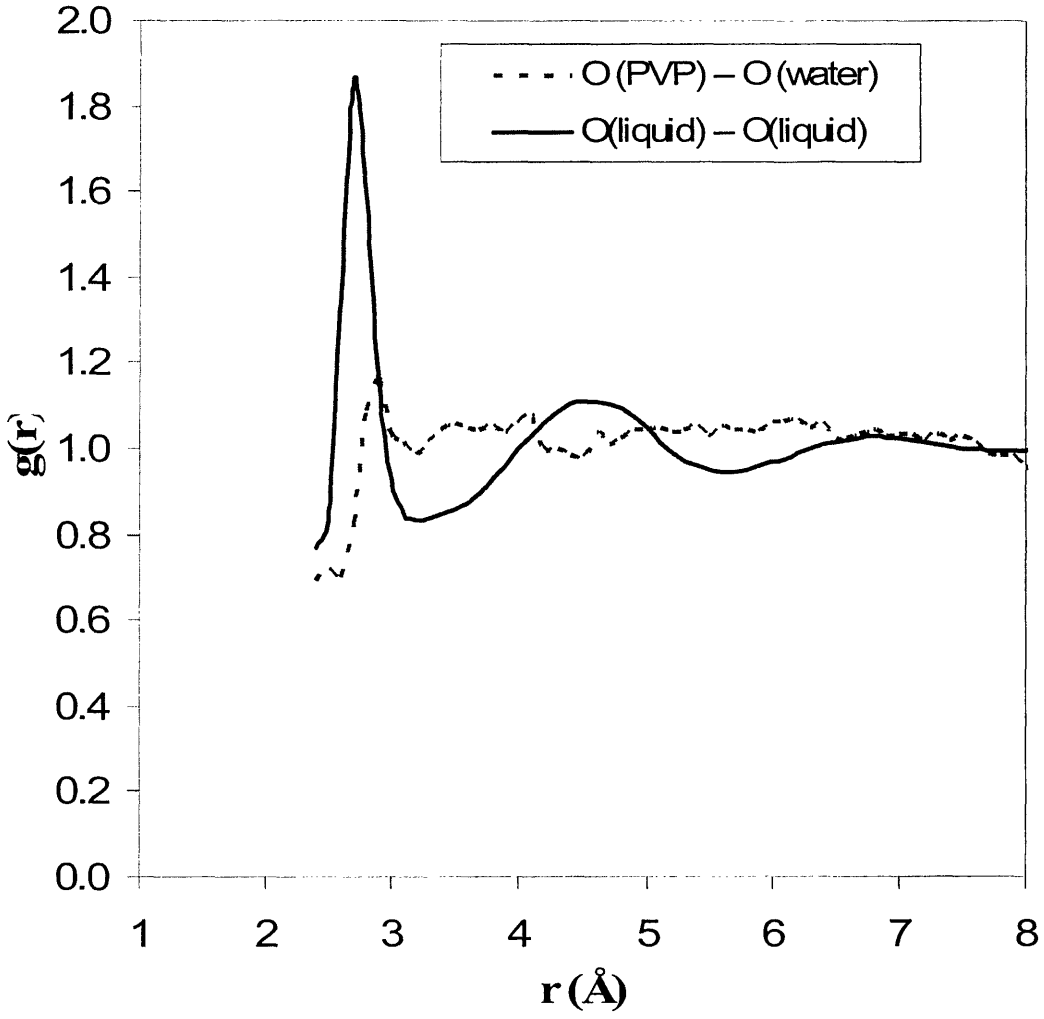

Figure 5.20b: Radial distribution functions between the double-bonded oxygen on PVP and the oxygen on water when the PVP is in solution away from the hydrate surface.

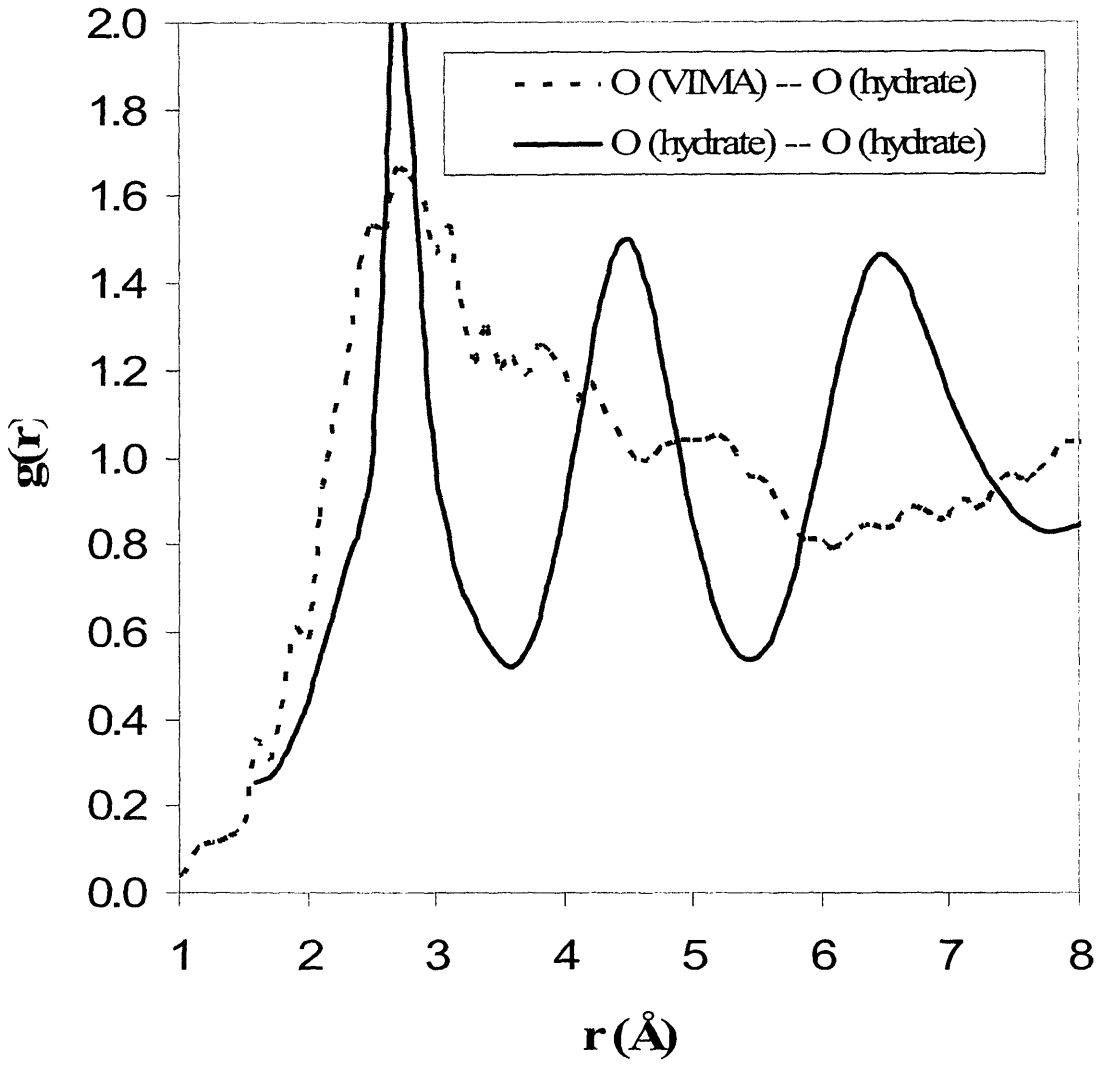

Figure 5.21a: Radial distribution functions between the double-bonded oxygen on VIMA and the oxygen on water when the VIMA is bound to the hydrate surface.

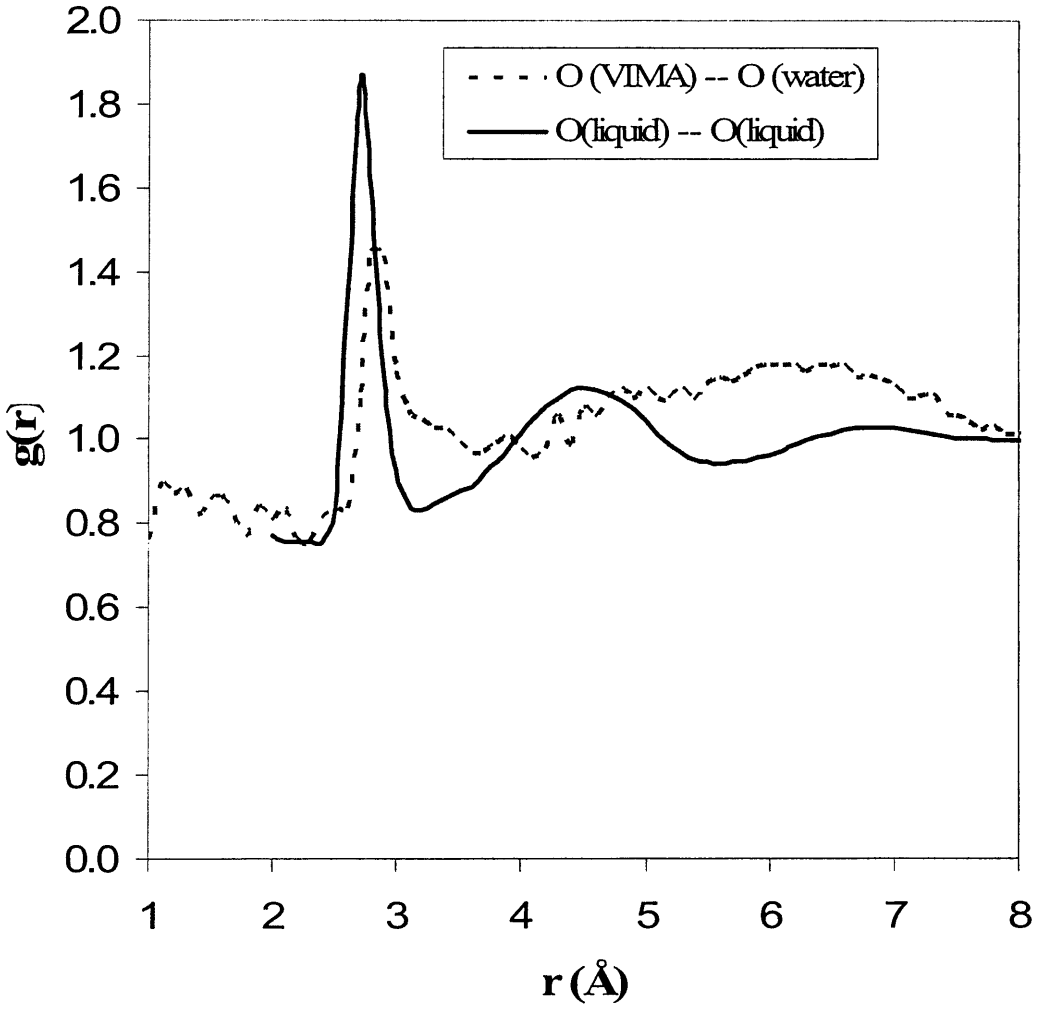

Figure 5.21b: Radial distribution functions between the double-bonded oxygen on VIMA and the oxygen on water when the VIMA is in solution away from the hydrate surface.

5.5 Molecular Characteristics Favoring Inhibition

From our molecular simulations, we have been able to identify two molecular characteristics that lead to the strong binding of PVCap: (1) a charge distribution on the edge of the PVCap (from O to CA in Figure 5.22a) that mimics the charge separation in the water molecules on the surface of the hydrate and (2) the congruence of the size of the PVCap with respect to the available space at the tetrakaidecahedron binding site. VIMA has been shown to have an inhibitor effect even stronger than PVCap and exhibits a similar charge distribution (see Figure 5.22b). However, unlike PVCap, there are two partially positive carbons (labeled CA and CN in Figure 5.22b) that double the opportunity for alignment with water to form hydrogen bonds.

PVP has a charge distribution similar to that of PVCap, thus allowing PVP to form hydrogen bonds with the waters on the hydrate surface. However, the size of the PVCap ring proves to be much more conducive to strong binding than that of the small PVP ring. When PVCap is bound in the open cage, its molecular motion is limited much more than the motion of the PVP monomer. The RMSD of the PVCap monomer is 1.155 Å while that of PVP is 2.466 Å, both over a period of 3 ns. More specifically, the atoms CO and CA on PVCap have RMSDs of 0.509 and 0.659 Å while the equivalent atoms on PVP have RMSDs of 0.844 and 2.390 Å, demonstrating that the motion of the carbon with the double-bonded oxygen (labeled CO) and its adjoining carbon (labeled CA), the bonding side of the ring, is much more restricted for PVCap compared to PVP. Therefore, the characteristics of this side of the ring should govern the strength of the binding interaction.

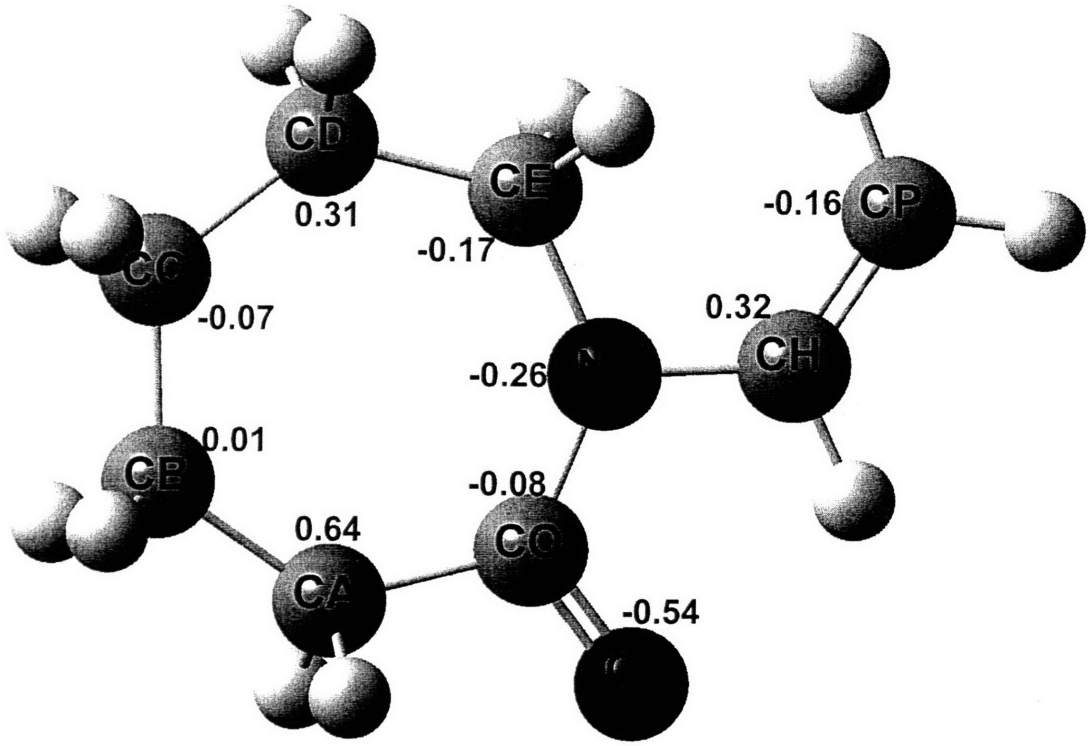

Figure 5.22a: Partial Charges on PVCap. Labels on atoms are simply to differentiate atoms of the same type from one another. For labels with two capital letters the first letter is the atom type and the second letter is to label that atom.

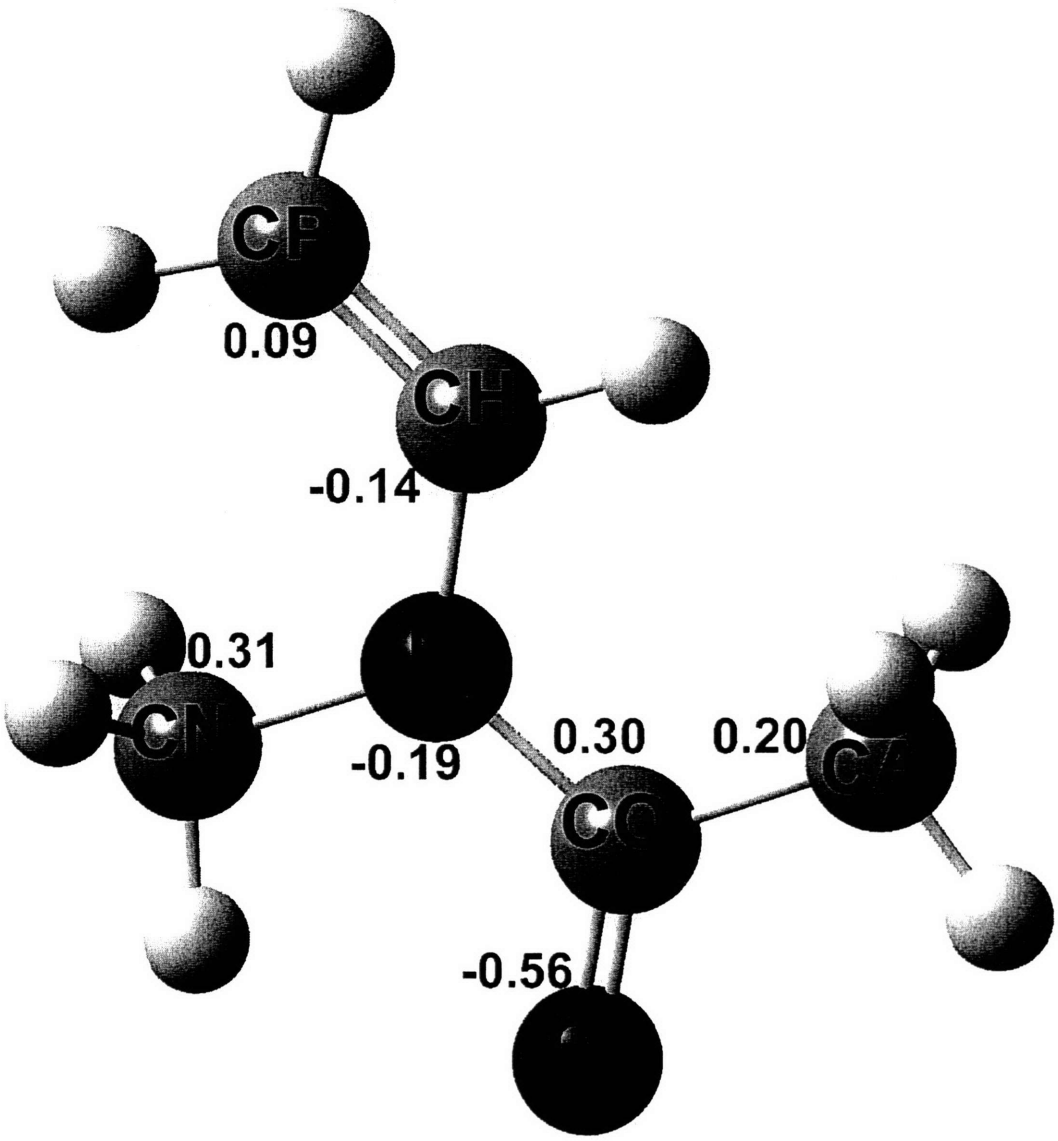

Figure 5.22b: Partial Charges on N-methyl, N-vinylacetamide. Labels on atoms are simply to differentiate atoms of the same type from one another. For labels with two capital letters the first letter is the atom type and the second letter is to label that atom.

5.6 Conclusions

Within we propose and test a two-fold mechanism for hydrate inhibition by four inhibitor molecules (PEO, PVP, PVCap, and VIMA) using molecular simulations. The mechanism hypothesizes that (1) as potential guest molecules become coordinated by water, form nuclei, and begin to grow, nearby inhibitor molecules disrupt the organization of the forming clathrate and (2) inhibitor molecules bind to the surface of the hydrate crystal precursor and retards further growth along the bound growth plane resulting in a modified planar morphology. Part one of this mechanism is supported by the results of our molecular dynamic simulations for the four inhibitor molecules studied. PVCap and VIMA, the more effective inhibitors, show strong interactions with the liquid water phase under hydrate forming conditions, while PVP and PEO appear relatively neutral to the surrounding water.

For part two, we test our hypothesis that the degree of inhibition is related to the strength of binding of the inhibitor to the surface of the hydrate crystal. We find that the free energy of binding between the inhibitor molecules and the hydrate surface does correlate directly with the effectiveness of the inhibitors. Inhibitors increasing in effectiveness, PEO<PVP<PVCap<VIMA, also have increasingly negative (exothermic) binding energies of -0.2 < -20.6 < -37.5 < -45.8 kcal/mol and binding free energies of increasing favorability (+0.4 ≈ +0.5 < -9.4 < -15.1 kcal/mol). The free energies of binding of PVP and PEO, +0.5 ± 3.7 and +0.4 ± 3.9 kcal/mol respectively, correspond to neutral equilibrium constants, $K_{eq} \cong 1$, for binding reactions while the free energies of binding for the stronger inhibitors, PVCap and VIMA result in $K_{eq} \gg 1$. With $K_{eq} \gg 1$ a relatively high fraction of the surfaces of ensuing nuclei would be bound by PVCap and

VIMA, disrupting growth. In addition, two molecular characteristics that lead to strongly binding inhibitors were found: (1) a charge distribution on the edge of the inhibitor that mimics the charge separation in the water molecules on the surface of the hydrate and (2) an inhibitor size similar to the available space at the hydrate-surface binding site. These two molecular characteristics result in strong hydrogen bonding between the inhibitor molecule and the surface of a forming hydrate crystal and thus lead to more effective inhibitor molecules.

5.7 References

(1) Sloan, E. D., Jr. *Clathrate Hydrates of Natural Gases - 2nd ed.*; Marcel Dekker, Inc.: New York, 1998.
(2) Buffett, B. A. *Annual Review of Earth and Planetary Sciences* **2000**, *28*, 477.
(3) Kvenvolden, K. A. *Reviews of Geophysics* **1993**, *31*, 173.
(4) Miller, S. L. *Science* **1970**, *170*, 531.
(5) Davy, H. *Phil. Trans. Roy. Soc. London* **1811**, *101*, 1.
(6) Hammerschmidt, E. G. *Ind. Eng. Chem.* **1934**, *26*, 851.
(7) Lederhos, J. P.; Long, J. P.; Sum, A.; Christiansen, R. L.; Sloan, E. D. *Chemical Engineering Science* **1996**, *51*, 1221.
(8) Radhakrishnan, R.; Trout, B. L. *Journal of Chemical Physics* **2002**, *117*, 1786.
(9) Radhakrishnan, R.; Trout, B. L. *Physical Review Letters* **2003**, *90*, 158301.
(10) Radhakrishnan, R.; Trout, B. L. *Journal of the American Chemical Society* **2003**, *125*, 7743.
(11) Storr, M. T.; Taylor, P. C.; Monfort, J. P.; Rodger, P. M. *Journal of the American Chemical Society* **2004**, *126*, 1569.
(12) Hawtin, R. W.; Moon, C.; Rodger, P. M. "Simulation of Hydrate Kinetic Inhibitors: The Next Level"; The Fifth International Conference on Gas Hydrates, 2005, Trondheim, Norway.
(13) Koh, C. A.; Westacott, R. E.; Zhang, W.; Hirachand, K.; Creek, J. L.; Soper, A. K. *Fluid Phase Equilibria* **2002**, *194*, 143.
(14) Storr, M. T.; Rodger, P. M. A molecular dynamics study of the mechanism of kinetic inhibition. In *Gas Hydrates: Challenges for the Future*; NEW YORK ACAD SCIENCES: New York, 2000; Vol. 912; pp 669.
(15) Makogon, T. Y.; E. Dendy Sloan, J. "Mechanism of Kinetic Hydrate Inhibitors"; Fourth International Conference on Gas Hydrates, 2002, Yokohama, Japan.
(16) Zeng, H.; Wilson, L. D.; Walker, V. K.; Ripmeester, J. A. *Canadian Journal of Physics* **2003**, *81*, 17.
(17) Hutter, J. L.; King, H. E.; Lin, M. Y. *Macromolecules* **2000**, *33*, 2670.
(18) Makogon, T. Y.; Larsen, R.; Knight, C. A.; Sloan, E. D. *Journal of Crystal Growth* **1997**, *179*, 258.
(19) Larsen, R.; Knight, C. A.; Sloan, E. D. *Fluid Phase Equilibria* **1998**, *151*, 353.
(20) Sakaguchi, H.; Ohmura, R.; Mori, Y. H. *Journal of Crystal Growth* **2003**, *247*, 631.
(21) Christiansen, R. L.; Sloan, E. D. *International Conference on Natural Gas Hydrates* **1994**, *715*, 283.
(22) Sloan, E. D.; Fleyfel, F. *AIChE J* **1991**, *37*, 1281.
(23) Kvamme, S. *Gas Hydrates: Challenges for the Future* **2000**, *912*, 496.
(24) Larson, M. A.; Garside, J. *Chemical Engineering Science* **1986**, *41*, 1285.
(25) King, H. E.; Hutter, J. L.; Lin, M. Y.; Sun, T. *Journal of Chemical Physics* **2000**, *112*, 2523.
(26) Carver, T. J.; Drew, M. G. B.; Rodger, P. M. *Journal of the Chemical Society-Faraday Transactions* **1995**, *91*, 3449.

(27) Carver, T. J.; Drew, M. G. B.; Rodger, P. M. *Journal of the Chemical Society-Faraday Transactions* **1996**, *92*, 5029.
(28) Kvamme, B.; Huseby, G.; Forrisdahl, O. K. *Molecular Physics* **1997**, *90*, 979.
(29) Carver, T. J.; Drew, M. G. B.; Rodger, P. M. *Gas Hydrates: Challenges for the Future* **2000**, *912*, 658.
(30) Carver, T. J.; Drew, M. G. B.; Rodger, P. R. *Physical Chemistry Chemical Physics* **1999**, *1*, 1807.
(31) Cao, Z. T.; Tester, J. W.; Trout, B. L. *J. Chem. Phys.* **2001**, *115*, 2550.
(32) Anderson, B. J.; Tester, J. W.; Trout, B. L. *Journal of Physical Chemistry B* **2004**, *108*, 18705.
(33) Cao, Z. T.; Tester, J. W.; Sparks, K. A.; Trout, B. L. *J. Phys. Chem. B.* **2001**, *105*, 10950.
(34) Anderson, B. J.; Tester, J. W.; Trout, B. L. *Journal of Physical Chemistry B* **2004**, *108*, 18705.
(35) Jorgensen, W. L.; Chandrasekhar, J.; Madura, J. D.; Impey, R. W.; Klein, M. L. *Journal of Chemical Physics* **1983**, *79*, 926.
(36) Jorgensen, W. L.; Madura, J. D. *Molecular Physics* **1985**, *56*, 1381.
(37) Jorgensen, W.; Severance, D. L. *J. Am. Chem. Soc.* **1990**, *112*, 4768.
(38) Kaminski, G.; Duffy, E. M.; Matsui, T.; Jorgensen, W. L. *J. Phys. Chem.* **1994**, *98*, 13077.
(39) Kirkwood, J. G. *J. Chem. Phys.* **1935**, *3*, 300.
(40) Frenkel, D.; Smit, B. *Understanding molecular simulation: from algorithms to applications*, 2nd ed.; Academic Press: San Diego, 2002.
(41) Flyvbjerg, H.; Petersen, H. G. *Journal of Chemical Physics* **1989**, *91*, 461.
(42) Sloan, E. D. *Clathrate hydrates of natural gases*, 2nd ed.; Marcel Dekker: New York, 1998.
(43) Freer, E. M.; Sloan, E. D. *Gas Hydrates: Challenges for the Future* **2000**, *912*, 651.

Chapter 6. Overall Conclusions and Recommendations

6.1 Conclusions

The overall thesis goal was to better understand hydrate processes, namely hydrate phase equilibrium and mechanisms of inhibition, at a molecular level through the use of quantum chemical, statistical mechanical, and molecular dynamic approaches. By evaluating previous methods of determining Langmuir constants used in the calculation of hydrate phase equilibria, we have illuminated flaws in schemes to determine potential parameters and their accompanying reference parameters. These flaws led to limitations in prediction outside of the range of experimental data. By applying first principles methods, we have refined the literature reference parameters for hydrate phase equilibria significantly, such that these refined parameters actually allow for *prediction* of macroscopic events such as phase equilibria and structural changes. We have also proposed and tested a two-fold mechanism for hydrate inhibition using "low-dosage", kinetic inhibitor molecules. Molecular characteristics have been examined that can lead to even more effective inhibitors.

More specifically we conclude that:

1. A site-site potential was developed that characterizes the three-dimensional hyperspace energy surface of the argon-water interaction and the six-dimensional surface for methane-water interactions. Many-body effects can be significant in the argon-water system due to the delocalization of electrons along the hydrogen bonds. These effects were accounted for by fitting the **Ar–H**OH potential characteristic energy to quantum mechanical calculations

on systems with up to five water molecules interacting with the argon. The many-body effects are negligible in the methane-water system when our methane-water site-site potential is used.

2. Precise values for Structure II reference parameters, $\Delta\mu_w^0$=1077±5 kcal/mol and ΔH_w^0 =1294±11 kcal/mol and Structure I reference parameters, $\Delta\mu_w^0$=1203±3 kcal/mol and ΔH_w^0=1170±19 kcal/mol (errors evaluated using 95% confidence intervals), were found using the *ab initio* site-site potentials. Using these reference values together with the *ab initio* site-site potentials, the equilibrium dissociation pressure was computed within ±3% of the experimental value for pure argon hydrates and within ±3.5% of the experimental value for methane hydrates.
3. Over the temperature range studied, we verified that argon forms Structure II hydrates as opposed to Structure I hydrates.
4. Methane cage occupancies were predicted to within ±5% of experimental values.
5. Phase equilibria for the mixed hydrate of argon and methane were predicted within ±3.4% without any fitting parameters. Also the existence of Structure I to Structure II phase transitions was determined using our *ab initio* approach.
6. Our cell potential approach was validated by making numerous predictions of multi-component phase data without fitting mixture data to experiments.
7. The spherically averaged Kihara potential form is adequate in representing the overall guest-host interaction in structure I; however, guest-host interactions in the large cage of structure II are not effectively reproduced, thus leading to

inaccurate reference parameters which have commonly appeared in the literature.

8. The reference parameters determined and used in this thesis were validated by their successful utilization in predicting mixed gas hydrate phase equilibrium data. All mixture predictions in this work are performed without fitting to any mixture data and nonetheless predict the experimental data accurately.
9. Overall, the cell potential method developed in this work has demonstrated its effectiveness and applicability to successfully model mixed hydrate systems without any adjustable parameters. For example, the structure I to structure II transition for methane-ethane gas mixtures was predicted to occur at 0.75 mol fraction methane at 274.2 K, within the experimental range measured to be 0.72-0.75 mol fraction methane.
10. We were able to extrapolate the results of the calculated cell potentials to other systems. The cell potential that is calculated for ethane in a structure I hydrate lattice provides sufficient quantitative insight into the interaction between ethane and the water surrounding it in the hydrate that we have been able to model the ethane-water interaction in a structure II lattice.
11. Several predictions were also developed that await experimental testing. For example, structure I to structure II phase transitions have been predicted for methane-cyclopropane gas mixtures outside the temperature range of the pure cyclopropane structure II envelope. Quintuple (L_w-SI-SII-L_{hc}-V) points have been predicted for the ethane-propane-water (277.3 K, 12.28 bar, and

$x_{eth,waterfree}$ = 0.676) and ethane-isobutane-water (274.7 K, 7.18 bar, and $x_{eth,waterfree}$ = 0.81) systems.

12. By starting directly from thermodynamic data at finite temperature, and by using a Boltzmann-weighting scheme over a large configuration space when calculating our *ab initio* potential[46], our method easily determines an appropriate cell potential, which accounts for statistical averaging of configurations over a wide range of temperatures. The basic idea of solving an inverse problem for an "exact" thermodynamic potential may find further successful applications in other areas of materials modeling, where *ad hoc* fitting ideal structures remains the standard theoretical approach.
13. A two-fold mechanism for hydrate inhibition has been proposed and tested using molecular dynamic simulations for PEO, PVP, PVCap, and VIMA. This mechanism hypothesizes that (1) as potential guest molecules become coordinated by water, form nuclei, and begin to grow, nearby inhibitor molecules disrupt the organization of the forming clathrate and (2) inhibitor molecules bind to the surface of the hydrate crystal precursor and retards further growth along the bound growth plane resulting in a modified planar morphology. This mechanism is supported by the results of our molecular dynamic simulations for the four inhibitor molecules studied. PVCap and VIMA, the more effective inhibitors, shows strong interactions with the liquid water phase under hydrate forming conditions, while PVP and PEO appear relatively neutral to the surrounding water.

14. The free energy of binding for the inhibitors directly correlates with the effectiveness of the inhibitors. Inhibitors increasing in effectiveness, PEO<PVP<PVCap<VIMA, also have increasing negative (exothermic) binding energies of -0.2 < -20.6 < -37.5 < -45.8 kcal/mol and binding free energies of increasing favorability (+0.4 ≈ +0.5 < -9.4 < -15.1 kcal/mol). The free energies of binding for PVP and PEO of 0.5 ± 3.7 and +0.4 ± 3.9 predict neutral equilibrium constants, $K_{eq} \cong 1$, for the binding reactions while the free energies of binding for the stronger inhibitors, PVCap and VIMA result in $K_{eq} \gg 1$. This would result in the PVCap and VIMA spending, at equilibrium, a much higher proportion of their time bound to the surface and prior to reaching equilibrium there would be a stronger free energy driving force pushing the inhibitors toward the bound state.

6.2 Recommendations

We recommend that future work in the areas covered by this thesis focus on applications of the methods described. Continued work on the prediction of multi-phase hydrate systems could have significant impact in the areas of hydrogen storage, resource characterization, and thermodynamic stability, while development of more effective kinetic inhibition is a ripe domain. More specifically, areas of recommended study are:

1. Application of the cell potential method to the library of available literature values for hydrate equilibrium in systems with occupancy of both cages. The potential parameters could be linked by physically-relevant potentials between the two cages, thus allowing for determination of the cell potentials directly from experimental data.

2. Application of the *ab initio* potential method paired with the inclusion of many-body interactions to multiple occupancy systems of structure I, structure II, and structure H. These systems are difficult to access and accurately characterize experimentally due to the extremely high pressures involved.
3. Incorporate equations of state for the fluid phase that are valid or more accurate at elevated pressures. The Peng-Robinson EOS was used exclusively in this work and accurately models the fluid fugacity at these relatively low pressures; however, at pressures in which hydrogen forms a hydrate clathrate the Peng-Robinson EOS is likely to fail to accurately model the fluid fugacity.
4. Validation of the mechanism for hydrate inhibition and development of more effective inhibitors, including testing of the hypothesized mechanism for inhibition.
5. Investigation of the effect of inhibitors on impending hydrate nuclei in order to quantify the disruption of the formation of nuclei.
6. Identification of new molecules and examination both on the hydrate growth surface and in solution with hydrate nuclei. These should be tested for their ability to disrupt nuclei formation and inhibit growth of microcrystals.